J-990929-1

Optical Absorption in Transparent Materials During 1.5 MeV Electron Irradiation

NASA Contract No. SNPC-70

UNITED AIRCRAFT CORPORATION

United Aircraft Research Laboratories

EAST HARTFORD, CONNECTICUT

United Aircraft Research Laboratories

UNITED AIRCRAFT CORPORATION

EAST HARTFORD, CONNECTICUT

J-990929-1

Optical Absorption in Transparent Materials During 1.5 MeV Electron Irradiation

NASA Contract No. SNPC-70

REPORTED BY Gary E. Palma
Gary E. Palma

Ronald M. Gagosz
Ronald M. Gagosz

APPROVED BY Robert K. Erf
Robert K. Erf, Chief
Optics and Acoustics

DATE October 1970

NO. OF PAGES 76

COPY NO. 29

FOREWORD

An exploratory experimental and theoretical investigation of gaseous nuclear rocket technology is being conducted by the United Aircraft Research Laboratories under Contract SNPC-70 with the joint AEC-NASA Space Nuclear Propulsion Office. The Technical Supervisor of the Contract for NASA is Captain C. E. Franklin (USAF). Results of portions of the investigation conducted during the period between September 16, 1969 and September 15, 1970 are described in the following eight reports (including the present report) which comprise the required first Interim Summary Technical Report under the Contract:

1. Klein, J. F. and W. C. Roman: Results of Experiments to Simulate Radiant Heating of Propellant in a Nuclear Light Bulb Engine Using a D-C Arc Radiant Energy Source. United Aircraft Research Laboratories Report J-910900-1, September 1970.

2. Jaminet, J. F. and A. E. Mensing: Experimental Investigation of Simulated-Fuel Containment in R-F Heated and Unheated Two-Component Vortexes. United Aircraft Research Laboratories Report J-910900-2, September 1970.

3. Vogt, P. G.: Development and Tests of Small Fused Silica Models of Transparent Walls for the Nuclear Light Bulb Engine. United Aircraft Research Laboratories Report J-910900-3, September 1970.

4. Roman, W. C.: Experimental Investigation of a High-Intensity R-F Radiant Energy Source to Simulate the Thermal Environment in a Nuclear Light Bulb Engine. United Aircraft Research Laboratories Report J-910900-4, September 1970.

5. Bauer, H. E., R. J. Rodgers and T. S. Latham: Analytical Studies of Start-Up and Dynamic Response Characteristics of the Nuclear Light Bulb Engine. United Aircraft Research Laboratories Report J-910900-5, September 1970.

6. Latham, T. S. and H. E. Bauer: Analytical Studies of In-Reactor Tests of a Nuclear Light Bulb Unit Cell. United Aircraft Research Laboratories Report J-910900-6, September 1970.

7. Palma, G. E. and R. M. Gagosz: Optical Absorption in Transparent Materials During 1.5 Mev Electron Irradiation. United Aircraft Research Laboratories Report J-990929-1, September 1970. (present report)

8. Krascella, N. L.: Analytical Study of the Spectral Radiant Flux Emitted from the Fuel Region of a Nuclear Light Bulb Engine. United Aircraft Research Laboratories Report J-910904-1, September 1970.

J-990929-1

Optical Absorption in Transparent Materials During 1.5 MeV Electron Irradiation

TABLE OF CONTENTS

Report J-990929-1

Optical Absorption in Transparent Materials During 1.5 MeV Electron Irradiation

SUMMARY

A program of in situ optical experiments was conducted to determine the level of irradiation-induced optical absorption that exists in Corning Grade 7940 fused silica and single crystal aluminum oxide during steady-state 1.5 MeV electron irradiation. These experiments were conducted at the Space Radiation Effects Laboratory of NASA Langley Research Center using a Dynamitron electron accelerator as the electron source. The optical transmission of a total of 25 fused silica specimens was measured during electron irradiation over a range of ionizing dose rates (0.02-10 Mrads/sec) and specimen temperatures (40-900 C). Three of these specimens had been previously reactor irradiated to a dose of 10^{17} fast neutrons per cm^2 at the Union Carbide Research Center. In addition to measuring the transmission at the peak of the strong irradiation-induced absorption band centered at 2150 Å, spectral scans over the wavelength interval 2050-2500 Å were also made. The decay of the irradiation-induced absorption due to optical bleaching and the rate of recoloration following optical bleaching were measured in order to determine the effectiveness of optical bleaching and to obtain information relating to the damage mechanism responsible for the irradiation-induced absorption. The most surprising and important result was the low level of irradiation-induced optical absorption at dose rates equal to those expected in a nuclear light bulb engine which is believed to be due to radiation annealing.

Also included in this investigation were four aluminum oxide specimens, of which two had been reactor irradiated to a dose of 10^{17} fast neutrons per cm^2 at the Union Carbide Research Center. The optical transmission of these specimens was measured during electron irradiation primarily at 2050 Å, the peak of the strong irradiation-induced absorption band in aluminum oxide.

RESULTS

1. Measurement of the optical transmission of fused silica specimens during 1.5 MeV electron irradiation indicates that:

a. the growth of the induced absorption coefficient at a wavelength of 2150 Å during ambient-temperature irradiation is linear with a slope of 0.05 cm^{-1}/Mrad;

b. at constant ionizing dose rate, the steady-state irradiation-induced absorption coefficient at a wavelength of 2150 Å decreases with increasing specimen temperature. At 0.4 Mrad/sec the absorption coefficient decreases from 5.8 cm^{-1} at 100 C to 0.4 cm^{-1} at 500 C;

c. at constant temperature, the induced absorption coefficient increases with increasing ionizing dose rate, up to a dose rate of 0.4 Mrad/sec. Above an ionizing dose rate of 0.4 Mrad/sec, the induced absorption coefficient decreases with increasing dose rate. At a specimen temperature of 300 C, the induced absorption coefficient at 0.4 Mrad/sec is 2 cm^{-1} which decreases to 0.1 cm^{-1} at 5 Mrads/sec;

d. the steady-state irradiation-induced absorption coefficient is independent of the previous irradiation history;

e. the rate of annealing at elevated temperatures is enhanced during irradiation due to radiation annealing. At 300 C the estimated annealing rate during irradiation at 5 Mrads/sec is 2 sec^{-1} as compared with 0.002 sec^{-1} measured in the absence of irradiation;

f. the growth of induced absorption during 1.5 MeV electron irradiation and during gamma irradiation are approximately equal at the same ionizing dose rate. The additional generation of induced absorption due to fission neutrons appears negligible. The radiation annealing effect observed during electron irradiation is expected to occur during gamma irradiation also since the ionizing processes are nearly identical;

g. the spectral shape of the irradiation-induced absorption band, centered at a wavelength of 2150 Å, as measured during elevated-temperature electron irradiation, does not differ appreciably from that measured after nuclear-reactor irradiation;

h. the value of the optical bleaching constant, measured at low light intensity, is approximately 0.08 watts^{-1}cm^{2}-sec^{-1};

i. the electron trapping constant, measured at low dose rate, is approximately 2 Mrads^{-1}; and

j. at a specimen temperature of 930 C and an ionizing dose rate of 5 Mrads/sec, no change in optical transmission was observed over an irradiation time of 1000 sec in the wavelength interval 2050-2500 Å.

2. The results indicate that in an operating full-scale nuclear light bulb engine:

a. the estimated heat deposition in the fused silica transparent wall due to irradiation-induced optical absorption at wavelengths longer than 2050 Å is 100 watts/cm^3 neglecting optical bleaching. Optical bleaching is expected to decrease this heat deposition to 10 watts/cm^3. Both values are negligible compared to the expected total heat deposition of 4.5 kW/cm^3 due to convection heating, nuclear energy deposition and intrinsic optical absorption; and

b. the fraction of the total radiant light intensity which is absorbed in the transparent wall due to the irradiation-induced optical absorption at wavelengths longer than 2050 Å is estimated to be between 0.02% and 0.002%.

3. Measurement of the optical transmission of aluminum oxide specimens during 1.5 MeV electron irradiation and following reactor irradiation indicates that:

a. 1.5 MeV electron irradiation does not result in appreciable induced optical absorption in the wavelength interval 2050-2500 Å in this material; and

b. reactor irradiation generates a strong induced absorption band centered at approximately 2050 Å. This induced absorption band anneals at 500 C in the absence of irradiation and was observed to anneal at less than 200 C during electron irradiation at an ionizing dose rate of 3.5 Mrads/sec.

INTRODUCTION

The Research Laboratories of United Aircraft Corporation have been conducting an extensive program to determine the effects of nuclear radiation on the optical transmission of transparent materials under NASA contracts NASw-768, NASw-847, and SNPC-70, and under corporate sponsorship. The purpose of this program has been to determine the level of irradiation-induced optical absorption to be expected in the transparent wall of a full-scale nuclear light bulb engine during normal operation. The material studied most extensively during this program has been Corning 7940 fused silica, whose optical transmission, resistance to thermal shock, structural properties, ease of fabrication and availability, make it a promising candidate for the transparent wall material. In addition, the irradiation-induced absorption bands at visible wavelengths, which are related to impurities, do not develop appreciably in Corning 7940 fused silica due to the low level of impurities in this material. The irradiation-induced absorption bands that are observed after exposure to nuclear radiations are centered at the ultraviolet wavelengths of approximately 2150 Å and 1650 Å with a subsidiary peak sometimes observed at approximately 2700 Å (Refs. 1 through 5). These absorption bands are believed to be due to radiation damage to the SiO_2 molecules, rather than to impurities.

To directly determine the level of irradiation-induced absorption that would exist in the transparent wall of a full-scale engine during normal operation would require a source whose radiation flux and operating time were equal to that of the full-scale engine. Since a source of this type has not been available, it has been the purpose of this program to: (1) conduct a series of related experiments using various available radiation sources, each of which simulates some aspect of the radiation flux or dose of the full-scale engine, and (2) develop a suitable model for the coloration process from which a reasonable estimate of the irradiation-induced absorption in an operating full-scale engine could be predicted.

These experimental programs have consisted of four distinct sets of experiments which include:

1. post-irradiation optical transmission measurements in which the reactor irradiation simulated the full-scale engine dose (Ref. 6);

2. in situ optical transmission measurements in a pulsed reactor which simulated the full scale engine dose rate (Refs. 7 and 8);

3. in situ optical transmission measurements in a steady-state reactor which simulated the full-scale engine dose (Ref. 9); and

4. in situ optical transmission measurements in an electron accelerator which simulated the full scale flux and dose of the ionizing radiation (Ref. 9).

The post-irradiation measurements were made over the wavelength range from 1500 Å in the vacuum ultraviolet to 4.5 microns in the near infrared. The in situ measurements, however, were made primarily at 2150 Å in the ultraviolet since the long optical path lengths and difficult instrumental problems associated with these in situ experiments precluded measurements in the vacuum ultraviolet.

The first set of experiments involved post-irradiation measurements of the irradiation-induced absorption coefficient in fused silica (Ref. 6). A growth curve of gamma irradiation-induced absorption coefficient vs. ionizing dose was obtained which had a slope of 0.045 cm^{-1}/Mrad at 2150 Å. The rate of thermal annealing of nuclear reactor irradiation-induced absorption at this wavelength was also measured and was found to be an increasing function of specimen temperature. In addition, some preliminary data on irradiation-induced absorption in aluminum oxide and beryllium oxide was obtained.

A second set of experiments was conducted in which the optical transmission of fused silica at 2150 Å was measured during pulsed neutron and gamma irradiation using the University of Illinois'TRIGA reactor as a radiation source (Refs. 7 and 8). The results of these experiments indicated that the generation of the irradiation-induced absorption in fused silica was primarily due to the effects of ionizing radiation and that the effects of neutron damage were not significant. In addition, the thermal annealing rates observed immediately following the reactor pulse were found to be much higher than those measured in the previous post-irradiation experiments. However, due to the short duration of the reactor pulse (~30 msec), only transient data was obtained; this was of limited value in predicting the steady-state absorption that would exist in a full-scale engine.

In order to obtain information on the steady-state irradiation-induced absorption in fused silica, two additional sets of in situ experiments were conducted during the FY 1969 program (Ref. 9). In one set of experiments the optical transmission of fused silica was measured during steady-state nuclear reactor irradiation at elevated specimen temperatures using the Nuclear Engineering Test Reactor at WPAFB as a radiation source. The results of these experiments were found to be consistent with a model in which the rate of thermal annealing during irradiation was equal to that measured in post-irradiation experiments. However, it was not certain how the results of these experiments could be extrapolated to the ionizing dose rate of the full-scale engine (5 Mrads/sec) which was a factor of 250 higher than that of the steady-state reactor. Indeed, as indicated above, the results of the pulsed reactor experiments of Refs. 7 and 8 indicated that the annealing rate immediately following high-dose rate irradiation was much faster than that measured in the post-irradiation experiments of Ref. 6.

The other set of experiments performed during the FY 1969 program was conducted to obtain information on the steady-state irradiation-induced absorption that would exist in fused silica at high ionizing dose rates and elevated temperatures. The high ionizing dose rates were obtained by 1.5 MeV electron irradiation

from a Dynamitron electron accelerator, which could provide ionizing dose rates as high as 10 Mrads/sec for times comparable to the 1000 sec running time of the full-scale engine. Since the generation of irradiation-induced optical absorption in fused silica is primarily due to ionizing radiation, these experiments could provide a full-scale simulation of the effects of nuclear radiation on the transparent wall.

During the Dynamitron experiments, conducted in the FY 1969 program, instrumental problems were encountered which limited the accuracy of the data obtained. These problems included the following: (1) inadequate control and measurement of electron beam current, (2) inadequate control of specimen temperature during irradiation, (3) inability to scan wavelength, and (4) large, anomalous loss of transmission during irradiation due to thermal effects not associated with irradiation-induced absorption. In addition, none of the previous experiments have included the effects of optical bleaching. Since the induced absorption is observed to bleach when exposed to ultraviolet light (Refs. 3 and 9), and since the light flux of the full-scale engine is so intense, the effects of optical bleaching in the full-scale engine could be significant.

The experimental program described in this report is a continuation of the Dynamitron experiments conducted in the FY 1969 program. The instrumental problems were eliminated in this program by a redesign of the optical system, furnace assembly, and current measurement system, and accurate measurements of the irradiation-induced optical absorption in fused silica at high dose rates and elevated temperatures were obtained. Additional experiments were also conducted to determine the effectiveness of optical bleaching and to determine the damage mechanism responsible for the irradiation-induced absorption in fused silica. The results of these and previous experiments were used to derive a mathematical model for the coloration process which was used to correlate the results of the various experiments and to predict the irradiation-induced absorption expected in the full-scale NLB engine.

In addition, preliminary investigations of the effects of electron and nuclear reactor irradiation on the optical transmission of aluminum oxide were conducted.

The motivation, design, procedure and results for each of the experiments and the details of the mathematical model are described in the following sections. A discussion of the level of irradiation-induced optical absorption expected in the full-scale engine is also given.

DESCRIPTION OF EQUIPMENT AND EXPERIMENTAL TECHNIQUE

The electron irradiations were conducted at the Space Radiation Effects Laboratory of the NASA Langley Research Center, Hampton, Virginia, using the Dynamitron electron accelerator as a source of 1.5 MeV electrons to provide the ionizing dose rates up to 10.0 Mrads/sec to simulate an operating full-scale engine. The system used to make the in situ measurements of optical transmission during the electron irradiation is similar to that described in Ref. 9. Appropriate modifications were incorporated to improve the accuracy of the transmission measurements and to provide a wider specimen temperature range independent of the electron irradiation conditions.

Dynamitron Electron Accelerator

The Dynamitron electron accelerator is a linear beam device that provides a continuous 1-cm-diameter electron beam through a water cooled, thin (0.001-in.) titanium window. In order to obtain an electron kinetic energy of 1.5 MeV at the output of the beam port, it is necessary to run at a beam energy of 1.6 MeV to correct for the 0.1 MeV energy loss due to the titanium window. Upon passing through the titanium window, the electron beam is also scattered resulting in a loss of collimation. In order to compensate for this effect, 1-cm-diameter apertures were used at the output beam port of the accelerator and at the input of the specimen furnace assembly to provide the necessary collimation. With this configuration, a maximum current density of 100 microamps/cm^2 in a well collimated 1-cm-diameter beam could be obtained at the location of the specimen, 1.5 in. from the beam port.

Specimen Configuration

The specimen configuration and its orientation with respect to the incident electron and optical beams are illustrated in Fig. 1. The specimens were in the form of thin wafers of square cross section (0.8 x 0.8 in.). The choice of specimen thickness was based on a number of requirements which include:

1. obtaining the correct uniform electron energy deposition that would result in the desired ionizing dose rate;

2. obtaining a sufficient optical path length through the specimen in order to allow accurate measurement of optical transmission;

3. minimizing the effects of thermally induced refractive gradients in the specimen on the optical beam; and,

4. minimizing the number of electrons stopping in the specimen which could result in induced birefringence or dielectric breakdown.

A suitable compromise among these various requirements was obtained by choosing a specimen thickness of 1.5 mm for the fused silica specimens and 1 mm for the aluminum oxide specimens. The thinner specimens are required in the case of aluminum oxide because the electron energy loss per unit length is higher than in fused silica.

In order to provide a large interaction region between the incident optical beam and the irradiated region, the specimens were mounted at an angle of 65 deg. with respect to the electron beam axis and at an angle of 25 deg. with respect to the optical beam axis as shown in Fig. 1. With this configuration, the optical beam passes through the irradiated region of the specimen only, and the optical transmission is averaged over the beam cross section as well as the specimen thickness. With the specimen oriented at this angle, the path length which the optical beam traverses is greater than the specimen thickness and can be calculated from the following equation:

$$\ell = \frac{nd}{\sqrt{n^2-\cos^2\phi_s}} \qquad (1)$$

where:

ℓ = path length (mm)

n = index of refraction

d = specimen thickness (mm)

ϕ_s = angle between specimen and optical beam (deg)

The calculated path lengths are 1.9 mm and 1.2 mm for the 1.5 mm fused silica and 1 mm aluminum oxide specimens, respectively. These values are approximately constant over the wavelength interval $2050<\lambda<2500$ Å.

The specimen transmission in the absence of optical absorption is less than 100% due to reflection losses at the surfaces of the specimen. The resulting optical transmission can be calculated from the following equation:

$$I_o = \frac{1}{2}\frac{\sin^2 2\phi_s \sin^2 2\phi_t[\sin^4(\phi_s+\phi_t)+1]}{\cos^4(\phi_t-\phi_s)\sin^4(\phi_s+\phi_t)} \qquad (2)$$

where:

$$\phi_t = \sin^{-1}\left(\frac{\cos\phi_s}{n}\right)$$

The calculated optical transmissions at 2150 Å are 78% and 73% for fused silica and aluminum oxide, respectively. These values are in close agreement with the values of optical transmission measured prior to irradiation on all specimens and is an indication of the purity and surface quality of the specimens used.

The relation between the ionizing dose rate, $\dot{D}$, and the electron current density, J, for an electron kinetic energy E can be calculated for this specimen configuration using the techniques described in Appendix B of Ref. (9). The results are:

$$\dot{D} = 0.125\ J \text{ for } 1.5 \text{ mm fused silica specimen} \quad (3)$$

$$\dot{D} = 0.14\ J \text{ for } 1 \text{ mm aluminum oxide specimen} \quad (4)$$

where:

$\dot{D}$ = ionizing dose rate (Mrads/sec)

J = electron current density (microamp/cm^2)

These results are, of course, approximate due to the extreme complexity of the processes involved. The major source of error is in the calculation of the divergence of the electron beam as it passes through the specimen. The resulting increase in the volume into which the energy is deposited cannot be exactly determined and contributes an uncertainty of approximately 25% in the estimation of the ionizing dose rate.

Optical and Electronic System

Figure 2 is a combined optical and electronic schematic that illustrates in functional form the important experimental equipment with their respective locations. The details of the specimen mounting and the furnace assembly will be described in the next section.

The light source used in these experiments was a Hanovia Model 771-B-32 hydrogen discharge lamp operated in a continuous flow configuration. The light beam is apertured at the lamp, collimated by an off-axis parabola (Perkin-Elmer 098-0041), and split by two plane mirrors into a specimen beam, S, and a reference beam, R, as shown in Fig. 2. The reference beam is included to provide a continuous check on variations in the source intensity and detector gain. Both light

beams are then chopped sequentially at a frequency of 13 Hz. The specimen beam is apertured a second time such that the light beam at the specimen has a circular cross-section of 0.3 cm diameter as shown in Fig. 1. Both the specimen and reference beams are collected and imaged by a second off-axis parabola on the monochromator (Perkin-Elmer Model 99) entrance slit. The light beams are monochromatized after passing through the specimen in order to prevent the broadband fluorescence generated by the specimen from saturating the photomultiplier (Ascop 543-1014) during the irradiations. The monochromator could be operated at a fixed wavelength or scanned over the wavelength range 2050 Å to 2500 Å. Extensive shielding of the photomultiplier tube and pre-amplifier was necessary in order to minimize the noise generated by X-rays incident on the photomultiplier and to eliminate the possibility of radiation damage to the pre-amplifier semiconductors. In order to further discriminate against this source of noise, as well as background light and specimen fluorescence, a phase-sensitive detection system, locked in phase with the sequential chopper, was used to extract the desired repetitive waveform. The phase-sensitive detection system and the remaining electronic equipment were located outside the irradiation area so that complete monitoring of all important functions was obtained during irradiation. The output of the phase-sensitive detection system consists of two d.c. signals, proportional to the intensity of the specimen beam and reference beam, respectively. The two signals are amplified and their ratio,(S/R), displayed on a chart recorder as shown in Fig. 2. This system has a response time of approximately 1 sec. which is limited primarily by the chart recorder response. The level of noise encountered during irradiation was such that measurement of optical transmission with an accuracy of $\pm 1\%$ was obtained. In the case of the fused silica specimens, the smallest value of induced absorption coefficient that could be detected was thus 0.05 cm^{-1}.

A remotely actuated Faraday cup was used in the present set of experiments to provide both rapid switching of the electron beam and accurate measurement of the electron beam current and stability prior to, during, or after a given specimen irradiation, as shown in Fig. 2. The Faraday cup was calibrated by comparing the measurements obtained with the cup at the location of the specimen with the measurements obtained with the cup at its location during the optical transmission experiments. The resulting conversion factor and the measured electron beam diameter at the location of the specimen can be used to calculate the current density from the microammeter reading. The current density is then used in Eqs. (3) or (4) to determine the ionizing dose rate.

Furnace Assembly and Specimen Mount

As described in Ref. 8, the furnace assembly used in the FY 1969 Dynamitron experiments was not capable of maintaining the specimens at temperatures in excess of 400 C in the absence of electron beam heating. Thus, high-temperature data could only be obtained at high ionizing dose rates and, as a result, only a few isolated data points were obtained. In addition, the accuracy of the limited data

so obtained was questionable in that it was not possible to determine if the loss of optical transmission observed during irradiation was due to actual specimen absorption or to effects of a thermal nature. For instance, the heating of the specimen by the electron beam could cause the specimen to warp or flex resulting in a displacement of the optical beam off of the monochromator slit. In order to determine if such effects could have influenced the data obtained during the FY 1969 experiments, an experiment was performed at UARL in which the optical transmission of a fused silica specimen was measured during irradiation by a CO_2 infrared laser beam. Such an experiment provides a reasonable simulation of the effects of electron beam heating on the optical transmission measurements without creating any irradiation-induced absorption in the specimen. The results of this simulation experiment indicated that a large decrease in optical transmission could result due to thermal effects if the specimen was rigidly clamped in its optical mount, as in the FY 1969 experiments. This was a preliminary indication that the decrease in optical transmission measured during the FY 1969 electron irradiation experiments could have been due to thermal effects and that the actual irradiation-induced absorption was much less than the measurements indicated. It was found that a redesigned optical mount, that included flexible gaskets between the specimen and its stainless steel holder, reduced the change in transmission due to thermal effects to a small predictable increase in transmission, probably due to focussing by the specimen. These results were confirmed in an electron irradiation experiment that was run for calibration purposes. The optical transmission of a fused silica specimen was measured during electron irradiation at various dose rates and specimen temperatures at a wavelength of 3000 Å at which the induced absorption is negligible. A large anomalous decrease in transmission was observed during irradiation when the specimen was clamped rigidly without the flexible gaskets. On turning off the electron beam, the transmission recovered immediately. When the specimen was mounted with the flexible gaskets, however, only a small increase in transmission was observed, as in the CO_2 laser simulation experiment. This small increase in transmission, due to thermal effects, was applied as a correction to the data taken at shorter wavelengths. The maximum correction was 0.1 cm^{-1} at a dose rate of 5 Mrads/sec and a specimen temperature of 900 C.

In addition to the modification of the specimen mounting configuration to eliminate thermal effects, the entire furnace assembly was redesigned and was capable of maintaining specimens at temperatures as high as 1100 C in the absence of electron beam heating for extended periods of time during the present set of experiments. Specimen temperature was measured with a Chromel-Alumel thermocouple in contact with the back surface of the specimen as shown in Fig. 2.

Optical Bleaching Light Source Calibration

Measurements of the relative spectral output of several available high-intensity light sources were made in the wavelength region from 2000-4000 Å. These included a General Electric 900 watt BH-6 mercury arc lamp, a Hanovia

hydrogen discharge lamp, a General Electric 500 watt xenon flashlamp, and a General Electric 1000 watt tungsten iodide lamp. The spectral measurements were made to locate the position of any intense spectral lines and to determine the spectral variation of the light intensity for the various light sources. The experimental arrangement that was used is shown in Fig. 3a. A single-beam monochromator system was used with the light source chopped mechanically as shown. The output of the photomultiplier was recorded on an oscilloscope and the voltage was recorded as a function of wavelength. No attempt was made to calibrate the monochromator-photomultiplier combination to give absolute measurements of light intensity. For this reason, the data in each scan has been normalized to the maximum value of intensity occurring in each scan. The results of these measurements are plotted in Figs. 4 through 7 as curves of normalized intensity vs wavelength in the wavelength band 2000-4000 Å for each light source measured. It is seen that none of the measured light sources have strong spectral lines in the wavelength region of interest 2050-2250 Å, but that the mercury arc and the hydrogen discharge lamp do exhibit output in this region.

Absolute intensity measurements were made of the light intensity in the spectral region 2050-2250 Å with the experimental system shown in Fig. 3b. The detector consisted of a radiometer with a narrowband ultraviolet filter as an aperture. The ultraviolet filter had a transmission of approximately 10 percent in the spectral region 2050-2250 Å and essentially zero transmission at other wavelengths. The output of the radiometer was recorded on a digital voltmeter as shown in Fig. 3b. Using this system, it was possible to measure intensities as low as 100 microwatts/cm^2. The only light source with sufficient light intensity for detection in the spectral region of interest was the BH-6 mercury arc lamp. The light intensity was recorded as a function of the distance between source and detector, and the results are presented in Fig. 8, which includes a correction to account for the filter attenuation. Similar measurements of total intensity, made without the ultraviolet filter, are presented in Fig. 9. It can be seen that the radiated power in the spectral region between 2050-2250 Å is approximately 0.2 percent of the total radiated power, which agrees with the manufacturer's specifications. The intensity in the spectral range of interest was measured to be 2.1 milliwatts/cm^2 at a distance of 4 cm from the arc. The light intensity is approximately inversely proportional to distance from the arc for distances less than 6 cm and changes to an inverse square variation at about 10 cm, as shown in Figs. 8 and 9. The intensity at the surface of the arc can be calculated by extrapolating the curve in Fig. 8 to the radius of the arc (0.2 cm). This yields a maximum obtainable intensity in the spectral range 2050-2250 Å of 40 milliwatts/cm^2. This can be approached using an elliptical cavity in which the arc is placed at one focus and imaged at the other focus.

An unfocussed BH-6 mercury arc lamp was used as the bleaching light source in the present set of experiments, and the light intensity at a given specimen-lamp separation was obtained from Fig. 8.

EXPERIMENTAL RESULTS

The experimental results are expressed as induced absorption coefficients which are calculated from the chart recorder data using the following equation:

$$\alpha(\lambda) = \frac{1}{\ell} \ln \left[\frac{I(\lambda,T,\dot{D},t)}{I_o(\lambda)} \right] \qquad (5)$$

where:

$\alpha(\lambda)$= irradiation-induced absorption coefficient at the wavelength $\lambda(cm^{-1})$

ℓ = optical path length through specimen (cm)

$I_o(\lambda)$ = chart recorder amplitude prior to irradiation

$I(\lambda,T,\dot{D},t)$ = chart recorder amplitude at a time t after turn-on of electron beam.

Fused Silica Specimen Irradiations

A total of 25 Corning 7940 fused silica specimens were investigated in this portion of the experimental program. The irradiation history of each of these specimens is presented in Table I. Three of these specimens (SC-N-1, SC-N-2, and SC-N-3) had received a prior irradiation to a dose of $10^{17}/cm^2$ fast neutrons at the Union Carbide Research Center Nuclear Reactor. A total of fifty electron irradiations were conducted during which the optical transmission was measured at wavelengths in the interval 2050-2500 Å, but primarily at 2150 Å.

This experimental program can be divided into several distinct areas of investigation: the measurement of the steady-state irradiation-induced optical absorption during elevated-temperature electron irradiation; and independent measurements of the growth and removal of irradiation-induced optical absorption which include radiation annealing, defect generation and removal, optical bleaching and absorption spectra.

Steady-State Absorption

Measurements of the steady-state irradiation-induced optical absorption were obtained during electron irradiation runs 1 through 28, 31 and 42 with specimens SC-1 through SC-12, SC-14 and SC-20 as indicated in Table I. The resulting steady-state values of irradiation-induced absorption coefficient at 2150 Å along with the

corresponding ionizing dose rates and specimen temperatures are summarized in Table II. Data was obtained over a broad range of ionizing dose rates (0.08-5 Mrads/sec) and specimen temperatures (100-900 C). The variation of the ionizing dose rate, specimen temperature, and irradiation-induced absorption coefficient during several of these irradiations are illustrated in Figs. 10 through 19. In all cases the induced absorption coefficient was observed to reach a steady-state value during the irradiation. In certain of the irradiations, as shown in Figs. 10, 11, 13 and 14, the induced absorption coefficient was observed to rise to a maximum value before returning to a lower steady-state value at a given ionizing dose rate. This overshoot phenomena probably occurs because the specimen does not achieve thermal equilibrium immediately. Increasing the specimen temperature during a given irradiation causes the induced absorption coefficient to decrease to a lower steady-state value, as shown in Figs. 12, 15, 17, 18, and 19. This phenomena is expected since the annealing rate increases with increasing specimen temperature. It was also found that the steady-state induced absorption coefficient measured during a given irradiation was reversible. That is, the steady-state induced absorption coefficient is determined by the steady-state ionizing dose rate and specimen temperature and not by the previous irradiation history of the specimen. This is illustrated in Fig. 11, which presents the results of two consecutive irradiations of specimen SC-2 at an ionizing dose rate of 1.25 Mrads/sec. The same value of steady-state induced absorption coefficient is observed in each irradiation, although the initial values are significantly different.

Data showing the steady-state irradiation-induced absorption coefficient at temperatures of 100, 200, 300, 400 and 500 C from Table II are plotted against ionizing dose rate in Fig. 20. Also included in Fig. 20 are representative steady-state data from the reactor-irradiation experiments described in Ref. 9. A smooth curve can be drawn through the data points at each temperature and the extrapolation from the electron-irradiation data to the reactor-irradiation data appears reasonable.

The important characteristics exhibited by the steady-state data can be summarized as follows:

1. The induced absorption coefficient at a given ionizing dose rate decreases with increasing specimen temperature.

2. A reasonable extrapolation can be made from the steady-state reactor-irradiation data to the electron-irradiation data.

3. The induced absorption coefficient at a given temperature first rises with increasing ionizing dose rate, reaches a maximum value, and then begins to decrease with increasing dose rate. This maximum value of the induced absorption coefficient occurs at an ionizing dose rate of approximately 0.4 Mrad/sec.

Radiation Annealing

All but one of the important features of the steady-state data mentioned above are consistent with the results of previous experiments. First, the induced absorption at a given dose rate is expected to decrease with increasing specimen temperature due to the corresponding increase in the thermal annealing rate. Second, the results of the nuclear reactor irradiations should be consistent with the results of the electron irradiations when plotted against the corresponding ionizing dose rates, since it is believed that ionization effects, rather than displacement effects, are primarily responsible for the coloration of fused silica. However, the behavior of the induced absorption coefficient at high dose rates, referred to in item 3 above, represents a new phenomenon in that the steady-state induced absorption coefficient has not been observed to decrease with increasing dose rate in any of the previous experiments. This behavior can be explained if it is assumed that the annealing process is enhanced during irradiation and that the annealing rate at a given temperature increases with increasing ionizing dose rate. This behavior is referred to as radiation annealing.

Direct evidence of the existence of a radiation annealing effect is illustrated in Fig. 21. Specimen SC-18, which had previously been irradiated at ambient temperature to an induced absorption coefficient of 1.6 cm^{-1} during run 37, was re-irradiated at a dose rate of 10 Mrads/sec during run 38. The induced absorption coefficient decreases to 1/e of its initial value in a time of 26 sec and is completely removed before the specimen temperature exceeds 200 C. The thermal annealing time constants reported in Ref. 5 were 3×10^4 sec at 200 C and 500 sec at 300 C so that thermal annealing alone cannot be used to explain this behavior. In order for thermal annealing to result in a removal time constant of 26 sec, the specimen temperature would have to be greater than 900 C which is well outside the error in temperature measurement of ±10%.

Defect Generation and Removal

The growth of the irradiation-induced absorption coefficient at 2150 Å during an ambient-temperature electron irradiation of specimen SC-17 is illustrated in Fig. 23. Except for a small initial portion, the curve is linear with a slope of 0.042 cm^{-1}/Mrad up to a total dose of 140 Mrads. The induced absorption coefficient does not saturate indicating that the coloration process may be due to the generation of defects by the ionizing radiation rather than to defects initially present in the specimen. The slopes of the linear portions of the remaining ambient-temperature electron irradiation growth curves are summarized in Table III. The values range from 0.073 cm^{-1}/Mrad to 0.039 cm^{-1}/Mrad with an average value of 0.05 cm^{-1}/Mrad. This is in excellent agreement with the value of 0.045 cm^{-1}/Mrad obtained as a result of the Co-60 gamma irradiations described in Ref. 6.

The degree to which thermal annealing and radiation annealing remove the defects generated by the ionizing radiation was obtained by comparing the shapes of the ambient-temperature growth curves measured prior to and immediately following the appropriate annealing treatment. Representative results of these experiments

are presented in Figs. 23 through 29. Figure 23 illustrates the results of an ambient-temperature electron irradiation, followed by a 300 C heat treatment, with a subsequent re-irradiation at ambient temperature. The value of induced absorption coefficient at the end of the initial irradiation, $\alpha_1 = 1.6$ cm^{-1}, decreases to a value, $\alpha_2 = 0.4$ cm^{-1} as a result of thermal annealing. However, complete removal of the defects responsible for the coloration is not obtained at this temperature. The fraction of the defects completely removed can be calculated in the following manner. Curve B is translated along the abscissa until it intersects curve A. Curve A is then subtracted from curve B to obtain the difference curve C, as shown in Fig. 23. Curve C saturates at an induced absorption coefficient, $\Delta\alpha = 0.24$ cm^{-1}, which is proportional to the number of defects remaining after the annealing treatment. The fraction of the defects removed, ξ, is then calculated from the following equation:

$$\xi = \frac{\alpha_1 - \alpha_2 - \Delta\alpha}{\alpha_1 - \alpha_2} \qquad (6)$$

Using the values appropriate to Fig. 23, the fraction of defects removed by the 300 C thermal anneal is calculated to be 79%. Thus, even at 300 C the removal of defects by thermal annealing is nearly complete. The results of this experiment substantiate the hypothesis of defect generation by ionizing radiation since the difference curve should have been zero with a fixed concentration of defects. The results of a similar experiment in which the thermal annealing was conducted at 900 C is illustrated in Fig. 24. The growth curves before and after the heat treatment are identical, indicating complete removal of defects at this temperature. The same procedure was used to obtain the results illustrated in Fig. 25, except that the irradiation-induced absorption was removed by a radiation annealing treatment at an ionizing dose rate of 5 Mrads/sec and a maximum specimen temperature of 200 C as shown in Fig. 26. The fraction of defects removed, calculated from Eq. (6), is 66%, as a result of this radiation annealing treatment.

Experiments involving thermal annealing and radiation annealing of reactor-irradiation-induced absorption, followed by ambient-temperature electron irradiation were also conducted. However, the growth of induced absorption during the initial reactor irradiation was not measured so that a detailed comparison of the consecutive growth curves was not possible. Specimen SC-N-3 was reactor irradiated to a dose of 10^{17}/cm^2 fast neutrons, resulting in an induced absorption coefficient of 7.3 cm^{-1} at 2150 Å. This absorption was completely removed by a 900 C heat treatment, after which the specimen was electron irradiated at ambient temperature and a dose rate of 0.02 Mrad/sec. The growth of the induced absorption coefficient during this re-irradiation is illustrated in Fig. 27. This curve is very similar to those obtained with previously unirradiated specimens and indicates that thermal annealing at 900 C results in complete removal of the defects generated by reactor irradiation. Specimen SC-N-1 was also reactor irradiated to a dose of 10^{17}/cm^2 fast neutrons, resulting in an induced absorption coefficient of 7.6 cm^{-1} at 2150 Å. The reactor-

induced absorption was then completely removed by radiation annealing at an ionizing dose rate of 5 Mrads/sec and a maximum specimen temperature of 250 C as shown in Fig. 28, illustrating that radiation annealing is effective in removing reactor irradiation-induced absorption as well as that due to electron irradiation. The growth of the induced absorption coefficient during the subsequent ambient-temperature electron irradiation of specimen SC-N-1 is illustrated in Fig. 29. The shape of the resulting growth curve is also similar to that obtained with unirradiated specimens, an indication that the radiation annealing has resulted in complete removal of the defects generated by the reactor irradiation.

Optical Bleaching

Experiments to determine the effects of optical bleaching on the irradiation-induced absorption were conducted using specimens SC-16, SC-21, SC-22, and specimen SC-N-2 which had been reactor irradiated to a dose of $10^{17}/cm^2$ fast neutrons. The results of several of these experiments are illustrated in Figs. 30, 31, and 32. As shown in Fig. 30, Specimen SC-21 was first given an ambient-temperature electron irradiation which resulted in an induced absorption coefficient of 1.42 cm^{-1} at 2150 Å. The specimen was then irradiated with ultraviolet light from the BH-6 mercury arc lamp for a period of 45 minutes. The specimen and arc were separated a distance of 4 cm, at which the intensity in the wavelength interval 2050-2250 Å was 2 mw/cm^2 based on the data presented in Fig. 8. The induced absorption coefficient decreased to a value of 0.96 cm^{-1} as a result of this optical bleaching treatment. Subsequent re-irradiation at ambient temperature indicates a drastic change in the shape of the growth curve as a result of optical bleaching as illustrated in Fig. 30. The induced absorption coefficient first increases rapidly to the value measured prior to the optical bleach and then increases at a slower rate that is approximately equal to the slope of the previous growth curve. Specimen SC-22 was given a similar treatment as shown in Fig. 31. However, the light intensity in this experiment was 1 mw/cm^2 and the duration of the optical bleach was increased proportionately to 90 minutes. Figure 32 illustrates the results of an experiment in which the specimen SC-N-2, which had been reactor irradiated to an induced absorption coefficient of 7.9 cm^{-1} at 2150 Å, was given an optical bleaching treatment at 2 mw/cm^2 for 45 minutes and then re-irradiated at ambient temperature. The induced absorption coefficient decreased from 7.9 cm^{-1} to 4.95 cm^{-1} as a result of the optical bleaching treatment.

The growth of the induced absorption coefficient during the subsequent re-irradiations exhibits the same behavior in each case as shown in Figs. 30, 31 and 32. The growth is characterized by an initial rapid rise to a value of induced absorption coefficient measured prior to optical bleaching, followed by a slower increase similar to that observed in previously unirradiated specimens.

Absorption Band Structure

Spectral scans of the induced absorption coefficient in the wavelength

interval 2050-2500 Å were also made on several specimens. Figure 33 illustrates the absorption spectra of specimens SC-N-1, and SC-N-3 which were measured after a reactor irradiation to a dose of $10^{17}/cm^2$ fast neutrons. Figure 34 illustrates the absorption spectra of specimen SC-10 which were measured during electron irradiation at an ionizing dose rate of 0.42 Mrad/sec and specimen temperatures of 100, 300, and 400 C. An additional spectral scan of specimen SC-14 made during run 41 at an ionizing dose rate of 5 Mrads/sec and a specimen temperature of 900 C did not reveal any induced absorption in the wavelength interval 2050-2500 Å. The curves of Figs. 33 and 34 and a representative post-irradiation spectrum from Ref. 6 were normalized to their respective peak values and the resulting curves are presented in Fig. 35. All the curves are centered at a wavelength of approximately 2150 Å, and the shapes of the curves do not differ appreciably although the specimen irradiation histories were quite different.

Aluminum Oxide Specimen Irradiations

A total of four single crystal ultraviolet grade aluminum oxide specimens were investigated in this portion of the experimental program. The material for these specimens was supplied by Linde and optically polished by Insico, Inc. The irradiation history of each of these specimens is presented in Table IV. Two of these specimens (AL-N-1 and AL-N-2) had received a prior irradiation to a dose of $10^{17}/cm^2$ fast neutrons at the Union Carbide Research Center Nuclear Reactor. Electron irradiations of previously unirradiated specimens AL-1 and AL-2 did not result in any change in optical transmission in the wavelength interval 2050-2500 Å. During the high-dose-rate irradiation of specimen AL-2, the specimen fractured, probably as a result of thermal shock or dielectric breakdown.

Although the electron irradiated specimens did not exhibit any measurable irradiation-induced absorption, a strong irradiation-induced absorption band with a peak occurring at approximately 2050 Å was observed in the reactor irradiated specimens, as illustrated in Fig. 36. Reactor irradiated specimen AL-N-2 was then given a heat treatment to investigate the thermal annealing rate as shown in Fig. 37. Thermal annealing begins at a specimen temperature of 500 C and resulted in complete removal of the reactor irradiation-induced absorption at a specimen temperature of 940 C.

Reactor irradiated specimen AL-N-1 was re-irradiated with 1.5 MeV electrons at a current density of 25 microamp/cm^2, corresponding to an ionizing dose rate of 3.5 Mrads/sec, as shown in Fig. 38. Although the specimen temperature did not exceed 150 C during this irradiation, the induced absorption coefficient was observed to decrease from 9.4 cm^{-1} to 4.6 cm^{-1} in a time of 120 sec. Since specimen AL-N-2 was not observed to anneal in the absence of irradiation until a specimen temperature of 500 C had been reached, this data can be interpreted as evidence for radiation annealing in aluminum oxide. However, as in the previous high-dose-rate irradiation of specimen AL-1, specimen AL-N-2 fractured at an elapsed time of 120 sec.

DISCUSSION OF RESULTS

The nuclear radiation incident on the transparent wall of the full-scale NLB engine during normal operation will consist primarily of fission neutrons and gamma rays. However, the results of this and previous experimental programs concerned with the irradiation-induced optical absorption band centered at 2150 Å in fused silica indicate that the generation of this absorption band is due to ionizing radiation and that the effects of fission neutrons can be neglected. In fact, it appears from the data obtained to date that the effects of fission neutrons and gamma rays can be simulated with 1.5 MeV electron irradiation at the same ionizing dose rate. The radiation annealing effects observed during the electron irradiation experiments are also expected to occur during gamma irradiation since the resulting ionization effects are the same at a given ionizing dose rate. Thus, the results of the steady-state electron irradiation experiments at the ionizing dose rate of the full-scale engine can be used to directly determine the level of induced absorption due to nuclear radiation that would be expected in the transparent wall at the appropriate wall temperature. In addition, it has been demonstrated in the present experimental program that exposure to ultraviolet light results in bleaching of the irradiation-induced optical absorption and that the rate of bleaching increases linearly with light intensity at the light levels used. Since the transparent wall will also be exposed to intense ultraviolet light during normal operation, the level of irradiation-induced optical absorption is expected to be lower than that measured in the electron irradiation experiments due to the effects of optical bleaching. As the optical bleaching rate was measured at light intensities that were several orders of magnitude lower than that of the full-scale engine, an extrapolation procedure is necessary if a reasonable estimate of these effects is to be made.

Verification that the generation of irradiation-induced absorption in fused silica is due to ionizing radiation alone will be demonstrated by comparing the results of this and previous experiments with the predictions of the mathematical equations presented in Appendix A in which the effects of fission neutrons are neglected. The results of the steady-state electron irradiation experiments will then be used to directly determine the level of irradiation-induced absorption expected in the transparent wall of the full-scale engine, neglecting the effects of optical bleaching. The effects of optical bleaching are included in the mathematical equations and an estimate of the level of irradiation-induced absorption including optical bleaching will be made by linear extrapolation from the bleaching rates measured at low light intensities.

The linear increase of the induced absorption coefficient with ionizing dose at ambient temperature, as predicted by Eq. (A-4) of Appendix A is in agreement with the results of the ambient-temperature electron irradiations conducted in the present program and the ambient-temperature ^{Co}-60 gamma irradiations described in Ref. 6. In fact, the average value of the slopes of the electron irradiation growth curves, presented in Table III, was 0.05 cm^{-1}/Mrad, in close agreement with the

value of 0.045 cm^{-1}/Mrad measured in the Co-60 irradiation experiments of Ref. 6. This indicates that the effects of gamma irradiation are adequately simulated by 1.5 MeV electron irradiation. The mathematical equations were based on a model for the coloration process in which positively charged defects and free electrons are generated by ionizing radiation. When a free electron is trapped at a positively charged defect, a color center is formed which gives rise to the observed irradiation-induced absorption band. As predicted by Eq. (A-4), the induced absorption coefficient is not expected to saturate at ambient temperature since defects are continuously being generated. Experimental evidence for this is illustrated in Fig. 22 in which the ambient temperature growth curve did not show signs of saturation up to an ionizing dose of 140 Mrads. The assumed model for the coloration process is also in agreement with the results of the optical bleaching experiments. Optical bleaching results in liberation of the trapped electron only, thus removing the optical absorption while leaving the defects intact. A subsequent re-irradiation should then exhibit a rapid initial growth due to trapping of free electrons at the existing defects, followed by a slower growth due to the generation of new defects. Experimental evidence for this behavior is illustrated in Figs. 30, 31, and 32 in which growth curves before and after optical bleaching of specimens SC-21, SC-22, and SC-N-2 are presented. These curves can be used with Eq. (A-8) to calculate the electron trapping constant, b, which gives the rate of trapping of free electrons at defects when multiplied by the appropriate ionizing dose rate. A sample graphical calculation is illustrated in Fig. 32 and the results of the calculations for specimens SC-21, SC-22, and SC-N-2 are summarized in Table V. The calculated values are approximately equal in each case, consistent with the equations, and the average value is b = 2 $Mrad^{-1}$.

The calculated value of the electron trapping constant and the measured value of the slope of the ambient-temperature growth curve can be used in Eq. (A-5) to predict the value of the induced absorption coefficient resulting from an ambient-temperature pulsed reactor irradiation such as the TRIGA experiments described in Refs. 7 and 8. The calculated value is given by:

$$\alpha_{calc} = \frac{\partial \alpha}{\partial D} \left[D_p - \frac{1}{b} \left(1 - e^{-bD_p} \right) \right] \qquad (7)$$

where:

$\frac{\partial \alpha}{\partial D}$ = 0.05 cm^{-1}/Mrad from Table III

b = 2 $Mrads^{-1}$ from Table V

D_p = 2 Mrads - Ionizing dose of reactor pulse from Refs. 6 and 7.

Substitution gives $\alpha_{calc} = 0.075$ cm^{-1} which is in excellent agreement with the experimental value of 0.073 cm^{-1} reported in Ref. 7.

Further evidence for the case of ionizing radiation can be obtained by comparing the results of the steady-state reactor-irradiation experiments described in Ref. 9 with the corresponding results predicted by the mathematical model. In this case, the solution for the steady-state irradiation-induced absorption coefficient at elevated temperatures is given as Eq. (A-10). The post-irradiation thermal annealing time constants of Ref. 6 are used in this equation since the effects of radiation annealing are negligible at the ionizing dose rate of 0.02 Mrad/sec that was present during these experiments. The values of the steady-state induced absorption coefficients calculated from Eq. (A-10) are compared with the experimentally determined values from Ref. 9 at temperatures of 700, 800, and 900 C in Table VI. The experimental values are slightly higher than the calculated values, but this difference can be accounted for by the observed spread in the measured values of the slopes of the ambient temperature growth curves presented in Table III.

The above results indicate that the dominant defect generation mechanism is due to ionization processes such as the rupturing of molecular bonds rather than the displacements of atoms from lattice sites since the effects of fission neutrons were excluded from the calculations in both cases. Fission neutrons are more effective in displacing atoms than either electrons or gamma rays. In fact, for a displacement threshold of 25 ev, the rate of generation of displacement type defects by nuclear reactor, 1.5 MeV, and Co-60 gamma irradiations should be in the approximate ratio 1000:10:1 respectively (see Refs. 10 and 11) at a given ionizing dose rate. Since the same generation rate is observed in each of the above types of irradiation, there is strong evidence that the dominant defect generation mechanism is due to ionization processes such as the rupturing of molecular bonds. A model for the structure of the color center, consisting of an electron trapped at a ruptured Si-O bond has been proposed in Ref. 12 and the calculated energy levels are in reasonable agreement with the observed location of the peak of the absorption band at 2150 Å.

It appears, therefore, that the assumption that the irradiation-induced optical absorption in fused silica is due primarily to the effects of ionizing radiation, is well founded. The results of the steady-state electron irradiation experiments summarized in Table II and illustrated in Fig. 20 can, thus, be used to directly determine the level of irradiation-induced optical absorption expected in a full-scale engine in the absence of optical bleaching. The ionizing dose rate for the transparent wall of the full-scale engine is given in Ref. 13 as approximately 5 Mrads/sec. At this ionizing dose rate and a wall temperature of 300 C the curves of Fig. 20 indicate a steady-state induced absorption coefficient at 2150 Å of only 0.1 cm^{-1}. This small value of induced absorption is due to the effects of radiation annealing which results in very rapid annealing at high ionizing dose rates. The rate of annealing at 5 Mrads/sec and 300 C can be calculated by

substituting the measured value of $\alpha_s = 0.1$ cm^{-1} and the appropriate values of b, $\partial\alpha/\partial D$, and $\dot{D}$ into Eq. (A-11) and solving for the annealing rate, ν_A. The result is:

$$\nu_A(\dot{D} = 5 \text{ Mrads/sec}, T = 300 \text{ C}) = 2 \text{ sec}^{-1}$$

This is a factor of 1000 times greater than the thermal annealing rate measured at 300 C in the post-irradiation experiments of Ref. 6.

The results of the low-light-intensity optical bleaching experiments conducted during the present experimental program can be used in conjunction with the mathematical model to obtain an estimate, that includes the effects of optical bleaching, of the level of irradiation-induced absorption expected in the full-scale NLB engine. The effects of optical bleaching are included in the mathematical model by a bleaching rate that is linearly proportional to the light intensity within the absorption band. The constant of proportionality, c, referred to as the optical bleaching constant, can be determined from the results of the optical bleaching experiments using Eq. (A-7). A sample calculation is presented in Fig. 32, and the results of the calculations for specimens SC-16, SC-21, SC-22, and SC-N-2 are summarized in Table V. Although the optical bleaching experiments were conducted at different light intensities, durations of exposure, and initial absorption coefficients, the calculated values of the optical bleaching constant are approximately equal with an average value of 0.08 watts^{-1}-cm^2-sec^{-1}. This indicates that at the light levels used the optical bleaching rate was linearly proportional to light intensity. According to the calculations presented in Ref. 14, the light intensity of the full scale NLB engine in the wavelength interval 2050-2250 Å is approximately $I_W = 1000$ watts/cm^2. If it is assumed that the optical bleaching rate varies linearly with light intensity at this level also, then Eq. (A-12) can be used to predict the steady-state irradiation-induced absorption coefficient for the full-scale engine due to the combined effects of generation, annealing and optical bleaching of color centers. The appropriate equation is:

$$\alpha_s(\dot{D}_W, T_W, I_W) = \left(\frac{\partial\alpha}{\partial D}\right) \frac{b\dot{D}_W}{b\dot{D}_W + \nu_A(\dot{D}_W, T_W) + cI_W} \quad \frac{\dot{D}_W}{\nu_A(\dot{D}_W, T_W)}$$

$\left(\frac{\partial\alpha}{\partial D}\right)$ = 0.05 cm^{-1}/Mrad - from data in Table III

b = 2 Mrads^{-1} - from data in Table V

c = 0.08 watts^{-1}-cm^2-sec^{-1} - from data in Table V

$\dot{D}_W$ = 5 Mrads/sec - from Ref. 13

$$T_W = 300 \text{ C}$$

$$\nu_A(\dot{D}_W, T_W) = 2 \text{ sec}^{-1} \text{ - calculated from Eq. (A-11)}$$

$$I_W = 1000 \text{ watts/cm}^2 \text{ - from Ref. 14}$$

The resulting calculated value of induced absorption coefficient at 300 C is 0.01 cm^{-1}, which is a factor of ten lower than the value of 0.1 cm^{-1} measured directly at the same ionizing dose rate and specimen temperature in the absence of optical bleaching. Thus, even at the moderate wall temperature of 300 C, the irradiation-induced absorption coefficient at 2150 Å is estimated to be between 0.01 and 0.1 cm^{-1} during full-power operation. At higher temperatures, the induced absorption is expected to be less due to the corresponding increase in the annealing rate.

The resulting heat deposition in the transparent wall due to this absorption is given by Eq. (A-13).

$$\dot{Q}_W = \alpha_s(\dot{D}_W, T_W, I_W) I_W \text{ watts/cm}^3 \qquad (9)$$

At a wall temperature of 300 C and the light intensity of 1000 watts/cm^2 from Ref. 14, the resulting heat deposition is between 10 and 100 watts/cm^3. The total heat deposition in the transparent wall is approximately 4500 watts/cm^3 based on calculations presented in Ref. 15 so that the additional heat load due to irradiation-induced optical absorption appears negligible even at 300 C and neglecting optical bleaching. The fraction of the total radiant light intensity which is absorbed in the transparent wall due to irradiation-induced absorption in the band centered at 2150 Å, for a wall thickness of 0.005 in., is between 0.02% and 0.002% at 300 C and is also negligible.

REFERENCES

1. Compton, W. D. and G. W. Arnold, Jr.: Radiation Effects in Fused Silica and α-Al_2O_3. Disc Faraday Soc. 31, 130 (1961).

2. Nelson, C. M. and J. H. Crawford, Jr.: Optical Absorption in Irradiated Quartz and Fused Silica. J. Phys. Chem. Sol. 13, 296 (1960).

3. Nelson, C. M. and R. A. Weeks: Trapped Electrons in Irradiated Quartz and Silica. Journal of the American Ceramic Society 43, 396 (1960).

4. Nelson, C. M. and R. A. Weeks: Vacuum-Ultraviolet Absorption Studies of Irradiated Silica and Quartz. Journal of Applied Physics 32, 883 (1961).

5. Levy, P. W.: Reactor and Gamma-Ray Induced Coloring of Corning Fused Silica. J. Phys. Chem. Sol. 13, 287 (1960).

6. Gagosz, R. M., F. C. Douglas and M. A. DeCrescente: Optical Absorption in Transparent Materials Following High-Temperature Reactor Irradiation. United Aircraft Research Laboratories Report F-910485-2, September 1967. Also issued as NASA CR-1032.

7. Gagosz, R. M., J. P. Waters, F. C. Douglas and M. A. DeCrescente: Optical Absorption in Fused Silica during Triga Reactor Pulse Irradiations. United Aircraft Research Laboratories Report F-910485-1, September 1967. Also issued as NASA CR-1031.

8. Gagosz, R. M. and J. P. Waters: Optical Absorption and Fluorescence in Fused Silica during Triga Pulse Irradiations. United Aircraft Research Laboratories Report G-910485-3, April 1968. Also issued as NASA CR-1191.

9. Palma, G. E. and R. M. Gagosz: Optical Absorption in Fused Silica during Irradiation at High-Temperature. United Aircraft Research Laboratories Report H-930709-1, October 1969.

10. Corbett, J. W.: Electron Radiation Damage in Semiconductors and Metals. Academic Press, New York and London (1966).

11. Billington, D. S. and J. H. Crawford, Jr.: Radiation Damage in Solids. Princeton University Press, Princeton, New Jersey (1961).

12. Ruffa, A. R.: Model for the E_1' Center in SiO_2. Physical Review Letters 25, 650 (1970).

13. Latham, T. S.: Nuclear Studies of the Nuclear Light Bulb Rocket Engine. United Aircraft Research Laboratories Report G-910375-3, September 1968. Also issued as NASA CR-1315.

14. Krascella, N. L.: Analytical Studies of the Spectral Radiant Flux Emitted from the Fuel Region of the Nuclear Light Bulb Engine. United Aircraft Research Laboratories Report J-910904-1, October 1970.

15. Latham, T. S., H. E. Bauer and R. J. Rodgers: Studies of Nuclear Light Bulb Start-up Conditions and Engine Dynamics. United Aircraft Research Laboratories Report H-910375-4, September 1969.

LIST OF SYMBOLS

a	Defect generation constant, cm^{-3}-$Mrad^{-1}$
b	Electron trapping constant, $Mrad^{-1}$
c	Optical bleaching constant, $watt^{-1}$-cm^{2}-sec^{-1}
D	Ionizing dose, Mrad
D_p	Ionizing dose of reactor pulse, Mrad
$\dot{D}$	Ionizing dose rate, Mrad/sec
$\dot{D}_W$	Ionizing dose rate deposited in transparent wall, Mrad/sec
d	Specimen thickness, mm
E	Electron kinetic energy, MeV
I	Light intensity, $watts/cm^2$
$I(\lambda,T,\dot{D},t)$	Chart recorder amplitude during irradiation, dimensionless
$I_o(\lambda)$	Chart recorder amplitude prior to irradiation, dimensionless
I_W	Light intensity incident on transparent wall, $watt/cm^2$
J	Current density, $microampere/cm^2$
ℓ	Optical path length, mm
N_c	Concentration of color centers, cm^{-3}
N_d	Concentration of defects, cm^{-3}
n	Index of refraction, dimensionless
$\dot{Q}_W$	Heat deposition in transparent wall, $watts/cm^3$
R_e	Radius of electron beam, cm
R_o	Radius of optical beam, cm
T	Specimen temperature, Deg C

T_W	Transparent wall temperature, Deg C
t	Elapsed time during irradiation, sec
α_{calc}	Calculated induced absorption coefficient, cm^{-1}
α_p	Absorption coefficient at peak of induced absorption band, cm^{-1}
α_s	Steady-state induced absorption coefficient, cm^{-1}
$\alpha(\lambda)$	Induced absorption coefficient at a wavelength, λ, cm^{-1}
Δt	Duration of optical bleaching treatment, sec.
λ	Wavelength, $\mathring{A}$
ξ	Fraction of defects removed by annealing, dimensionless
$\sigma_{ph}(\lambda)$	Optical absorption cross section at a wavelength, λ, cm^2
$\tau_A(T)$	Thermal annealing time constant, sec.
$\nu_A(\dot{D},T)$	Annealing rate, sec^{-1}
ϕ_s	Angle between specimen and incident light beam, deg
ϕ_t	Angle between specimen and refracted light beam, deg

APPENDIX A

KINETIC EQUATIONS FOR COLOR CENTER GENERATION IN FUSED SILICA

The kinetic equations that were presented in Ref. 9 have been modified to incorporate the information obtained in the present experimental program. It has been determined that the coloration process responsible for the irradiation-induced absorption band centered at 2150 A occurs in two steps. First, defects are generated by ionizing radiation, probably as a result of rupturing of molecular bonds. Free electrons, which are also generated by the ionizing radiation, are then trapped by these defects resulting in the formation of color centers. Annihilation of the color centers results from both bleaching and annealing processes. A bleaching process results in liberation of the trapped electron only, while an annealing process results in complete annihilation of the center. Thermal decoloration results in almost complete removal of the centers at moderate temperatures ($\sim$300 C) and complete removal at high temperatures ($\sim$900 C) so that the interpretation of thermal decoloration as an annealing process seems justified. In addition, it was found that the rate of thermal annealing during irradiation was more rapid than in the absence of irradiation. This is interpreted as a radiation annealing effect which has been accounted for in the kinetic equations by making the annealing rate an increasing function of both temperature and ionizing dose rate. Optical decoloration by irradiation with ultraviolet light results in liberation of trapped electrons but does not remove defects and is thus a bleaching effect.

The effects of optical bleaching and radiation annealing are included in the following kinetic equations which describe the generation of defects and the subsequent trapping of electrons at these defects to form color centers, respectively.

$$\frac{dNd}{dt} = a\dot{D} - \nu_A(\dot{D},T)\ N_d \qquad \text{(A-1)}$$

$$\frac{dN_c}{dt} = b\dot{D}(N_d-N_c)-\nu_A(\dot{D},T)N_c-cIN_c \qquad \text{(A-2)}$$

where:

$\dot{D}$ = ionizing dose rate (Mrad/sec)

I = light intensity in absorption band (watt/cm^2)

T = specimen temperature (Deg C)

N_d = concentration of defects (cm^{-3})

N_c = concentration of color centers (cm^{-3})

a = defect generation constant (cm^{-3}-$Mrad^{-1}$)

b = electron trapping constant ($Mrad^{-1}$)

c = optical bleaching constant ($watts^{-1}$-cm^2-sec^{-1})

$\nu_A(\dot{D},T)$ = annealing rate (sec^{-1})

The resulting irradiation-induced absorption coefficient is directly proportional to the concentration of color centers and is given by:

$$\alpha(\lambda) = \sigma_{ph}(\lambda)N_c \qquad \text{(A-3)}$$

where:

$\alpha(\lambda)$ = induced absorption coefficient at the wavelength, λ, (cm^{-1})

$\sigma_{ph}(\lambda)$ = optical absorption cross section at the wavelength, λ, (cm^2)

Certain solutions to the kinetic equations and the way in which they relate to the results of this and previous experimental programs are summarized below.

Kinetic Equation Solutions

Ambient-Temperature Growth Curves - Previously Unirradiated Specimens

In this case, the effects of annealing and optical bleaching are negligible and the increase of the induced absorption coefficient with ionizing dose is given by:

$$\alpha(D) = a\sigma_{ph}\left[D-\frac{1}{b}(1-e^{-bD})\right] \qquad \text{(A-4)}$$

The growth curve becomes a straight line for $D>>\frac{1}{b}$ with a slope given by:

$$\frac{\partial\alpha}{\partial D} = a\sigma_{ph}$$

Ambient-Temperature Pulsed Reactor Experiments

If the effects of neutron damage are neglected, Eq. (A-4) can be used to calculate the induced-absorption coefficient due to an ambient temperature pulsed reactor irradiation of total dose D_p.

$$\alpha(D_p) = \frac{\partial \alpha}{\partial D} \left[D_p - \frac{1}{b}(1-e^{-bD_p})\right] \qquad \text{(A-5)}$$

where $\frac{\partial \alpha}{\partial D}$ is the measured slope of the linear portion of an ambient-temperature electron or gamma irradiation.

Optical Bleaching of Previously Irradiated Specimens

In this case the specimen is irradiated to an induced absorption coefficient α_1 and then given an optical bleach of duration Δt, at a temperature at which thermal annealing is negligible. The induced absorption coefficient after the optical bleach, α_2, is given by:

$$\alpha_2 = \alpha_1 e^{-cI\Delta t} \qquad \text{(A-6)}$$

where:

c = optical bleaching constant (watts^{-1}-cm^2-sec^{-1})

I = total light intensity incident on the specimen with wavelengths in the absorption band (watts/cm^2)

Δt = duration of optical bleach (sec)

The optical bleaching constant can then be calculated from the following equation:

$$c = \frac{1}{I\Delta t} \ln\left(\frac{\alpha_1}{\alpha_2}\right) \qquad \text{(A-7)}$$

Ambient-Temperature Growth Curve Following Optical Bleach

After the optical bleaching described above, a fixed concentration of defects proportional to $(\alpha_1-\alpha_2)$ remains in the specimen. If the specimen is re-irradiated at ambient temperature, the growth of the induced absorption coefficient will be characterized by an initial rapid increase due to electron trapping at the remaining defects and a much slower increase due to the creation of new defects.

The latter contribution can be neglected during the initial portion of the growth curve which is then given by:

$$\alpha(D) = \alpha_2+(\alpha_1-\alpha_2)(1-e^{-bD}) \tag{A-8}$$

The electron trapping constant, b, is then given by the reciprocal of the ionizing dose at which the induced absorption coefficient reaches the value α_3, where:

$$\begin{aligned}\alpha_3 &= \alpha_2+(\alpha_1-\alpha_2)(1-e^{-1}) \\ &= \alpha_2+0.63\ (\alpha_1-\alpha_2)\end{aligned} \tag{A-9}$$

Steady-State Reactor Irradiation at Elevated Temperatures

In this case the induced absorption coefficient reaches a steady-state value during irradiation due to the competing effects of the generation and annealing of color centers. The effects of optical bleaching are negligible and the annealing rate should be equal to that measured in post-irradiation experiments due to the low value of ionizing dose rate. The steady-state absorption coefficient is given by:

$$\alpha_s(\dot{D},T) = \left(\frac{\partial\alpha}{\partial D}\right) \frac{b\dot{D}}{b\dot{D} + \dfrac{1}{\tau_A(T)}}\ \dot{D}\tau_A(T) \tag{A-10}$$

where:

$\tau_A(T)$ = thermal annealing time constant at specimen temperature T as measured in post-irradiation experiments (sec).

All of the parameters in Eq. (A-10) are independently measurable quantities so that comparison with experiment is possible. This can be used to check the validity of the assumed mathematical model.

Steady-State Electron Irradiation at Elevated Temperatures*

This case is similar to the steady-state reactor experiments except that at the high dose rates employed the annealing rate becomes an increasing function of dose rate due to radiation annealing:

$$\alpha_s(\dot{D},T) = \left(\frac{\partial\alpha}{\partial D}\right) \frac{b\dot{D}}{b\dot{D}+\nu_A(\dot{D},T)} \cdot \frac{\dot{D}}{\nu_A(\dot{D},T)} \qquad \text{(A-11)}$$

A knowledge of $\alpha_s(\dot{D},T)$ can be used to calculate the annealing rate at a given ionizing dose rate and specimen temperature from the above equation.

Power Deposited in Transparent Wall of Full Scale NLB due to 2150 Å Absorption Band

In the case of the full-scale engine, the effects of radiation annealing and optical bleaching must both be included: The resulting equation for the steady-state irradiation-induced absorption coefficient is:

$$\alpha_s(\dot{D}_W,T_W,I_W) = \left(\frac{\partial\alpha}{\partial D}\right) \frac{b\dot{D}_W}{b\dot{D}_W+\nu_A(\dot{D}_W,T_W)+cI_W} \quad \frac{\dot{D}_W}{\nu_A(\dot{D}_W,T_W)} \qquad \text{(A-12)}$$

where:

$\dot{D}_W$ = predicted ionizing dose rate deposited in the transparent wall at full power. (Mrad/sec)

T_W = transparent wall temperature at full power (Deg C)

I_W = predicted light intensity at full power within the absorption band incident on the transparent wall (watts/cm^2).

If the product of the absorption coefficient and the transparent wall thickness is much less than one, the resulting volumetric heat deposition is uniform and is given by:

$$\dot{Q}_W = \alpha_s(\dot{D}_W,T_W,I_W)I_W \qquad \text{(A-13)}$$

* Transient solutions for the case of elevated temperature electron irradiations are difficult to obtain due to a lack of knowledge of the variation of the annealing rate with time during the onset of irradiation.

TABLE I

IRRADIATION HISTORY OF CORNING 7940 FUSED SILICA SPECIMENS

Specimen No.	Run No.	Initial Absorption Coefficient $\alpha(cm^{-1})$	Ionizing Dose Rate $\dot{D}$(Mrads/sec)	Ionizing Dose (D-Mrads)	Maximum Specimen Temperature (T - Deg C)
SC-1	1	0.0	0.84	172	340
SC-1	2	0.0	1.7	600	400
SC-1	3	0.0	3.4	680	400
SC-1	4	0.0	0.84	495	500
SC-1	5	0.0	3.40	1550	250
SC-2	6	0.0	1.25	325	400
SC-2	7	0.0	1.25	287	300
SC-2	8	0.0	1.25	525	170
SC-3	9	0.0	1.25	790	300
SC-3	10	0.0	1.25	230	500
SC-4	11	0.0	2.5	850	190
SC-4	12	0.0	2.5	350	370
SC-5	13	0.0	1.25	310	140
SC-5	14	3.8	2.50	1000	200
SC-5	15	1.4	3.40	630	220
SC-5	16	0.50	5.0	800	300
SC-5	17	0.25	1.25	225	100
SC-5	18	4.20	3.4	510	240
SC-6	19	0.0	3.7	930	230
SC-6	20	0.5	3.7	780	340
SC-7	21	0.0	5.0	800	300
SC-8	22	0.0	0.84	550	200
SC-9	23	0.0	0.42	395	100
SC-9	24	0.0	3.7	460	500
SC-10	25	0.0	0.42	1050	300
SC-10	26	1.3	0.42	1000	500
SC-11	27	0.0	0.17	600	500
SC-12	28	0.0	0.08	345	500
SC-13	29	0.0	0.02	56	40
SC-13	30	0.0	0.02	56	40
SC-14	31	0.0	5	5000	900
SC-15	32	0.0	0.02	18	40
SC-15	33	1.2	5	1200	200
SC-15	34	0.0	0.02	12	40
SC-16	35	0.0	0.02	15	40
SC-17	36	0.0	0.02	140	40
SC-18	37	0.0	0.02	30	40
SC-18	38	1.6	10	1000	400
SC-18	39	0.0	0.02	30	40
SC-19	40	0.0	0.02	26	40
SC-19	41	0.4	0.02	24	40
SC-20	42	0.0	0.42, 5	1750	400
SC-21	43	0.0	0.02	24	40
SC-21	44	0.96	0.02	12	40
SC-22	45	0.0	0.02	24	40
SC-22	46	0.7	0.02	12	40
SC-N-1*	47	7.8	5	1000	250
SC-N-1*	48	0.0	0.02	32	40
SC-N-2*	49	4.95	0.02	7	40
SC-N-3*	50	0.0	0.02	68	40

* Reactor irradiated to fast neutron dose of $10^{17} n/cm^2$ prior to electron irradiation.

TABLE II

STEADY-STATE VALUE OF INDUCED ABSORPTION COEFFICIENT DURING ELEVATED TEMPERATURE ELECTRON IRRADIATION AT λ = 2150 Å

Specimen No.	Run No.	Ionizing Dose Rate $\dot{D}$ (Mrads/sec)	Specimen Temperature T - Deg C	Steady-State Induced Absorption Coefficient α_s-cm^{-1}
SC-1	1	0.84	340	0.85
SC-1	2	1.7	400	0.15
SC-1	3	3.4	400	0.05
SC-1	4	0.84	300	1.35
SC-1	4	0.84	500	0.05
SC-1	5	3.4	250	0.20
SC-2	6	1.25	400	0.30
SC-2	7	1.25	300	1.10
SC-2	8	1.25	170	2.75
SC-3	9	1.25	140	3.40
SC-3	9	1.25	300	1.25
SC-3	10	1.25	500	0.0
SC-4	11	2.50	190	1.5
SC-4	12	2.50	370	0.35
SC-5	13	1.25	120	3.80
SC-5	14	2.5	200	1.40
SC-5	15	3.4	220	0.50
SC-5	16	5.0	300	0.25
SC-5	17	1.25	100	4.20
SC-5	18	3.4	240	0.30
SC-6	19	3.7	200	1.40
SC-6	19	3.7	230	0.70
SC-6	20	3.7	310	0.20
SC-6	20	3.7	340	0.10
SC-7	21	5.0	300	0.08
SC-8	22	0.84	120	4.60
SC-8	22	0.84	200	3.40
SC-9	23	0.42	100	5.0
SC-9	24	3.70	500	0.0
SC-10	25	0.42	100	5.7
SC-10	25	0.42	200	4.1
SC-10	25	0.42	300	2.2
SC-10	26	0.42	300	2.0
SC-10	26	0.42	400	0.75
SC-10	26	0.42	500	0.40
SC-11	27	0.17	100	5.50
SC-11	27	0.17	200	4.30
SC-11	27	0.17	300	1.60
SC-11	27	0.17	400	0.50
SC-11	27	0.17	500	0.20
SC-12	28	0.08	100	4.70
SC-12	28	0.08	200	3.50
SC-12	28	0.08	300	1.50
SC-12	28	0.08	400	0.40
SC-12	28	0.08	500	0.10
SC-14	31	5.0	900	0.0
SC-20	42	0.42	100	5.2
SC-20	42	0.42	250	2.9
SC-20	42	5	400	0.0
SC-20	42	0.42	250	2.5

TABLE III

SLOPE OF GROWTH OF INDUCED ABSORPTION COEFFICIENT AT λ = 2150 Å DURING AMBIENT TEMPERATURE ELECTRON IRRADIATION AT AN IONIZING DOSE RATE OF 0.02 MRAD/SEC

Specimen No.	Run No.	Slope $-\left(\frac{\partial \alpha}{\partial D}\right)$-cm^{-1}/Mrad
SC-13	29	0.044
SC-13	30	0.044
SC-15	32	0.070
SC-15	34	0.073
SC-16	35	0.067
SC-17	36	0.042
SC-18	37	0.045
SC-18	39	0.053
SC-19	40	0.054
SC-19	41	0.054
SC-21	43	0.053
SC-21	44	0.045
SC-22	45	0.042
SC-22	46	0.039
SC-N-1	48	0.042
SC-N-3	50	0.042

Average Slope - $\left(\frac{\partial \alpha}{\partial D}\right)$ = 0.05 cm^{-1}/Mrad

TABLE IV

IRRADIATION HISTORY OF ALUMINUM OXIDE SPECIMENS

Specimen	Reactor Irradiation Dose n/cm^2	Electron Irradiation Conditions		
		Dose Rate Mrad/sec	Temperature deg C	Elapsed Time min
AL-1	--	0.14	40	20
AL-2	--	7	200	2*
AL-N-1	10^{17}	3.5	150	2*
AL-N-2	10^{17}	--	--	--

* Run terminated due to specimen fracture.

TABLE V

CALCULATED VALUES OF OPTICAL BLEACHING
CONSTANT, c, AND ELECTRON TRAPPING CONSTANT, b

Specimen No.	Initial Absorption Coefficient $\alpha_1(cm^{-1})$	Light Intensity 2250<λ<2250 Å $I(mw/cm^2)$	Duration of Optical Bleach $\Delta t(sec)$	Absorption Coefficient After Optical Bleach $\alpha_2(cm^{-1})$	Calculated Optical Bleaching Constant $c(watts^{-1}-cm^2-sec^{-1})$	Calculated Electron Trapping Constant $b(Mrads^{-1})$
SC-16	1.07	2	600	0.97	0.079	--
SC-21	1.42	2	2700	0.96	0.073	2.4
SC-22	1.2	1	5400	0.70	0.098	1.9
SC-N-2	7.9	2	2700	4.95	0.087	1.8

Average Optical Bleaching Constant - $c = 0.08$ $watts^{-1}-cm^2-sec^{-1}$

Average Electron Trapping Constant - $b = 2$ $Mrads^{-1}$

TABLE VI

COMPARISON OF EXPERIMENTAL AND CALCULATED VALUES AT STEADY-STATE REACTOR-IRRADIATION-INDUCED ABSORPTION COEFFICIENT AT 2150 Å

$$\alpha_{calc} = \left(\frac{\partial \alpha}{\partial D}\right) \dot{D} \tau_A \frac{b\dot{D}}{b\dot{D} + \frac{1}{\tau_A}}$$

$$\dot{D} = 0.02 \text{ Mrad/sec}$$

$$\left(\frac{\partial \alpha}{\partial D}\right) = 0.05 \text{ cm}^{-1}/\text{Mrad}$$

$$b = 2 \text{ Mrads}^{-1}$$

Specimen Temperature T - Deg C	Thermal Annealing Time Constant* τ_A(sec)	Calculated Absorption Coefficient $\alpha_{calc}(cm^{-1})$	Experimentally Determined Absorption Coefficient** $\alpha_s(cm^{-1}$
700	61.5	0.044	0.054
800	57.7	0.040	0.050
900	34.4	0.023	0.034

* From Ref. 6

** From Ref. 9

FIG. 1

SPECIMEN CONFIGURATION FOR ELECTRON IRRADIATION EXPERIMENTS

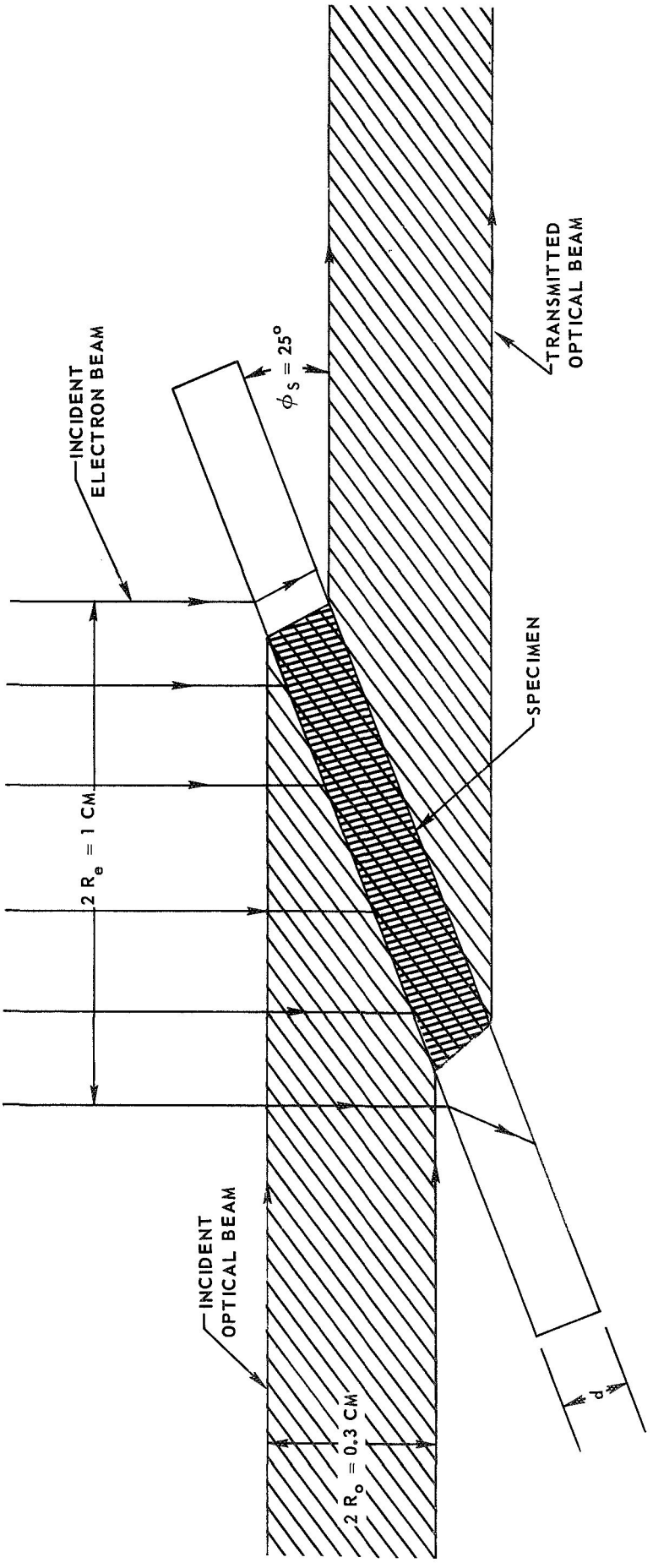

J-990929-1

FIG. 2

ELECTRICAL AND OPTICAL SCHEMATIC FOR ELECTRON IRRADIATION EXPERIMENTS

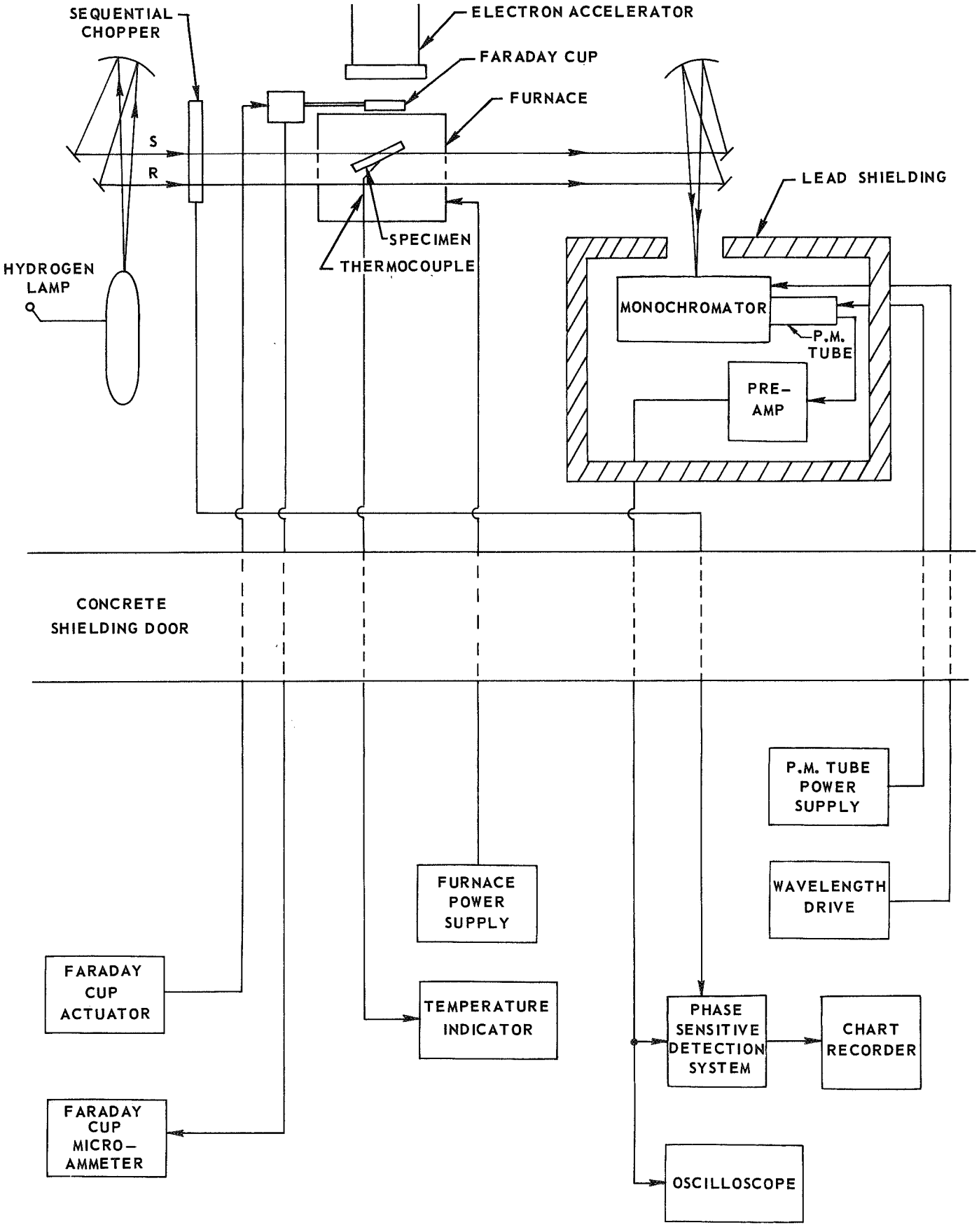

BLOCK DIAGRAMS OF OPTICAL SYSTEMS USED FOR LIGHT SOURCE MEASUREMENTS

a) EXPERIMENTAL ARRANGEMENT FOR SPECTRAL MEASUREMENTS

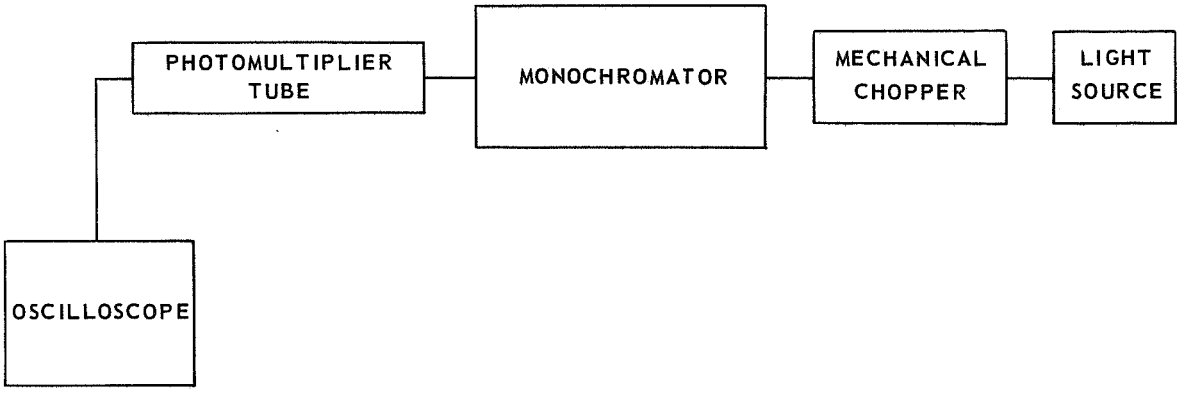

b) EXPERIMENTAL ARRANGEMENT FOR INTENSITY MEASUREMENTS

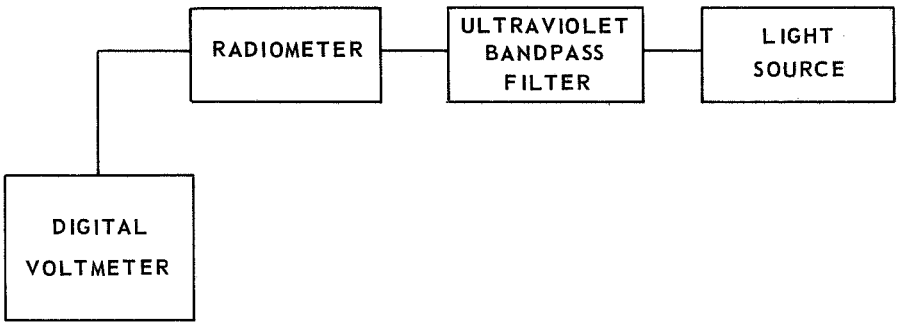

FIG. 4

BH-6 MERCURY ARC LAMP SPECTRUM

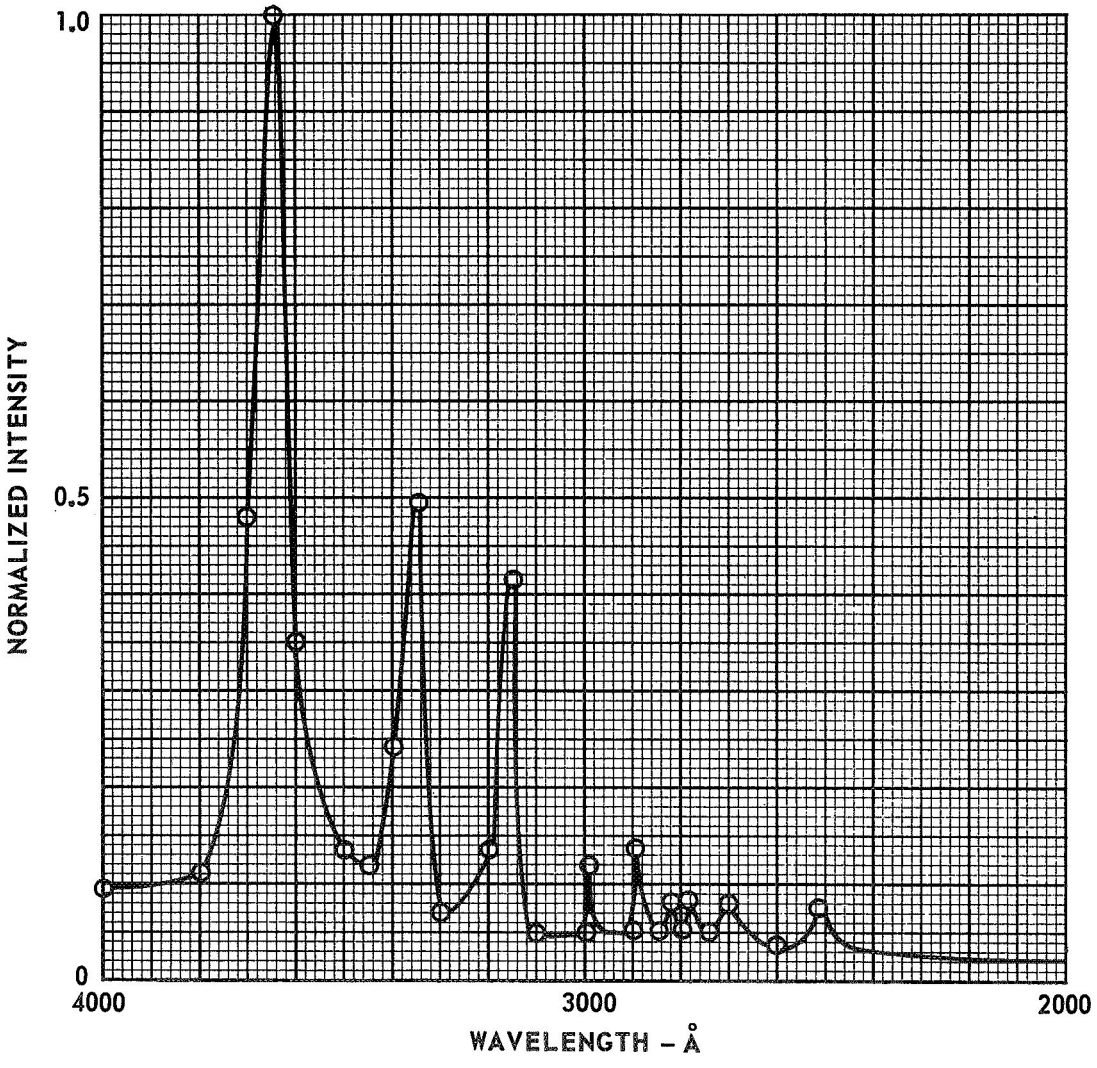

HYDROGEN DISCHARGE LAMP SPECTRUM

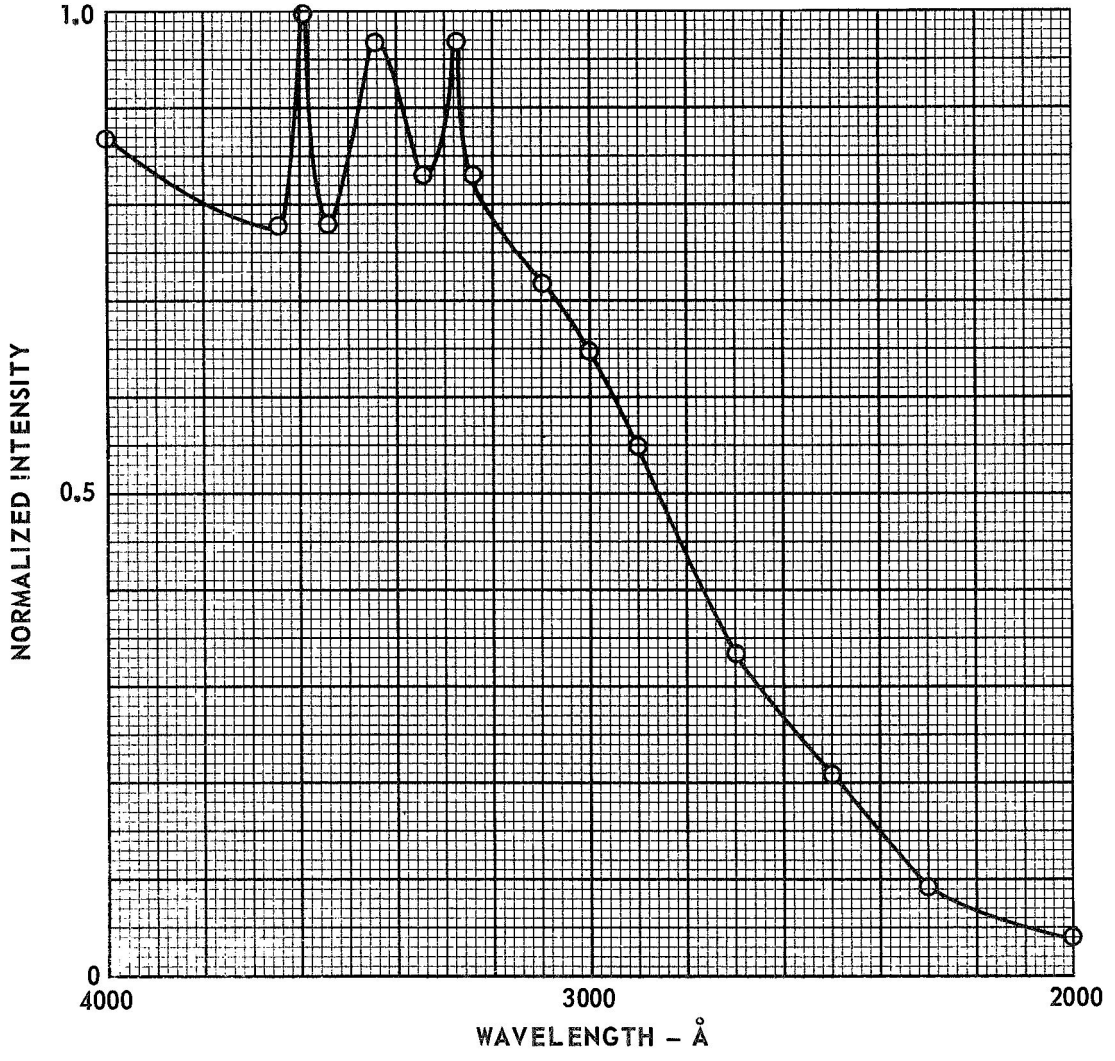

FIG. 6

TUNGSTEN- IODINE LAMP SPECTRUM

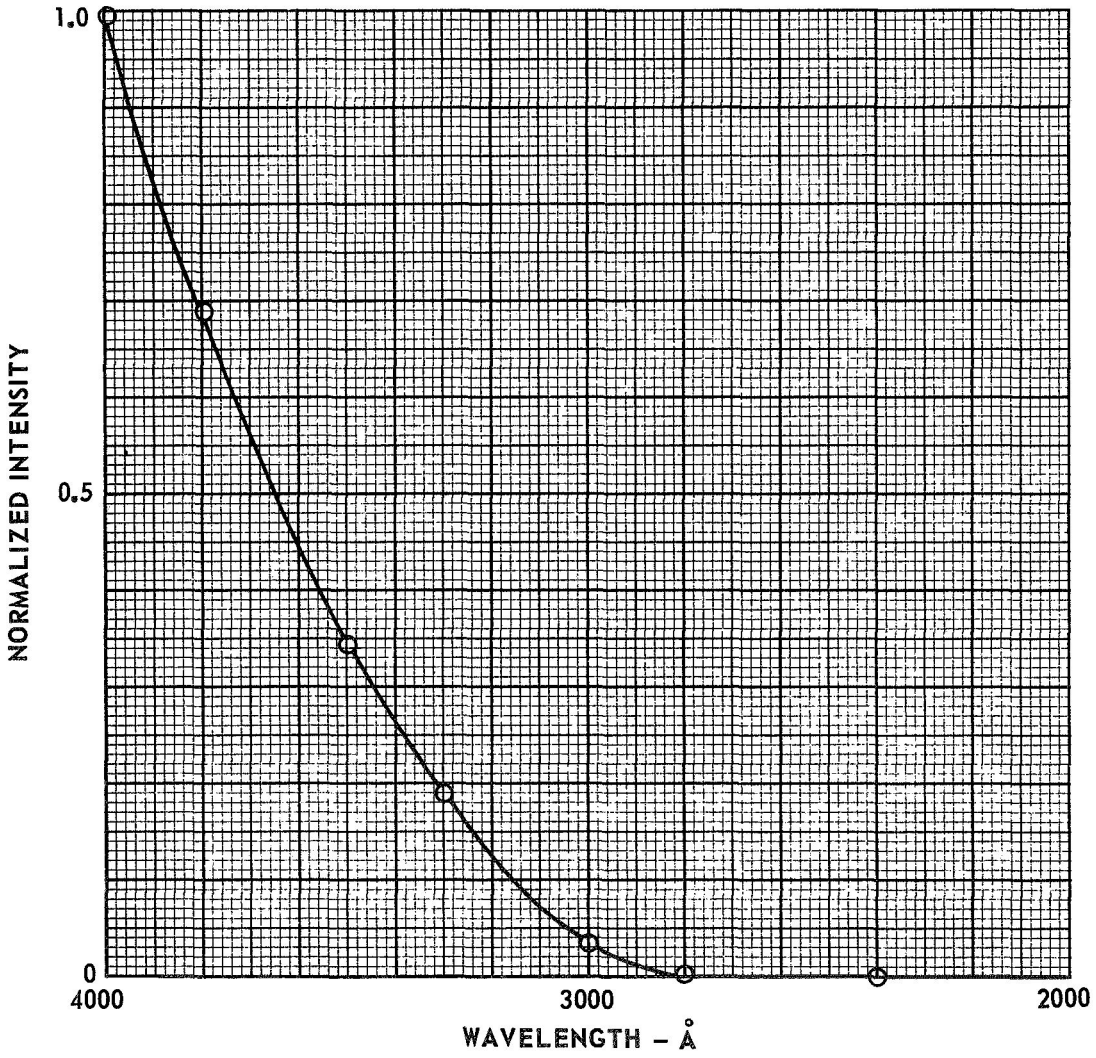

FIG. 7

XENON FLASHLAMP SPECTRUM

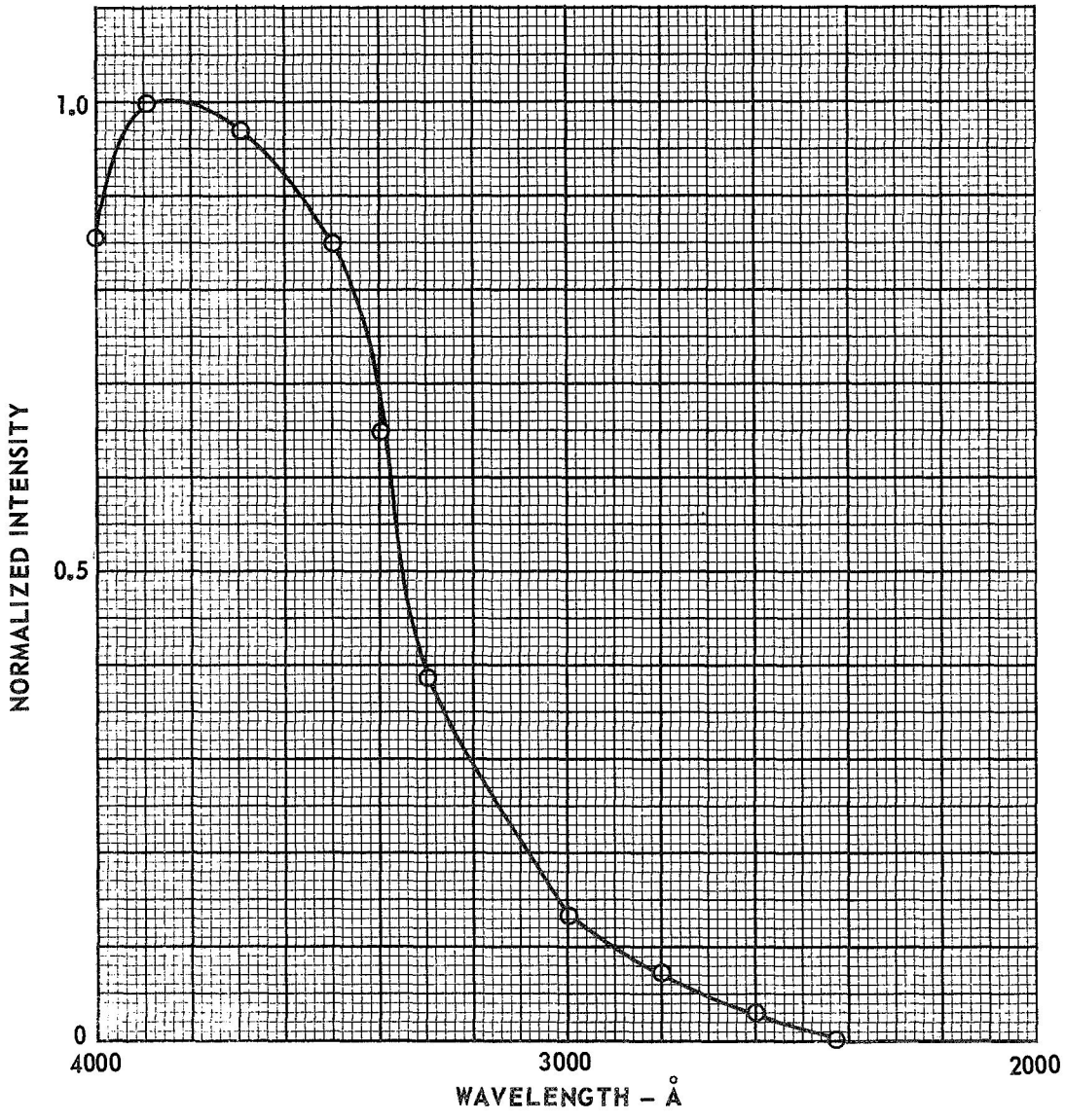

FIG. 8

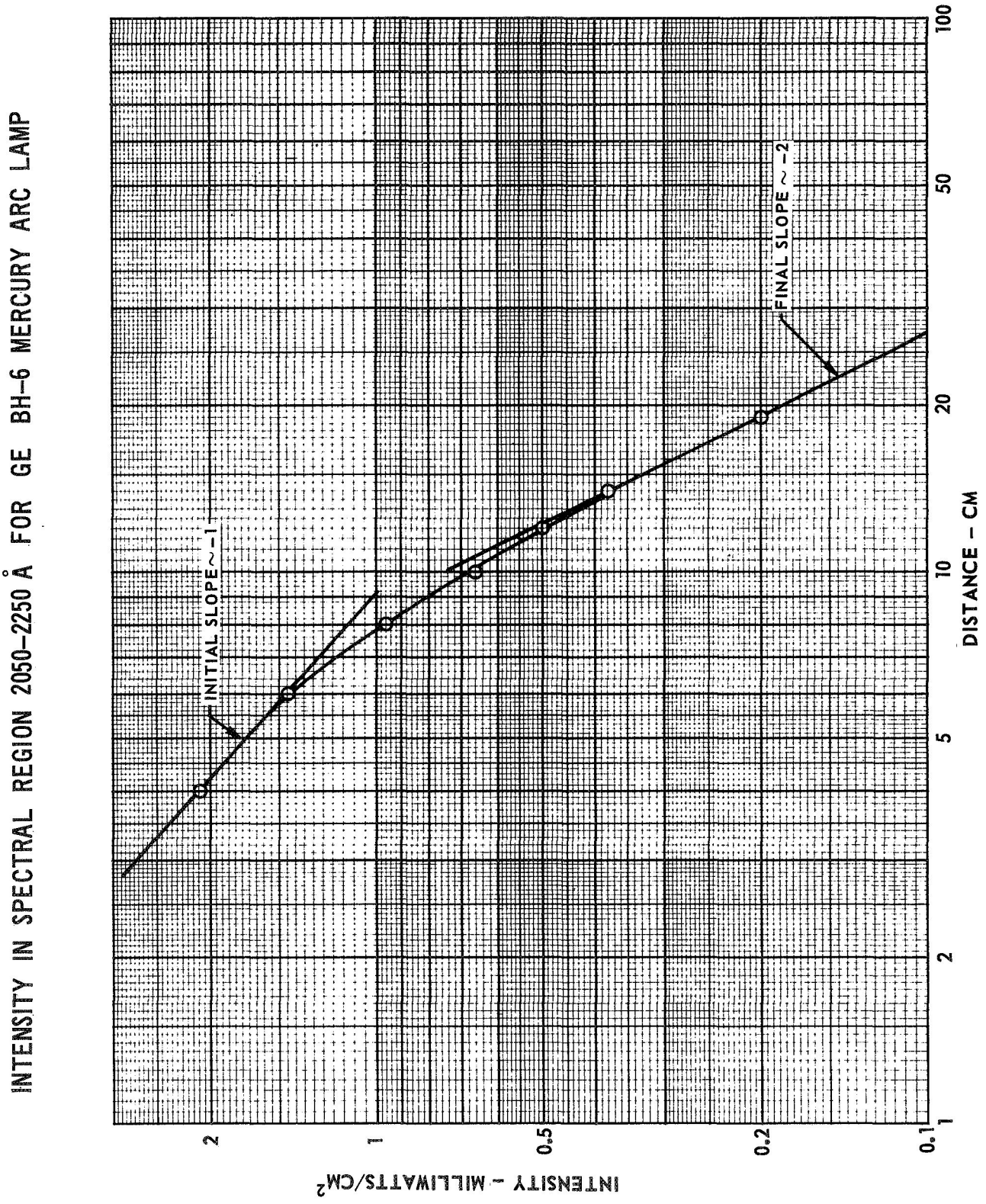
INTENSITY IN SPECTRAL REGION 2050-2250 Å FOR GE BH-6 MERCURY ARC LAMP
INITIAL SLOPE ~ -1
FINAL SLOPE ~ -2
INTENSITY - MILLIWATTS/CM²
2
1
0.5
0.2
0.1
1
2
5
10
20
50
100
DISTANCE - CM

J-990929-1

FIG. 9

TOTAL INTENSITY FOR GE BH-6 MERCURY ARC LAMP

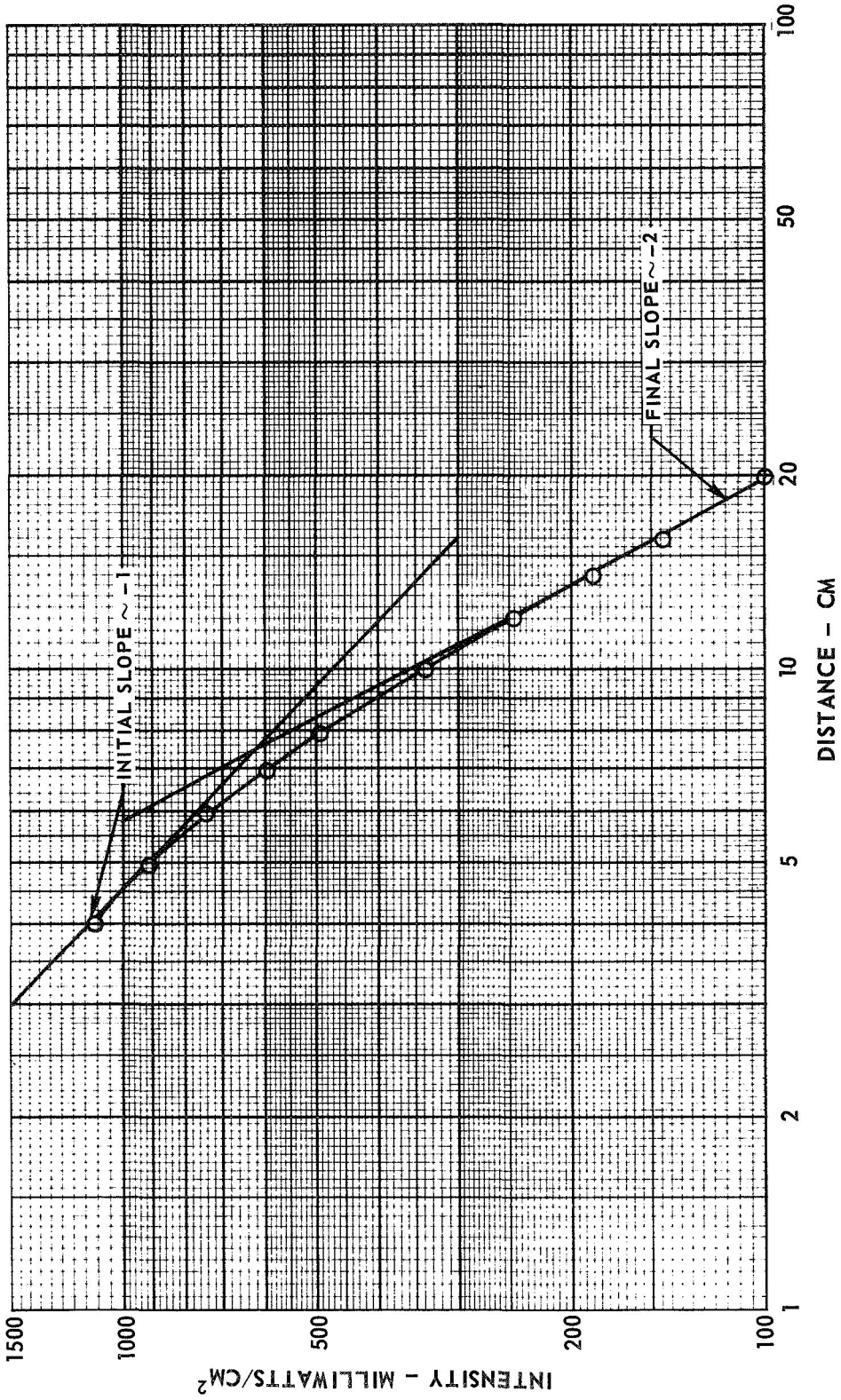

FIG. 10

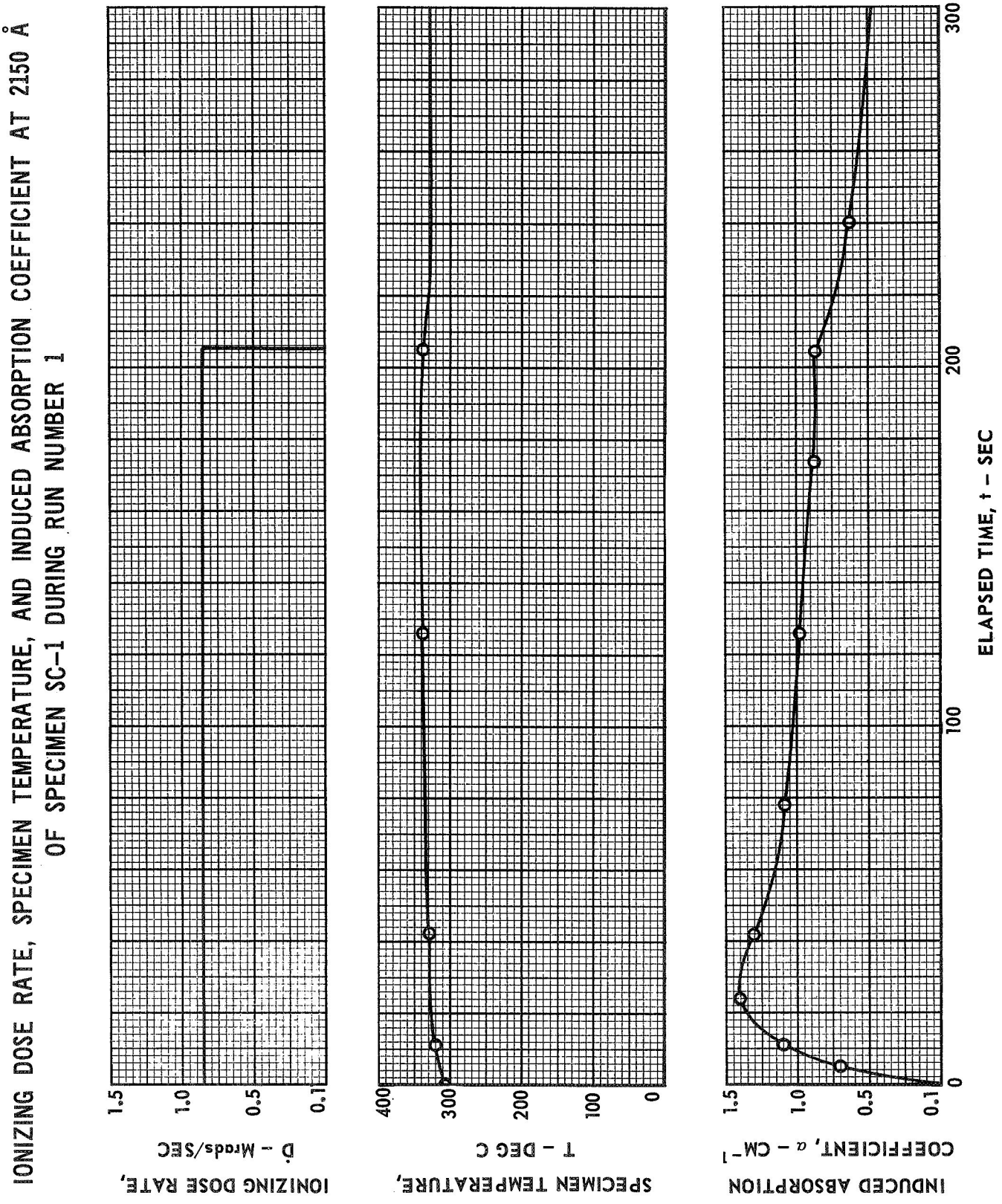
IONIZING DOSE RATE, SPECIMEN TEMPERATURE, AND INDUCED ABSORPTION COEFFICIENT AT 2150 Å OF SPECIMEN SC-1 DURING RUN NUMBER 1
IONIZING DOSE RATE, Ḋ – Mrads/SEC
1.5
1.0
0.5
0.1
SPECIMEN TEMPERATURE, T – DEG C
400
300
200
100
0
INDUCED ABSORPTION COEFFICIENT, α – CM⁻¹
1.5
1.0
0.5
0.1
0
100
200
300
ELAPSED TIME, t – SEC

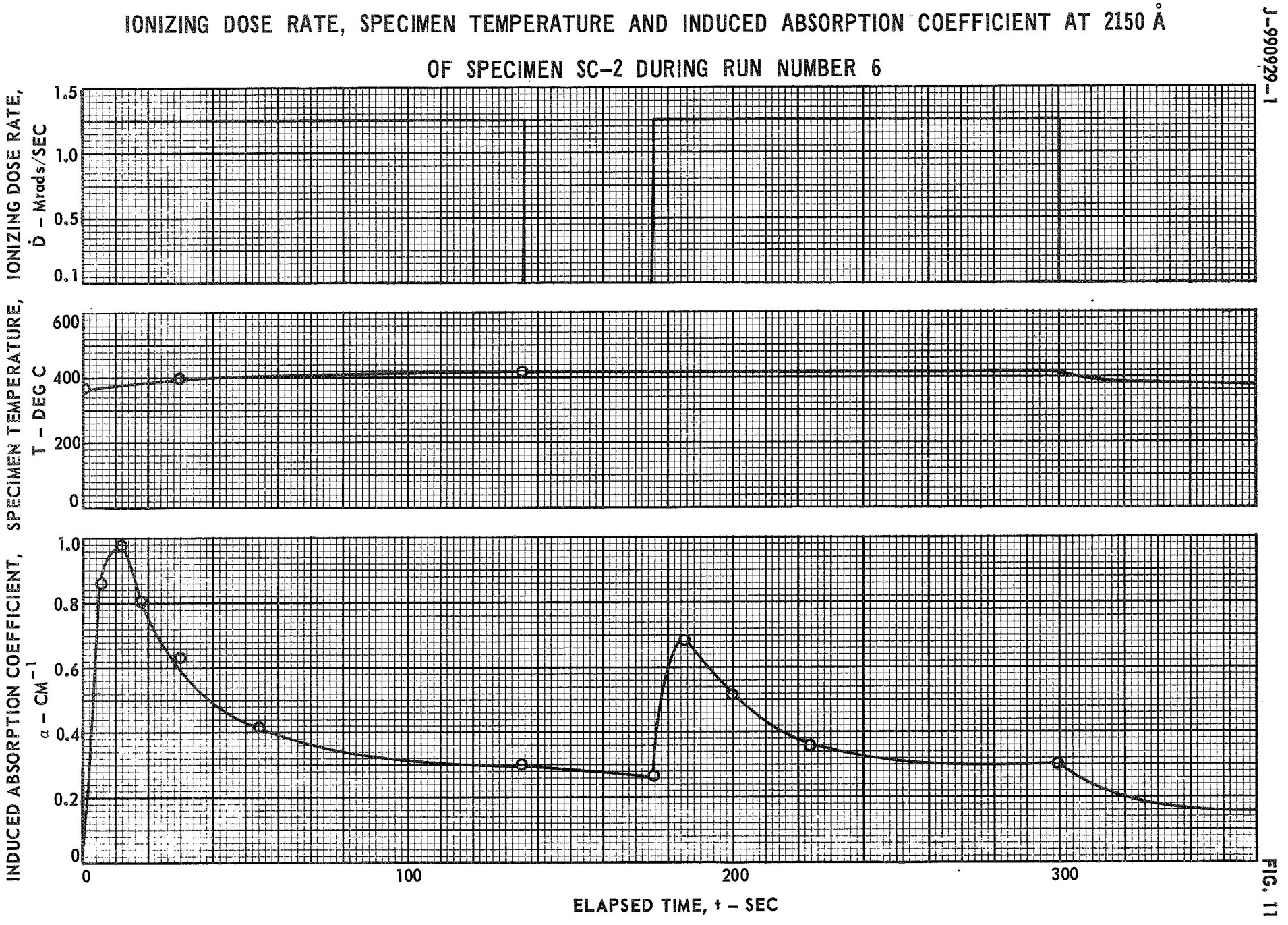
IONIZING DOSE RATE, SPECIMEN TEMPERATURE AND INDUCED ABSORPTION COEFFICIENT AT 2150 Å
OF SPECIMEN SC-2 DURING RUN NUMBER 6
J-990929-1
IONIZING DOSE RATE, Ḋ – Mrads/SEC
1.5
1.0
0.5
0.1
SPECIMEN TEMPERATURE, T – DEG C
600
400
200
0
INDUCED ABSORPTION COEFFICIENT, α – CM⁻¹
1.0
0.8
0.6
0.4
0.2
0
0
100
200
300
ELAPSED TIME, t – SEC
FIG. 11

IONIZING DOSE RATE, SPECIMEN TEMPERATURE, AND INDUCED ABSORPTION COEFFICIENT AT 2150 Å OF SPECIMEN SC-3 DURING RUN NUMBER 8

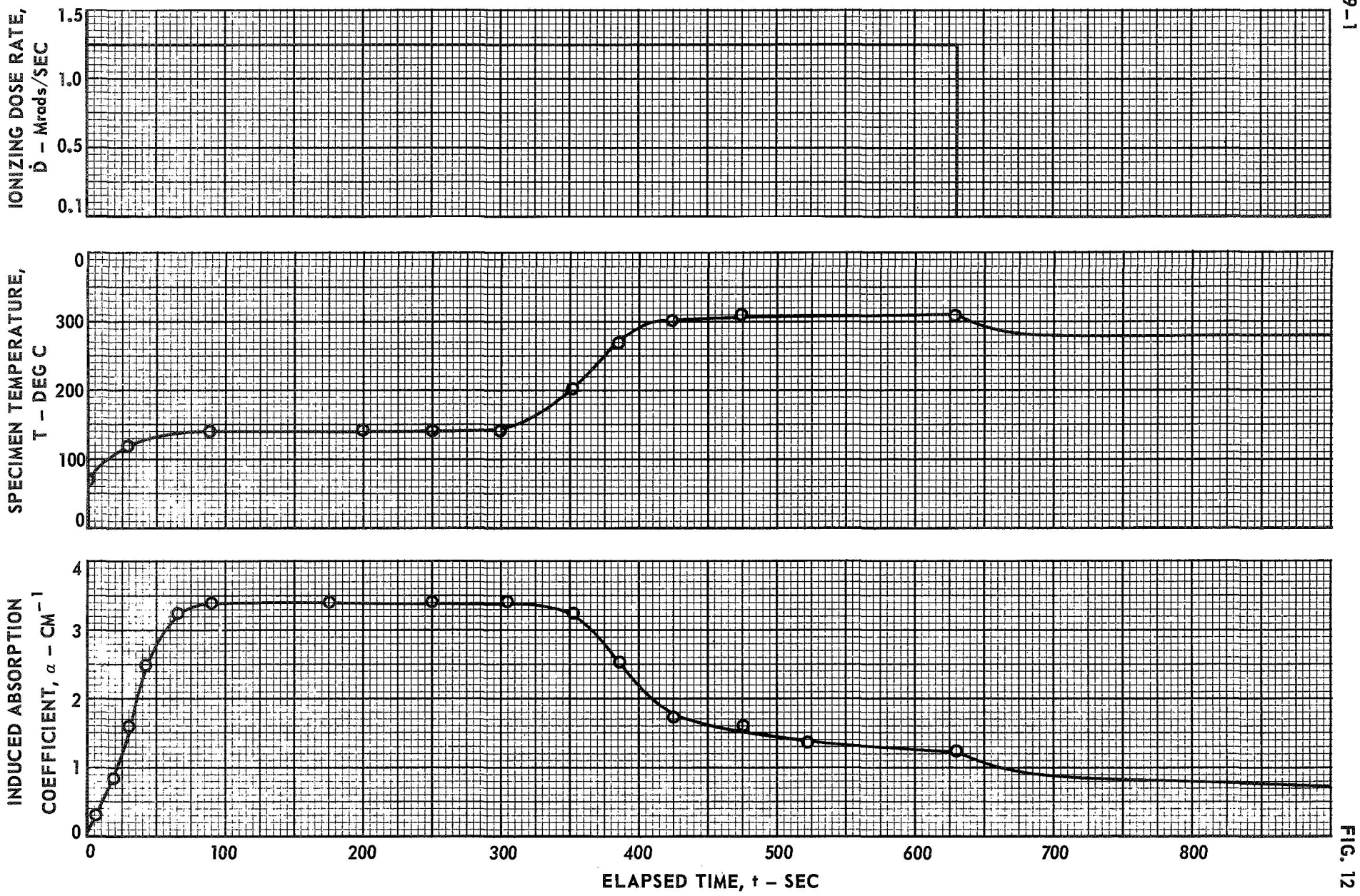

J-69029-1

FIG. 12

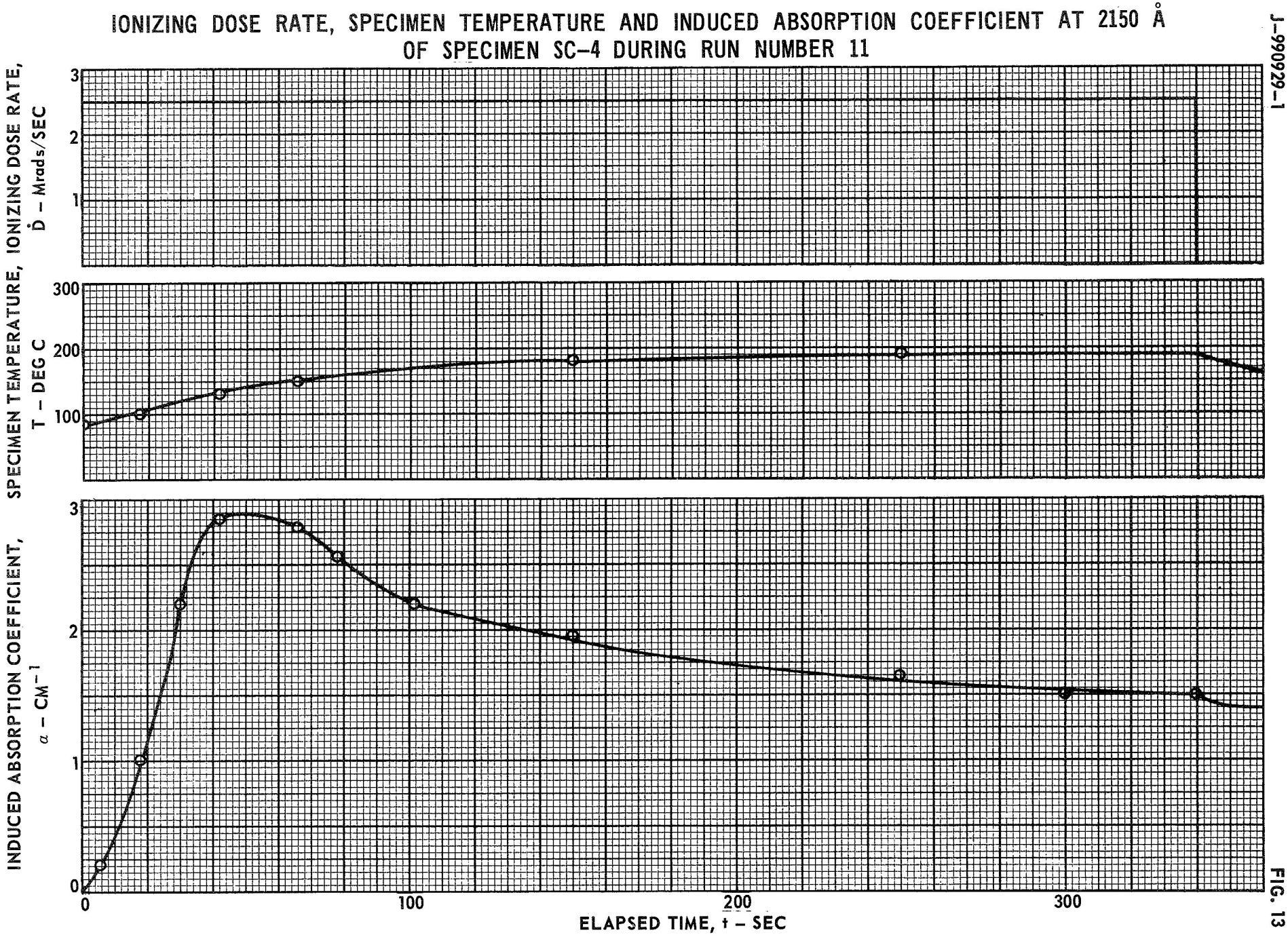
IONIZING DOSE RATE, SPECIMEN TEMPERATURE AND INDUCED ABSORPTION COEFFICIENT AT 2150 Å
OF SPECIMEN SC-4 DURING RUN NUMBER 11
INDUCED ABSORPTION COEFFICIENT, α – CM⁻¹
SPECIMEN TEMPERATURE, T – DEG C
IONIZING DOSE RATE, Ḋ – Mrads/SEC
ELAPSED TIME, t – SEC
0
100
200
300
1
2
3
100
200
300
J-69029-1

FIG. 13

IONIZING DOSE RATE, SPECIMEN TEMPERATURE AND INDUCED ABSORPTION COEFFICIENT AT 2150 Å OF SPECIMEN SC-7 DURING RUN NUMBER 21

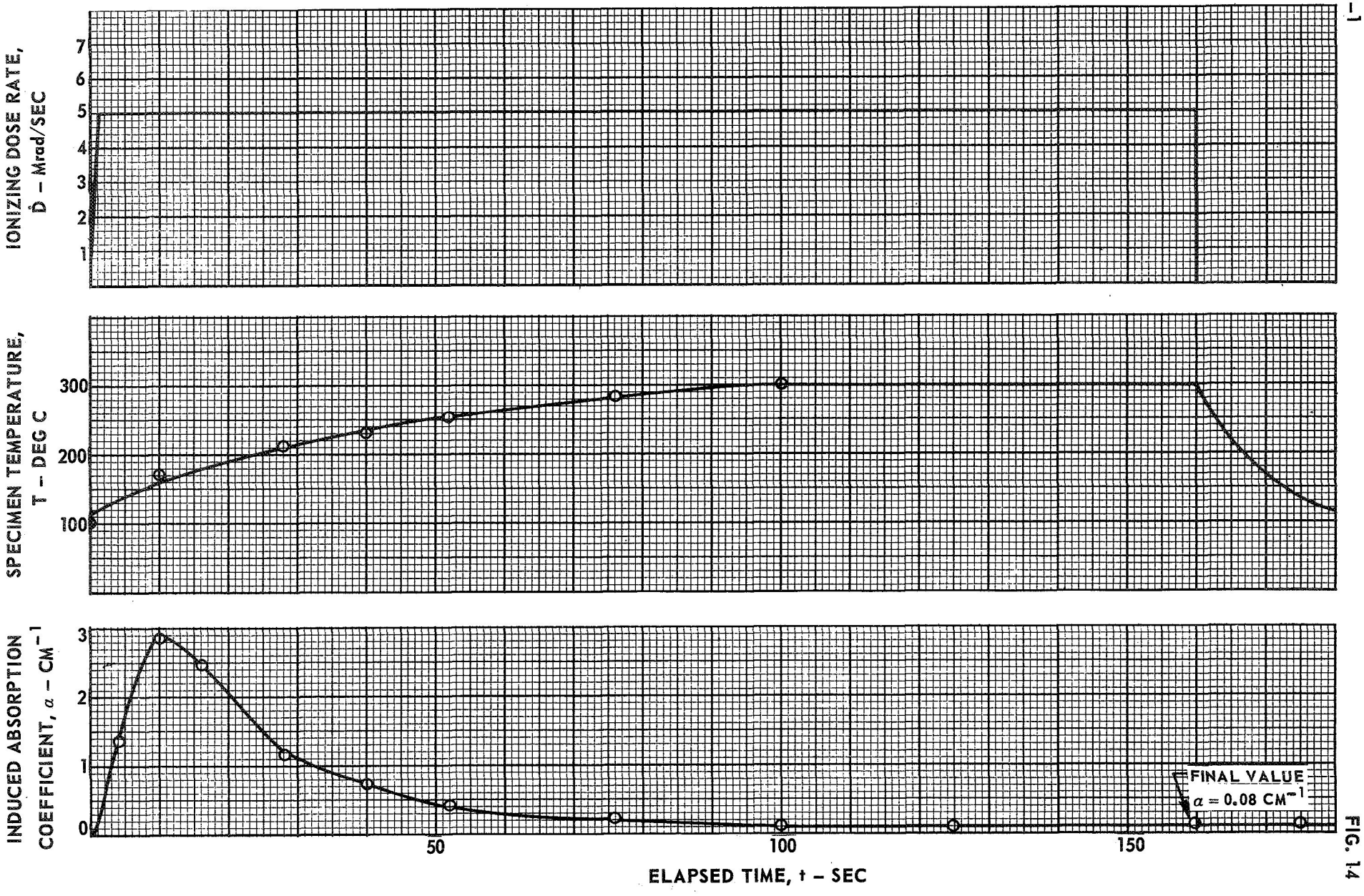

FIG. 14

J-990929-1

FIG. 15

IONIZING DOSE RATE, SPECIMEN TEMPERATURE AND INDUCED ABSORPTION COEFFICIENT AT 2150 Å OF SPECIMEN SC-8 DURING RUN NO. 22

FIG. 16

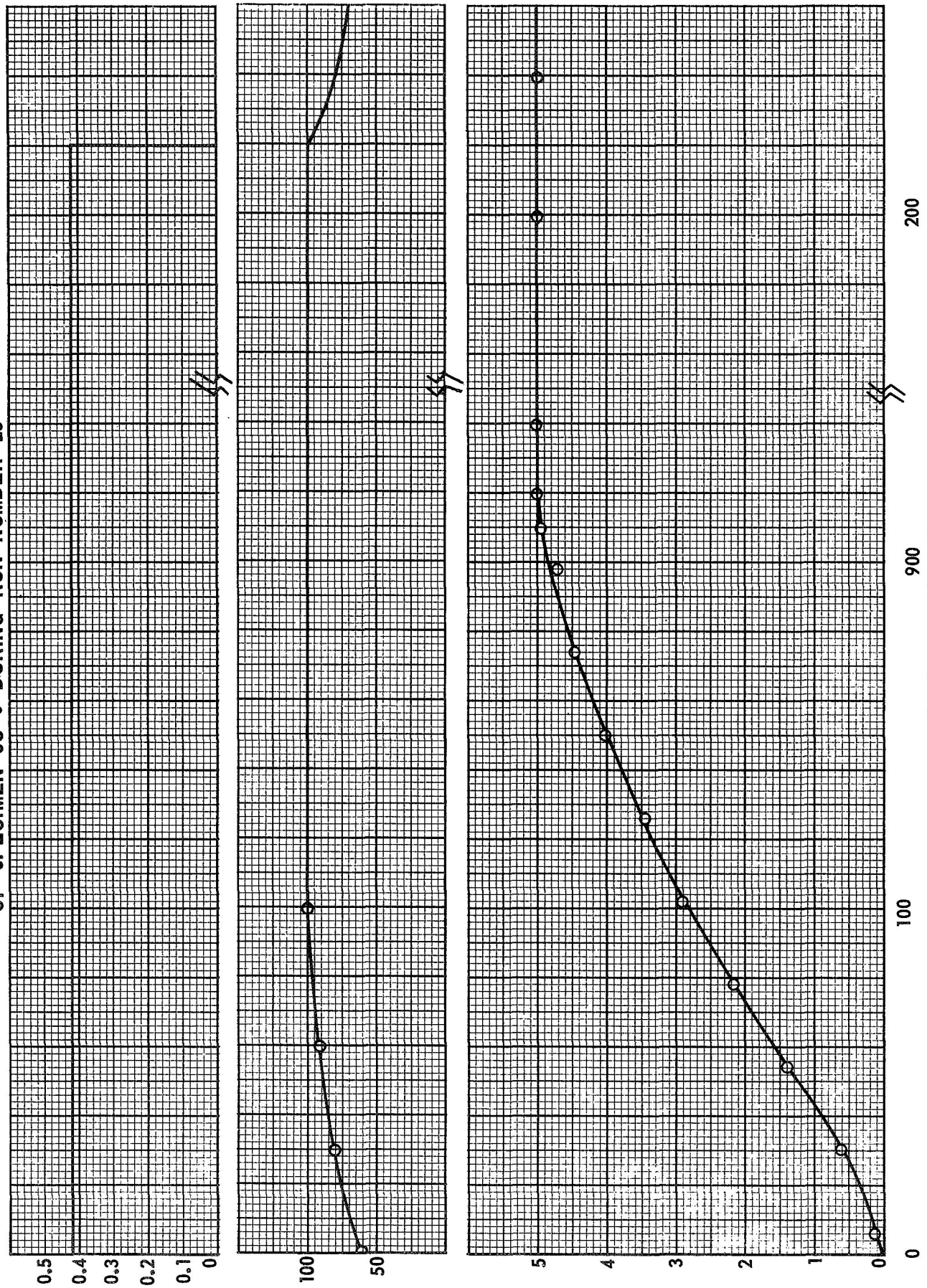
IONIZING DOSE RATE, SPECIMEN TEMPERATURE AND INDUCED ABSORPTION COEFFICIENT AT 2150 Å
OF SPECIMEN SC-9 DURING RUN NUMBER 23
IONIZING DOSE RATE, Ḋ – Mrads/SEC
0
0.1
0.2
0.3
0.4
0.5
SPECIMEN TEMPERATURE, T – DEG C
50
100
INDUCED ABSORPTION COEFFICIENT, α – CM⁻¹
0
1
2
3
4
5
0
100
900
200
ELAPSED TIME, t – SEC

FIG. 17

IONIZING DOSE RATE, SPECIMEN TEMPERATURE, AND INDUCED ABSORPTION COEFFICIENT AT 2150 Å OF SPECIMEN SC-10 DURING RUN NUMBER 25

IONIZING DOSE RATE, SPECIMEN TEMPERATURE, AND INDUCED ABSORPTION COEFFICIENT AT 2150 Å OF SPECIMEN SC-12 DURING RUN NUMBER 28

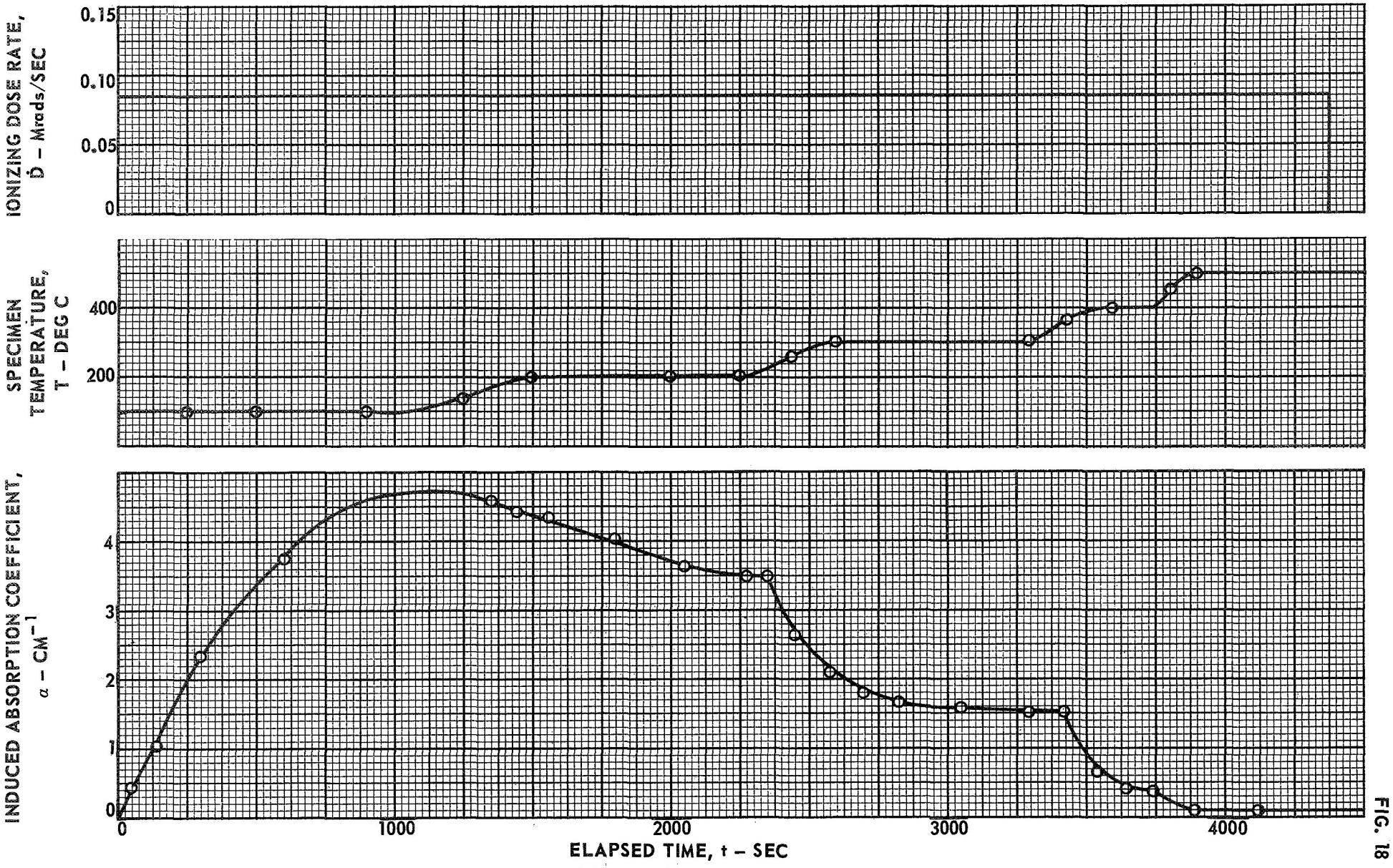

J-990929-1

FIG. 18

FIG. 19

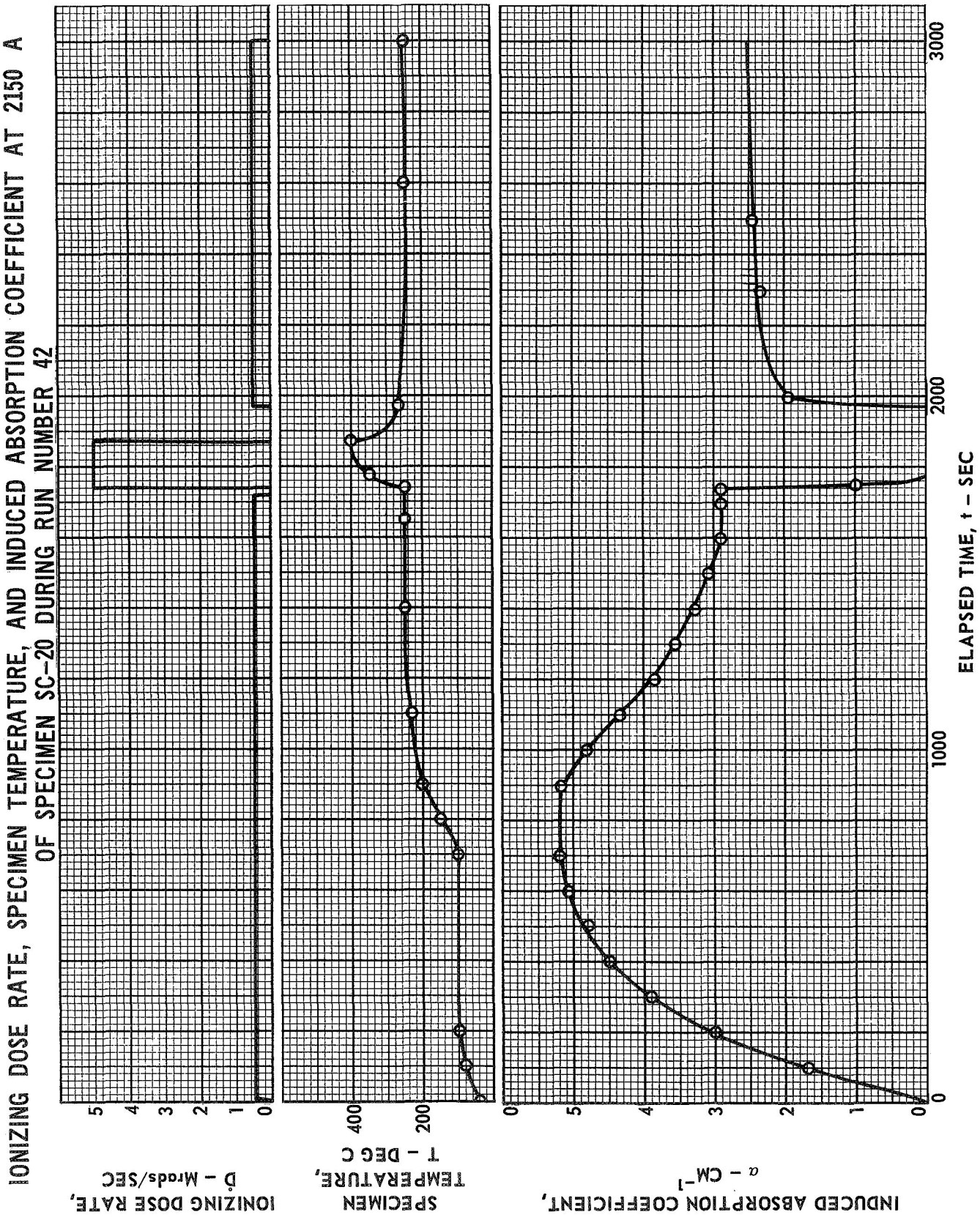
IONIZING DOSE RATE, SPECIMEN TEMPERATURE, AND INDUCED ABSORPTION COEFFICIENT AT 2150 Å OF SPECIMEN SC-20 DURING RUN NUMBER 42
IONIZING DOSE RATE, Ḋ – Mrads/SEC
SPECIMEN TEMPERATURE, T – DEG C
INDUCED ABSORPTION COEFFICIENT, α – CM⁻¹
ELAPSED TIME, t – SEC
0
1
2
3
4
5
200
400
1000
2000
3000

FIG. 20

STEADY-STATE INDUCED ABSORPTION COEFFICIENT AT ELEVATED SPECIMEN TEMPERATURES DURING ELECTRON AND REACTOR IRRADIATION

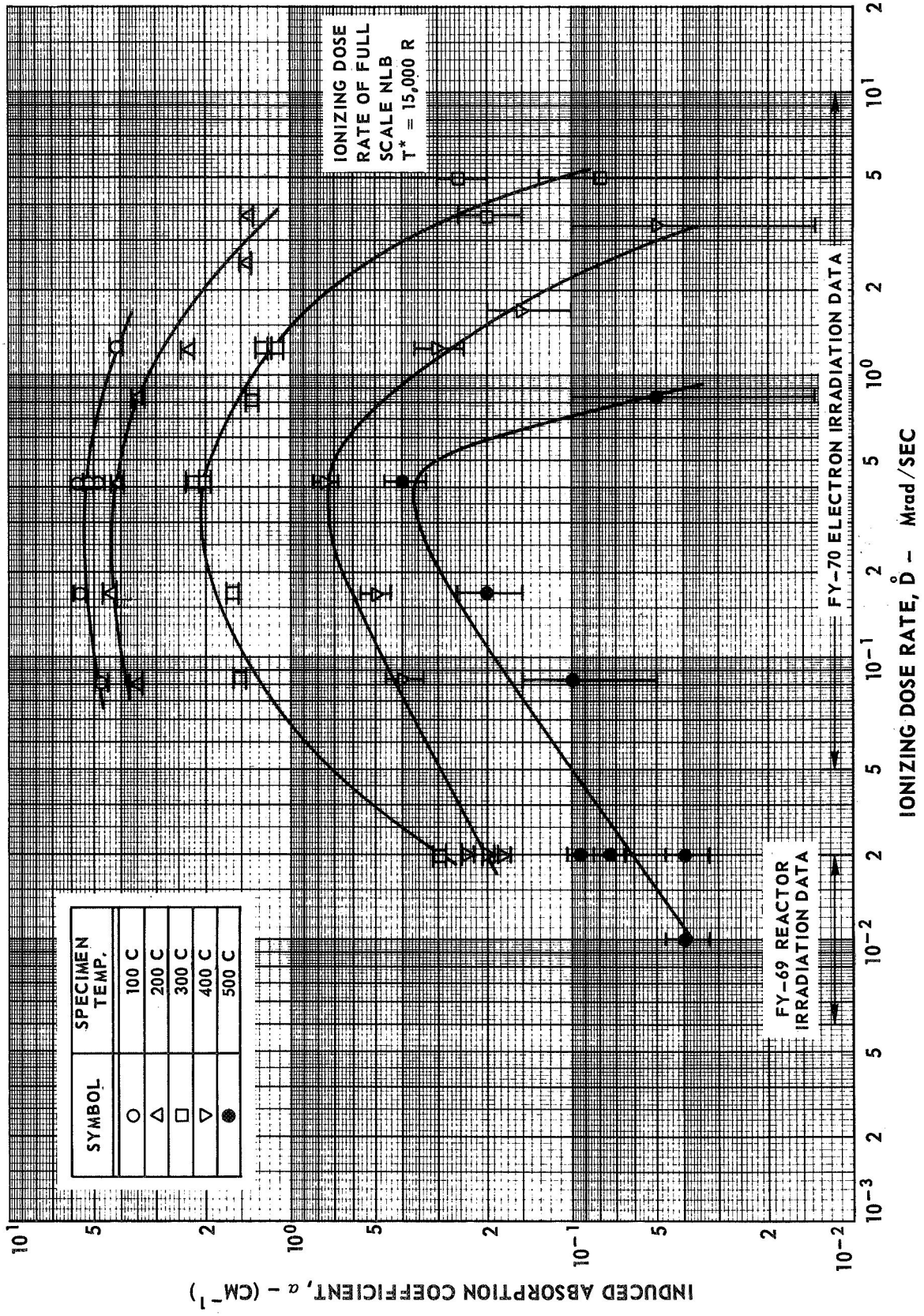

FIG. 21

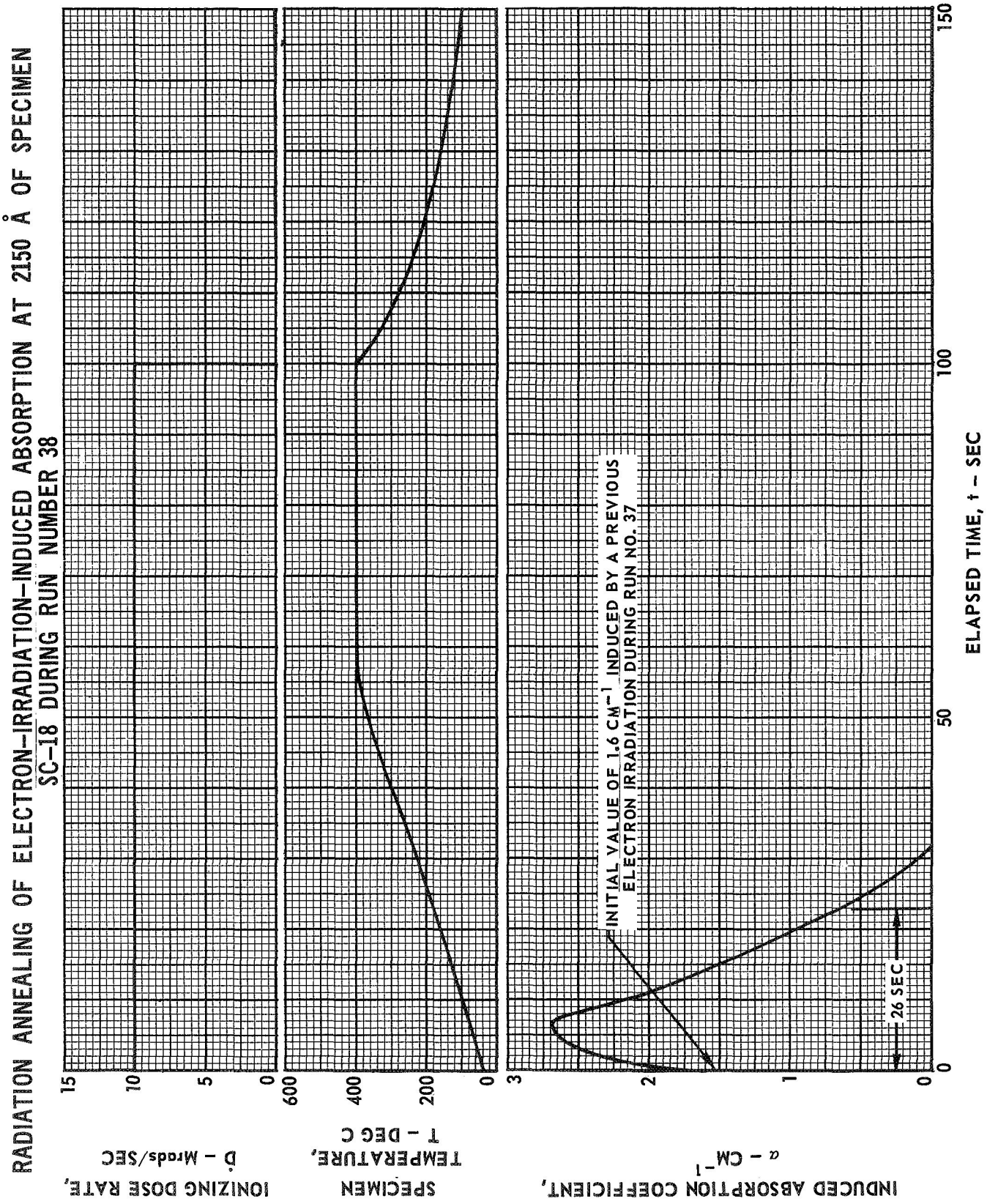
RADIATION ANNEALING OF ELECTRON-IRRADIATION-INDUCED ABSORPTION AT 2150 Å OF SPECIMEN SC-18 DURING RUN NUMBER 38
IONIZING DOSE RATE, $\dot{D}$ – Mrads/SEC
SPECIMEN TEMPERATURE, T – DEG C
INDUCED ABSORPTION COEFFICIENT, α – CM^{-1}
ELAPSED TIME, t – SEC
INITIAL VALUE OF 1.6 CM^{-1} INDUCED BY A PREVIOUS ELECTRON IRRADIATION DURING RUN NO. 37
26 SEC
15
10
5
0
600
400
200
0
3
2
1
0
0
50
100
150

FIG. 22

GROWTH OF INDUCED ABSORPTION FOR SPECIMEN SC-17 DURING ELECTRON IRRADIATION
RUN NUMBER 36

$\lambda = 2150$ Å
$\dot{D} = 0.02$ Mrad/SEC
T = 40 C

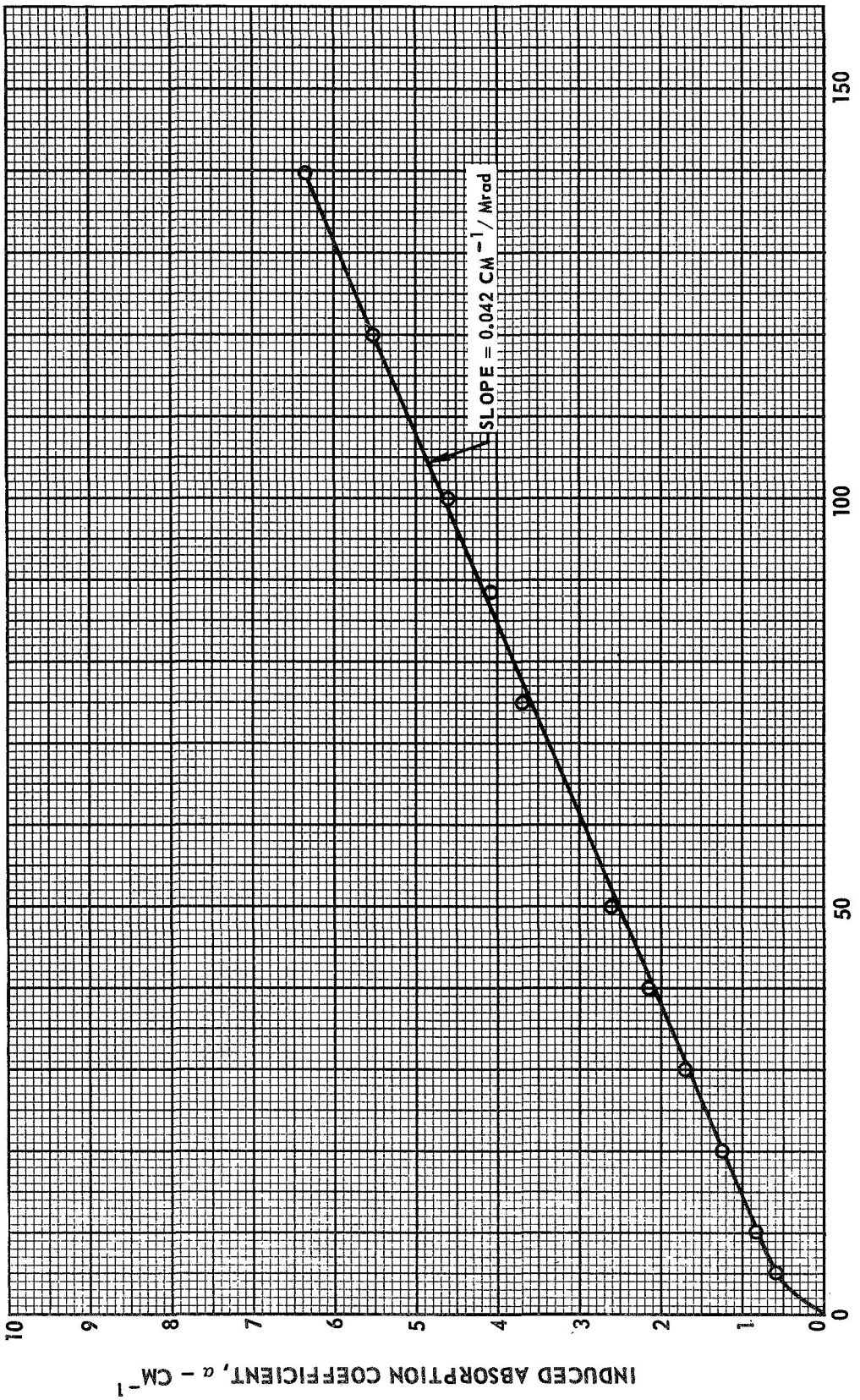

GROWTH OF INDUCED ABSORPTION FOR SPECIMEN SC-19 DURING ELECTRON IRRADIATION BEFORE AND AFTER THERMAL ANNEAL AT 300 C

SYMBOL	RUN NO.	CONDITIONS
○	40	BEFORE THERMAL ANNEAL
△	41	AFTER THERMAL ANNEAL AT 300 C FOR 10 MIN

FRACTION OF DEFECTS REMOVED BY THERMAL ANNEAL $\xi = 79\%$

$\lambda = 2150$ Å
$\dot{D} = 0.02$ Mrad/SEC
T = 40 C

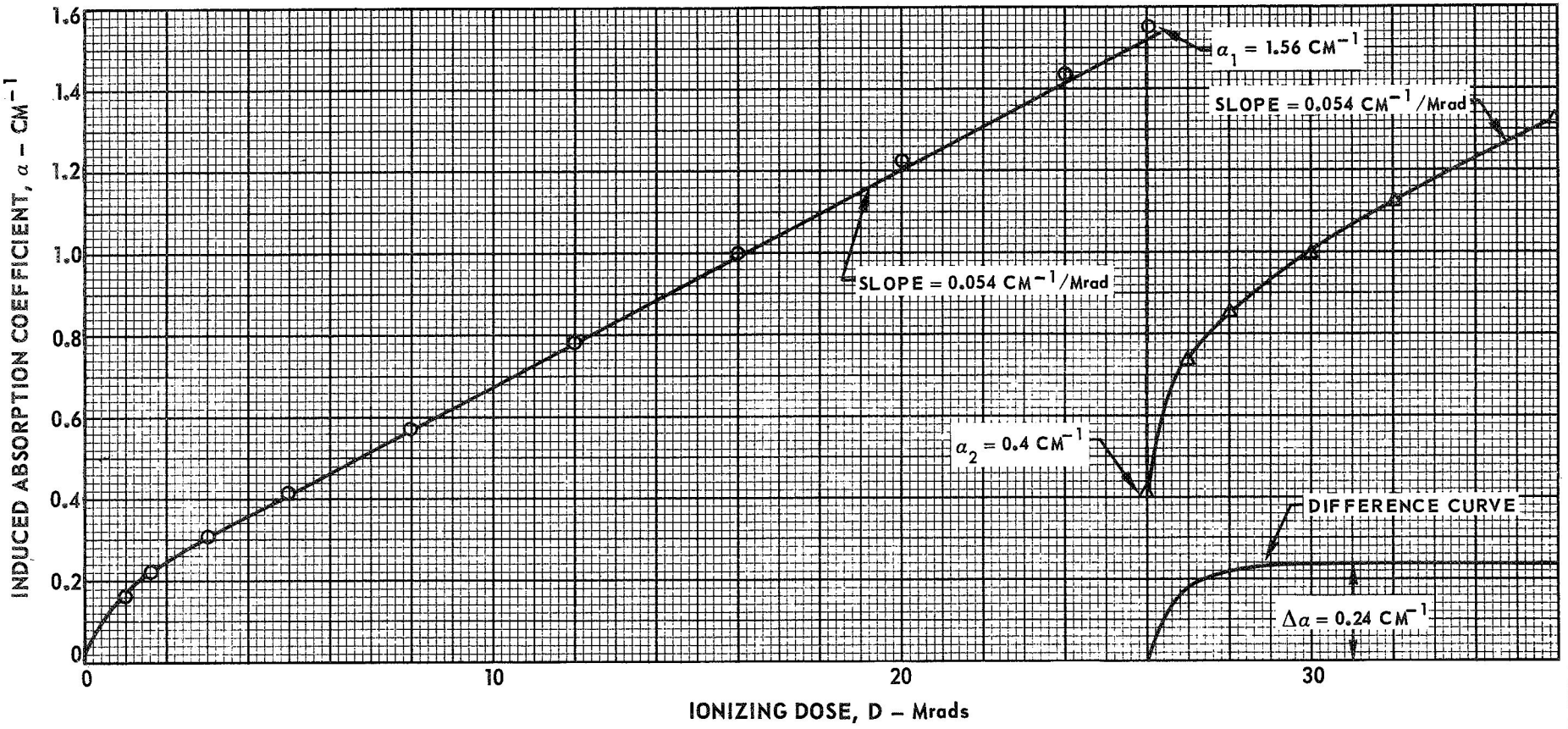

FIG. 23

FIG. 24

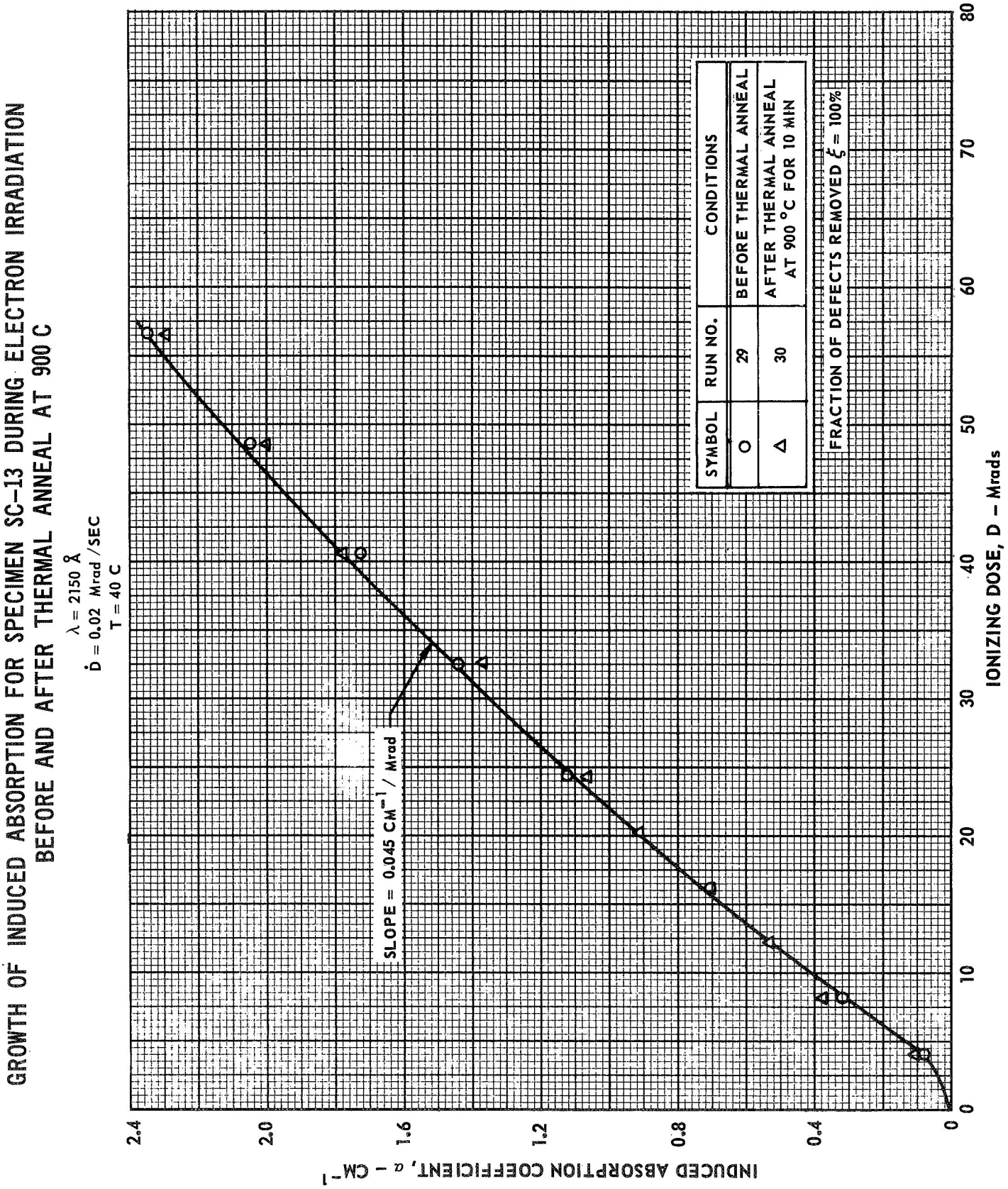
GROWTH OF INDUCED ABSORPTION FOR SPECIMEN SC-13 DURING ELECTRON IRRADIATION
BEFORE AND AFTER THERMAL ANNEAL AT 900 C
λ = 2150 Å
Ḋ = 0.02 Mrad/SEC
T = 40 C
SLOPE = 0.045 CM⁻¹ / Mrad
SYMBOL | RUN NO. | CONDITIONS
O | 29 | BEFORE THERMAL ANNEAL
Δ | 30 | AFTER THERMAL ANNEAL AT 900 °C FOR 10 MIN
FRACTION OF DEFECTS REMOVED ξ = 100%
INDUCED ABSORPTION COEFFICIENT, α – CM⁻¹
IONIZING DOSE, D – Mrads
0
0.4
0.8
1.2
1.6
2.0
2.4
10
20
30
40
50
60
70
80

GROWTH OF INDUCED ABSORPTION FOR SPECIMEN SC-15 DURING ELECTRON IRRADIATION BEFORE AND AFTER RADIATION ANNEAL

$\lambda = 2150$ Å

$\dot{D} = 0.02$ Mrads /SEC

T = 40 C

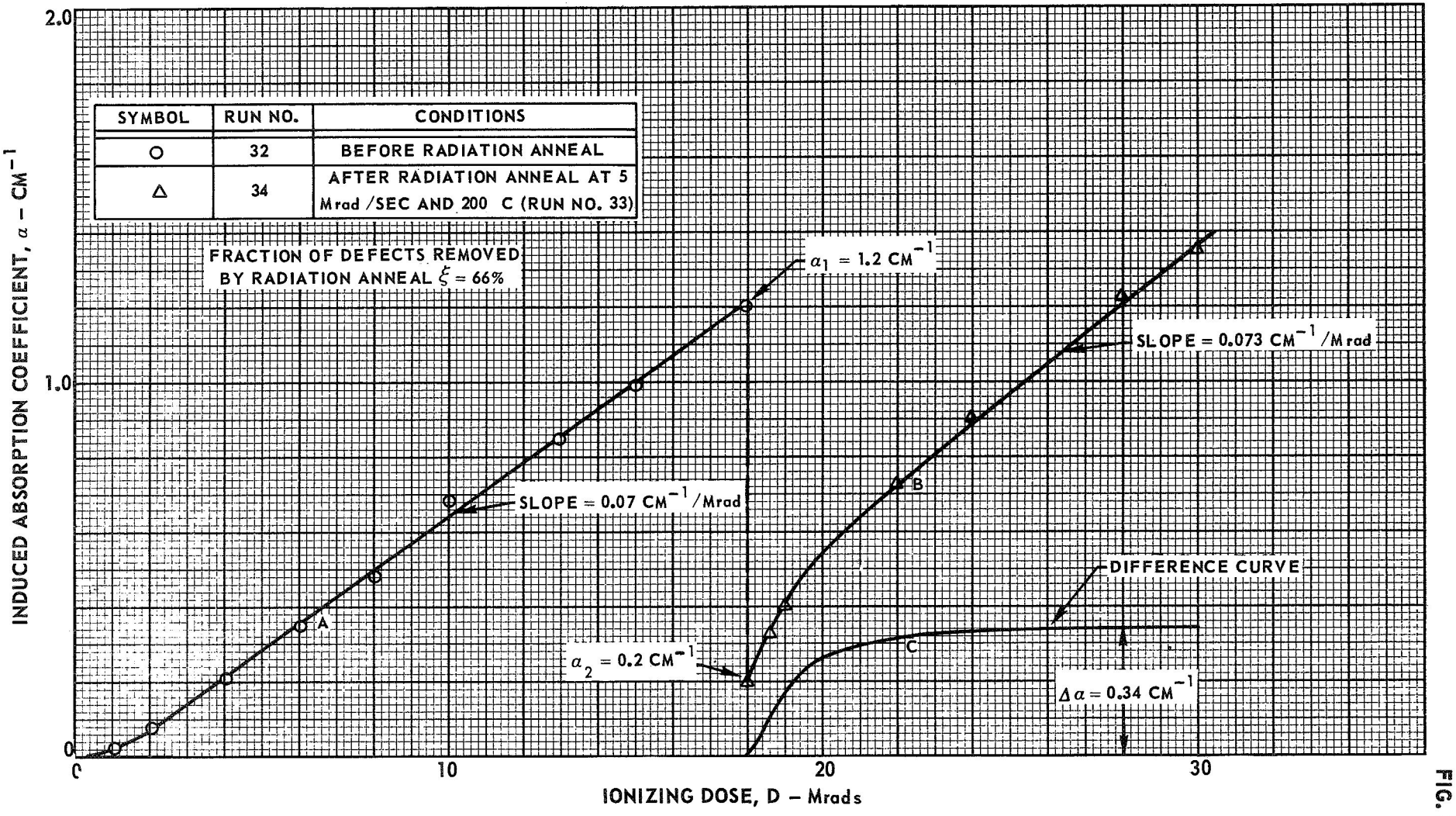

FIG. 25

J-990929-1

FIG. 26

FIG. 27

GROWTH OF INDUCED ABSORPTION FOR SPECIMEN SC-N-3 DURING ELECTRON IRRADIATION
RUN NUMBER 50 AFTER THERMAL ANNEAL AT 900 C

λ = 2150 Å
$\dot{D}$ = 0.02 Mrad/SEC
T = 40 C

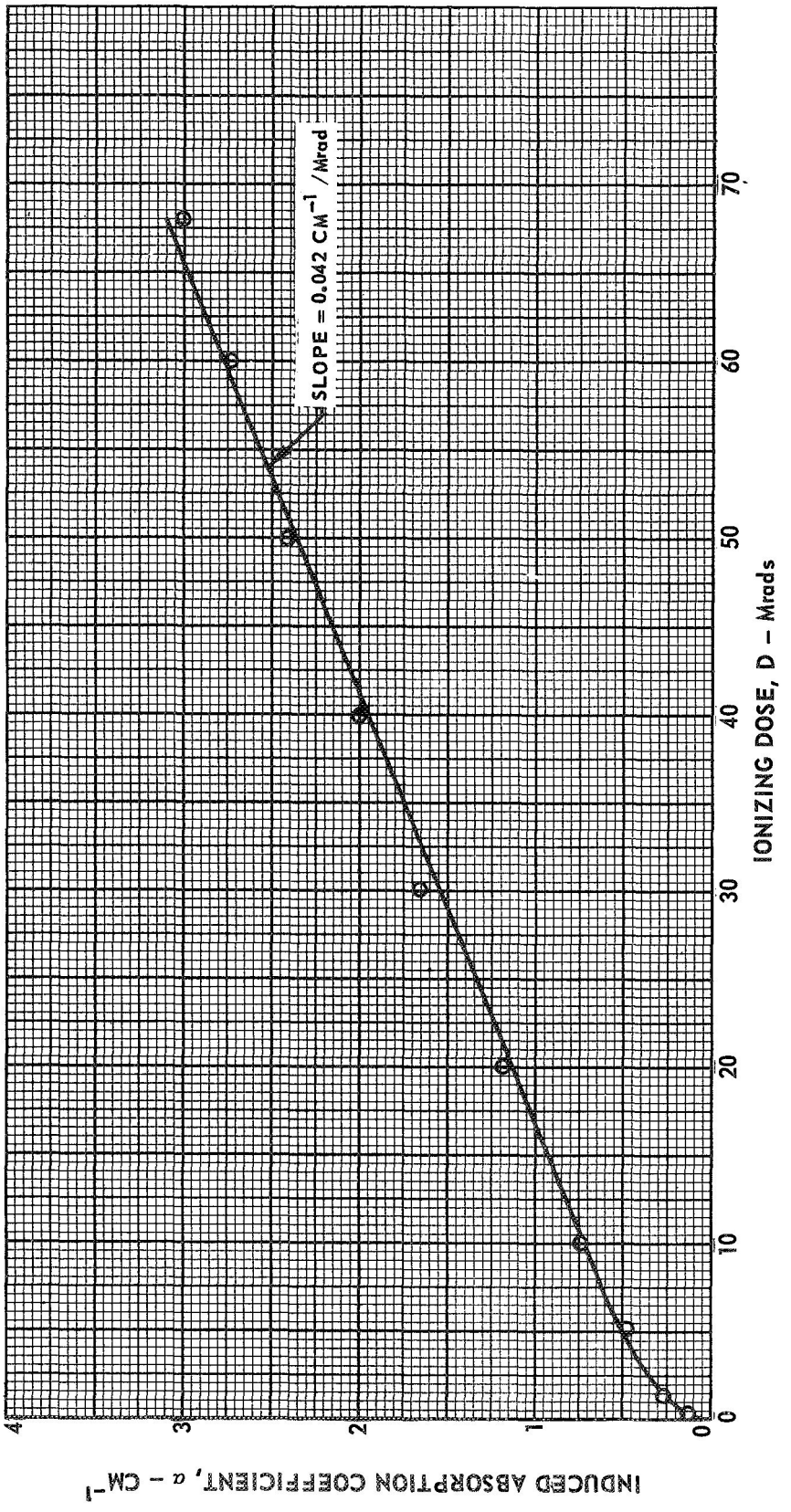

FIG. 28

RADIATION ANNEALING OF REACTOR-IRRADIATION-INDUCED ABSORPTION
AT 2150 Å OF SPECIMEN SC-N-1 DURING RUN NO. 47

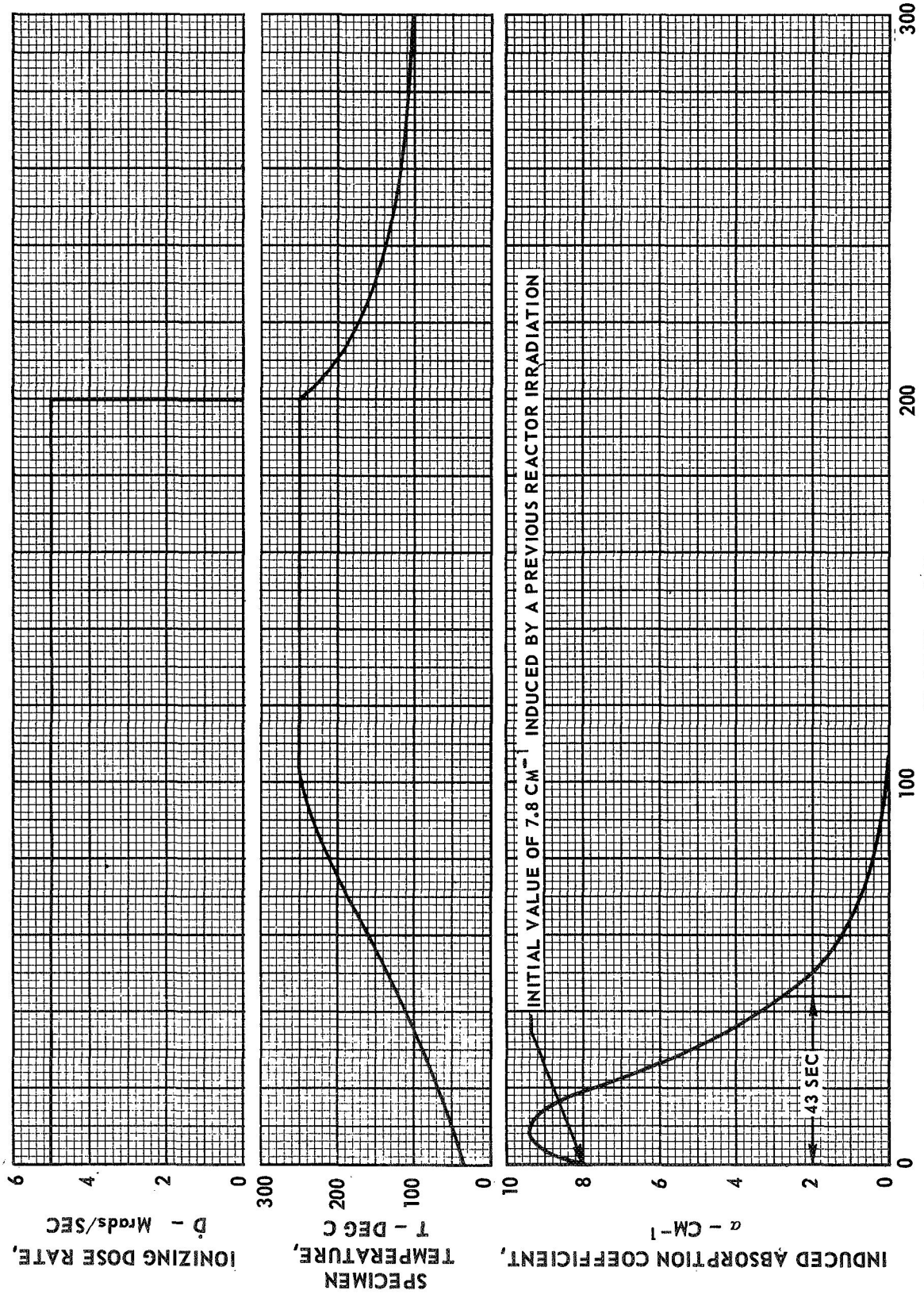

FIG. 29

GROWTH OF INDUCED ABSORPTION FOR SPECIMEN SC-N-1 DURING ELECTRON IRRADIATION RUN NUMBER 48 AFTER RADIATION ANNEAL AT 5 Mrads/SEC AND 250 C

$\lambda = 2150$ Å
$\dot{D} = 0.02$ Mrad/SEC
T = 40 C

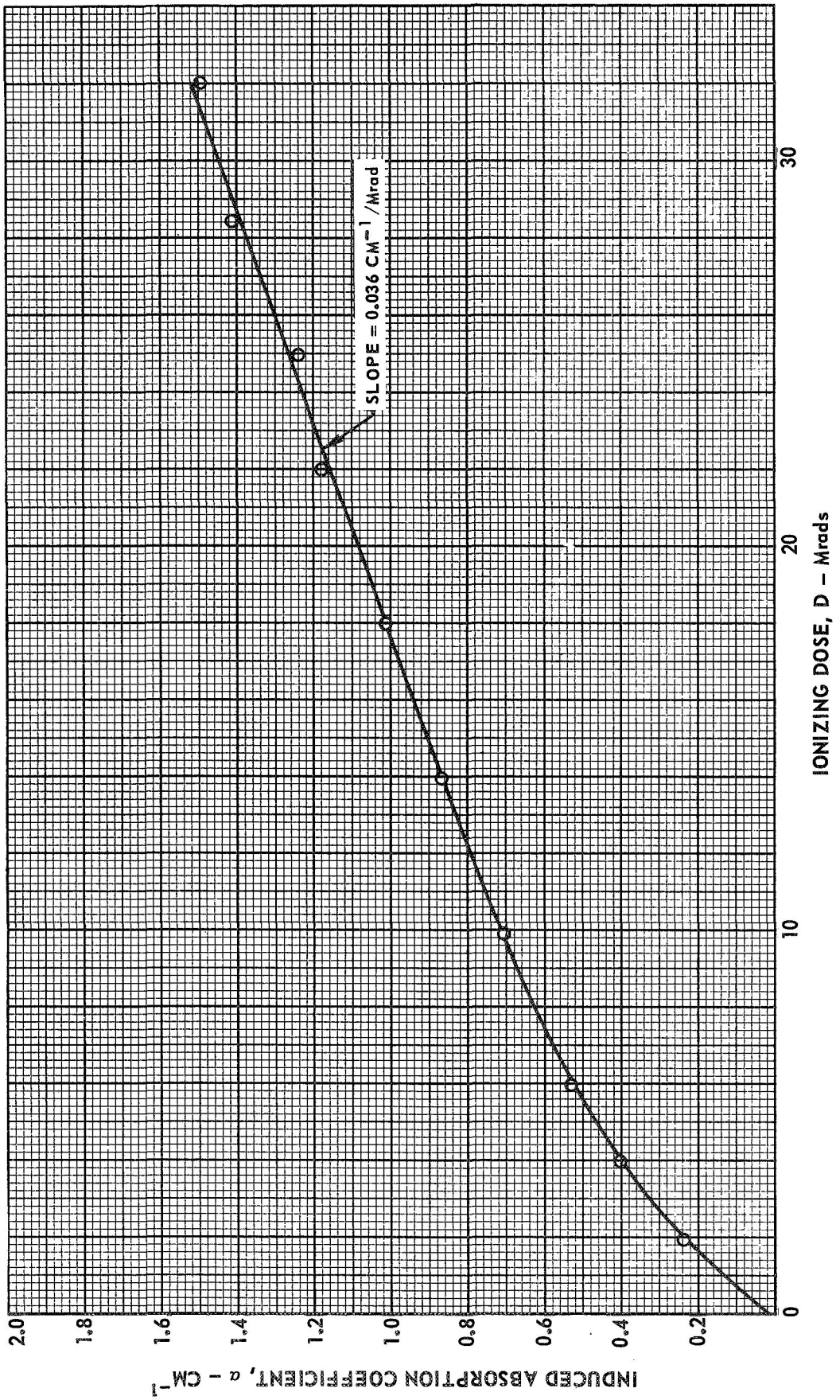

FIG. 30

GROWTH OF INDUCED ABSORPTION FOR SPECIMEN SC-21 DURING ELECTRON IRRADIATION
BEFORE AND AFTER OPTICAL BLEACH

$\lambda = 2150$ Å
$\dot{D} = 0.02$ Mrad/SEC
T = 40 C

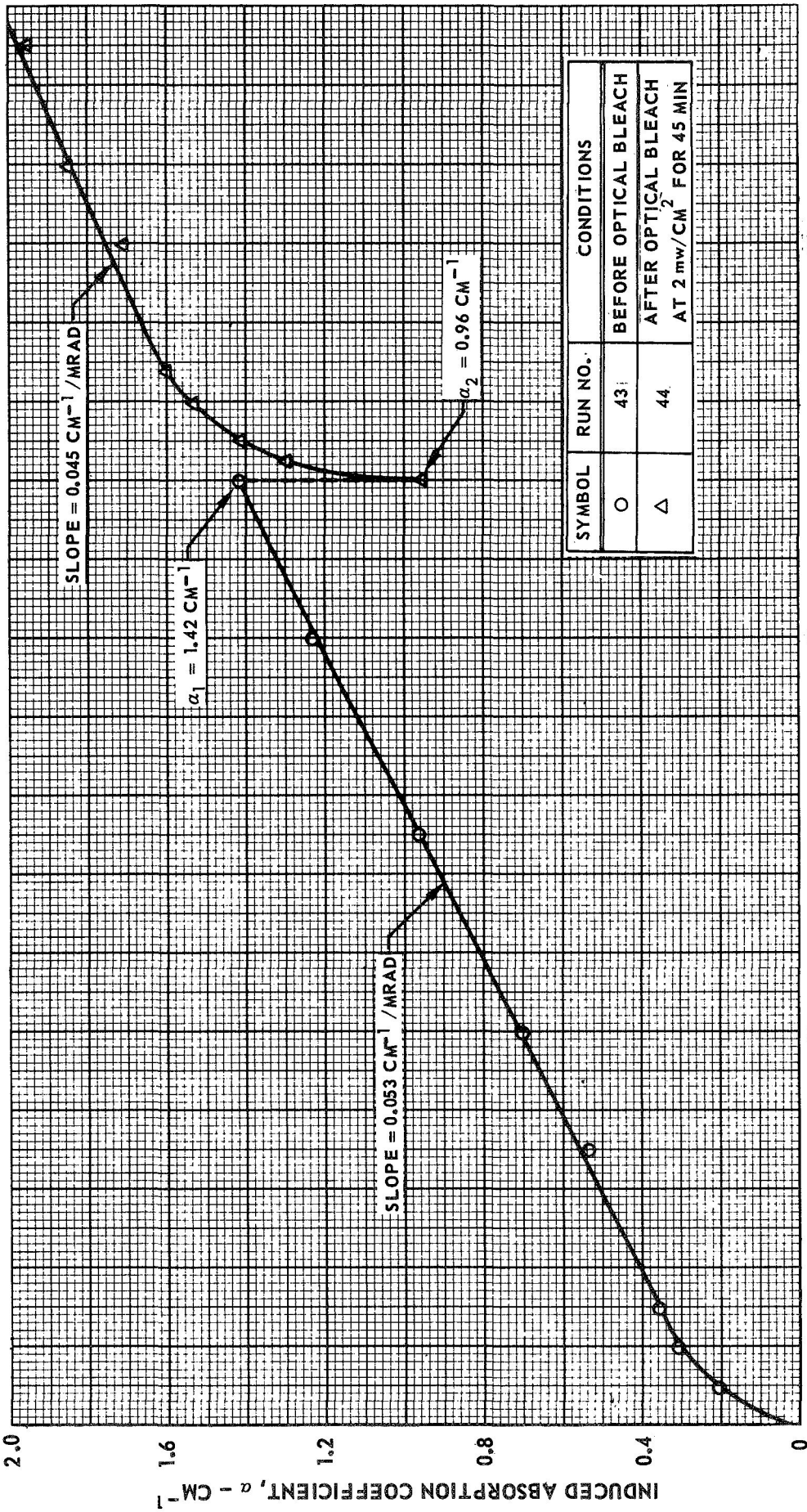

GROWTH OF INDUCED ABSORPTION FOR SPECIMEN SC-22 DURING ELECTRON IRRADIATION BEFORE AND AFTER OPTICAL BLEACH

$\lambda = 2150$ Å
$\dot{D} = 0.02$ Mrad/SEC
T = 40 C

SYMBOL	RUN NO.	CONDITIONS
○	45	BEFORE OPTICAL BLEACH
△	46	AFTER OPTICAL BLEACH AT 1 mw/CM^2 FOR 90 MIN

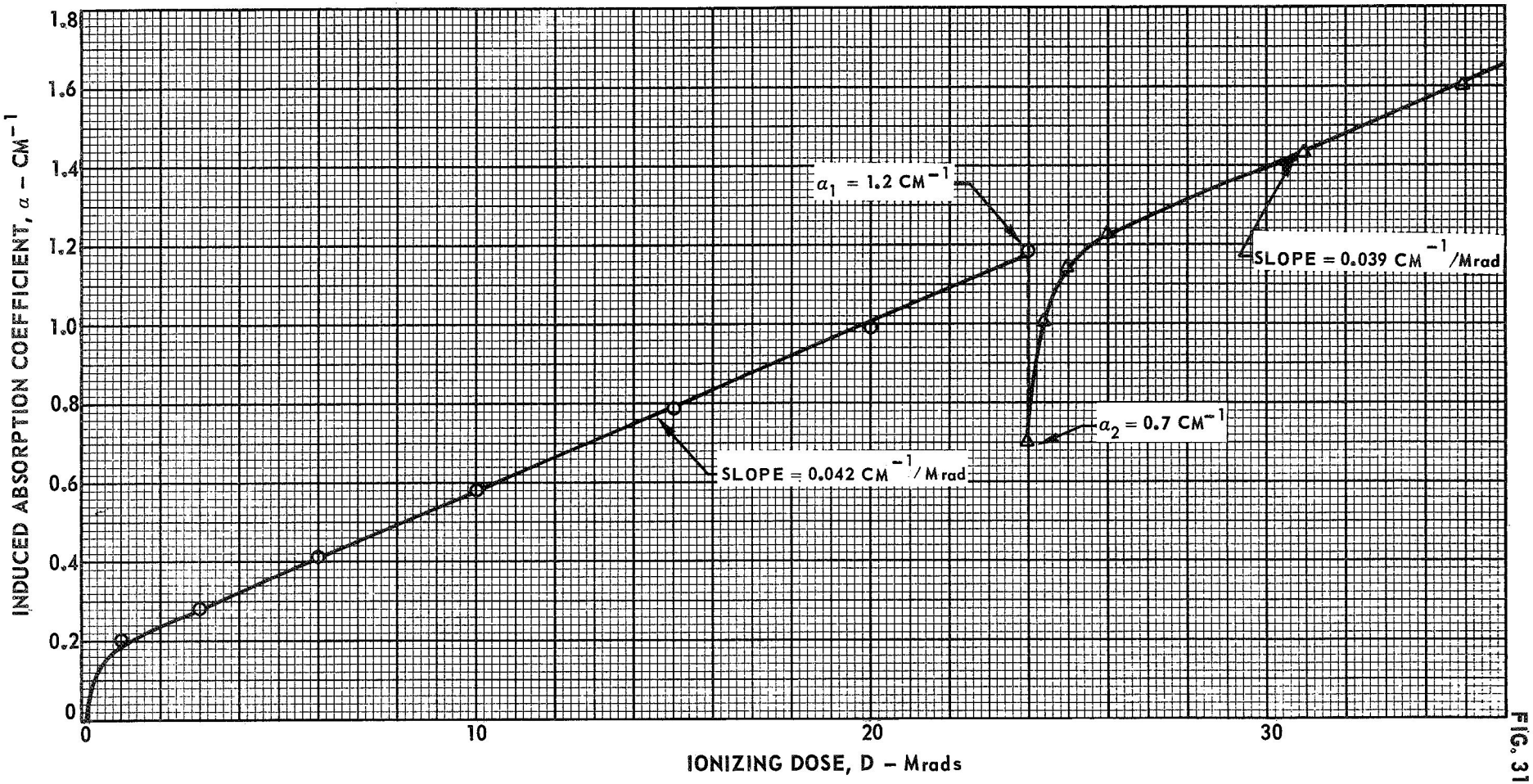

FIG. 31

FIG. 32

GROWTH OF INDUCED ABSORPTION FOR SPECIMEN SC-N-2 DURING ELECTRON IRRADIATION
RUN NUMBER 49 AFTER OPTICAL BLEACH

$\lambda = 2150$ Å
$\dot{D} = 0.02$ Mrad/SEC
$T = 40$ °C

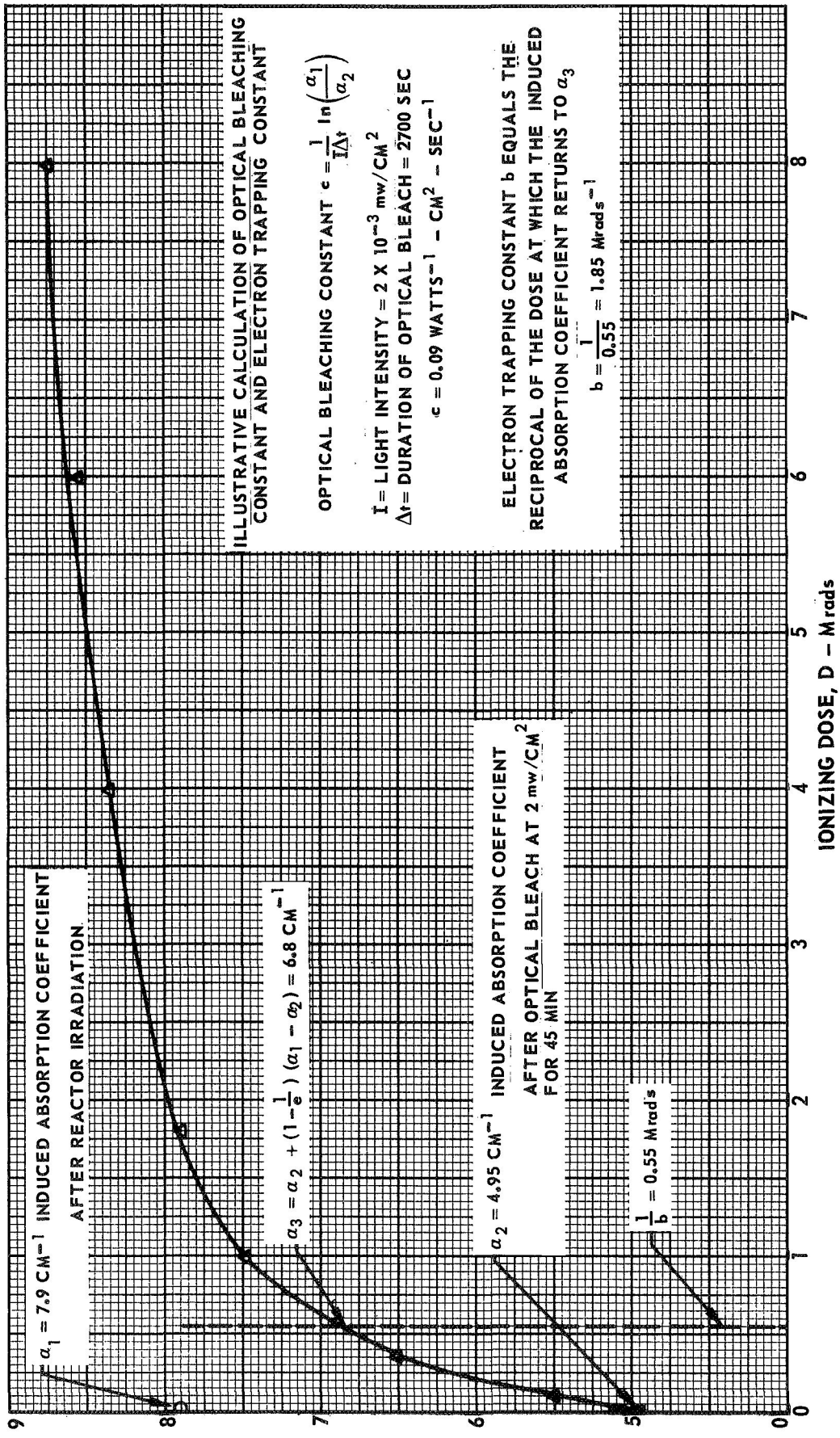

ABSORPTION SPECTRA OF FUSED SILICA AFTER REACTOR IRRADIATION TO 10^{17} n/CM^2 FAST NEUTRONS

SYMBOL	SPECIMEN
○	SC-N-1
△	SC-N-3

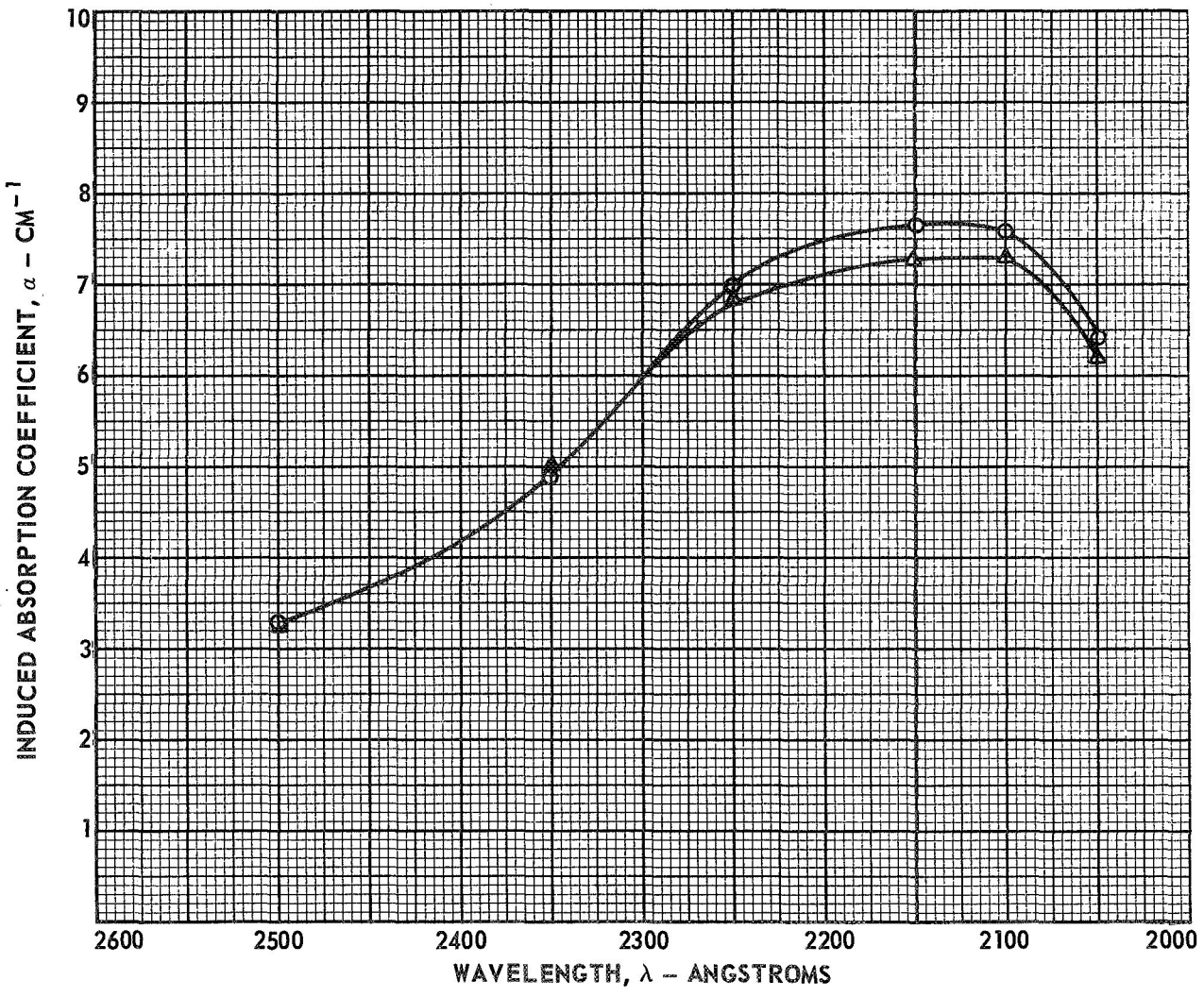

ABSORPTION SPECTRA OF FUSED SILICA AT ELEVATED TEMPERATURES DURING ELECTRON IRRADIATION

SYMBOL	SPECIMEN TEMP
○	100 C
□	300 C
▽	400 C

SPECIMEN SC-10
$\dot{D}$ = 0.42 Mrads/SEC

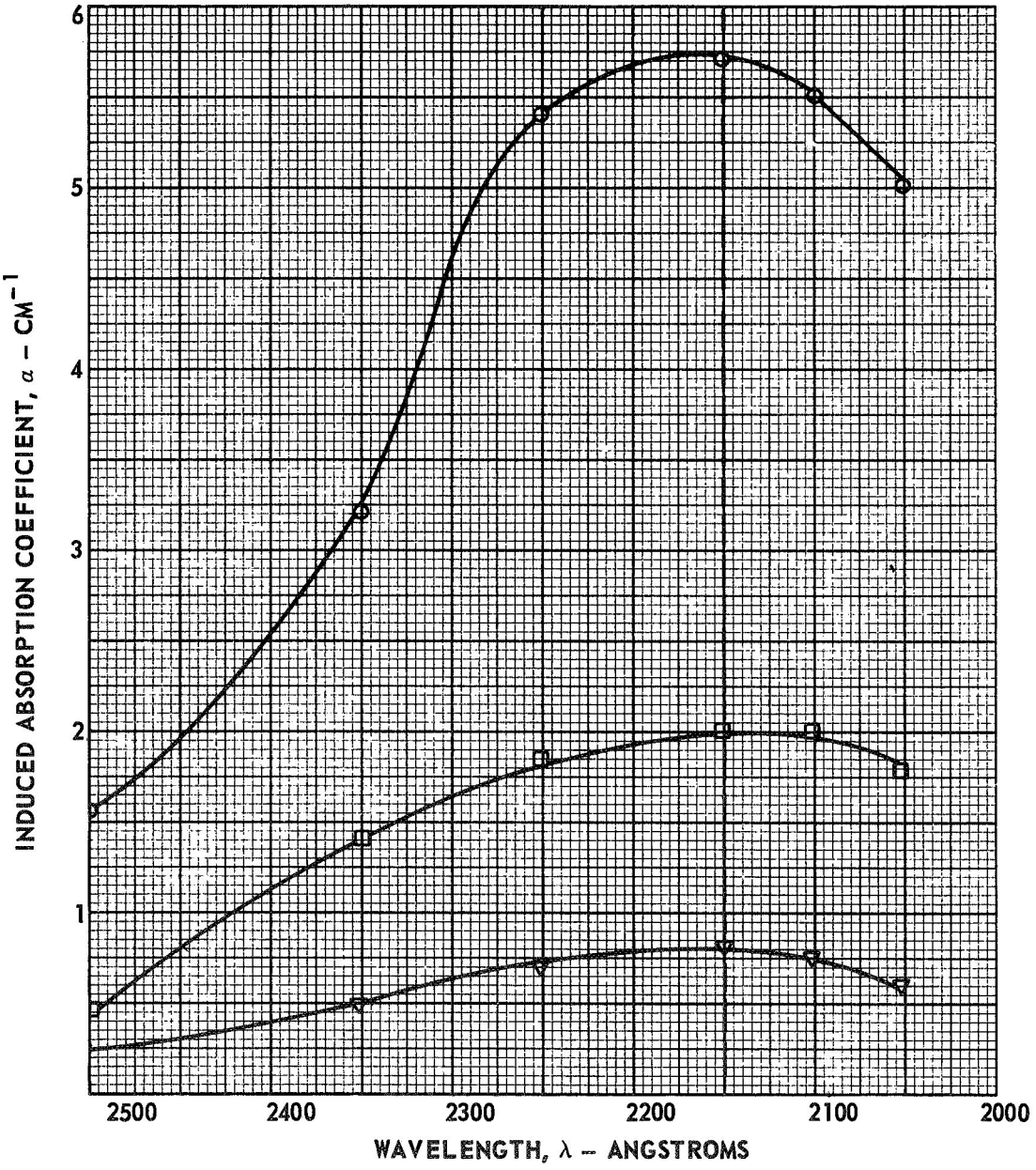

FIG. 35

NORMALIZED IRRADIATION-INDUCED ABSORPTION SPECTRA OF FUSED SILICA

SYMBOL	SPECIMEN	MEASUREMENT
△	SC-N-1 SC-N-3	POST REACTOR-IRRADIATION
○	SC-10	IN-SITU ELECTRON IRRADIATION AT T = 100 C
□	SC-10	IN-SITU ELECTRON IRRADIATION AT T = 300 C
▽	SC-10	IN-SITU ELECTRON IRRADIATION AT T = 400 C

— — — — — — DASHED CURVE IS A TYPICAL NORMALIZED SPECTRUM OBTAINED FROM PREVIOUS POST REACTOR-IRRADIATION MEASUREMENTS; SEE REF. 5

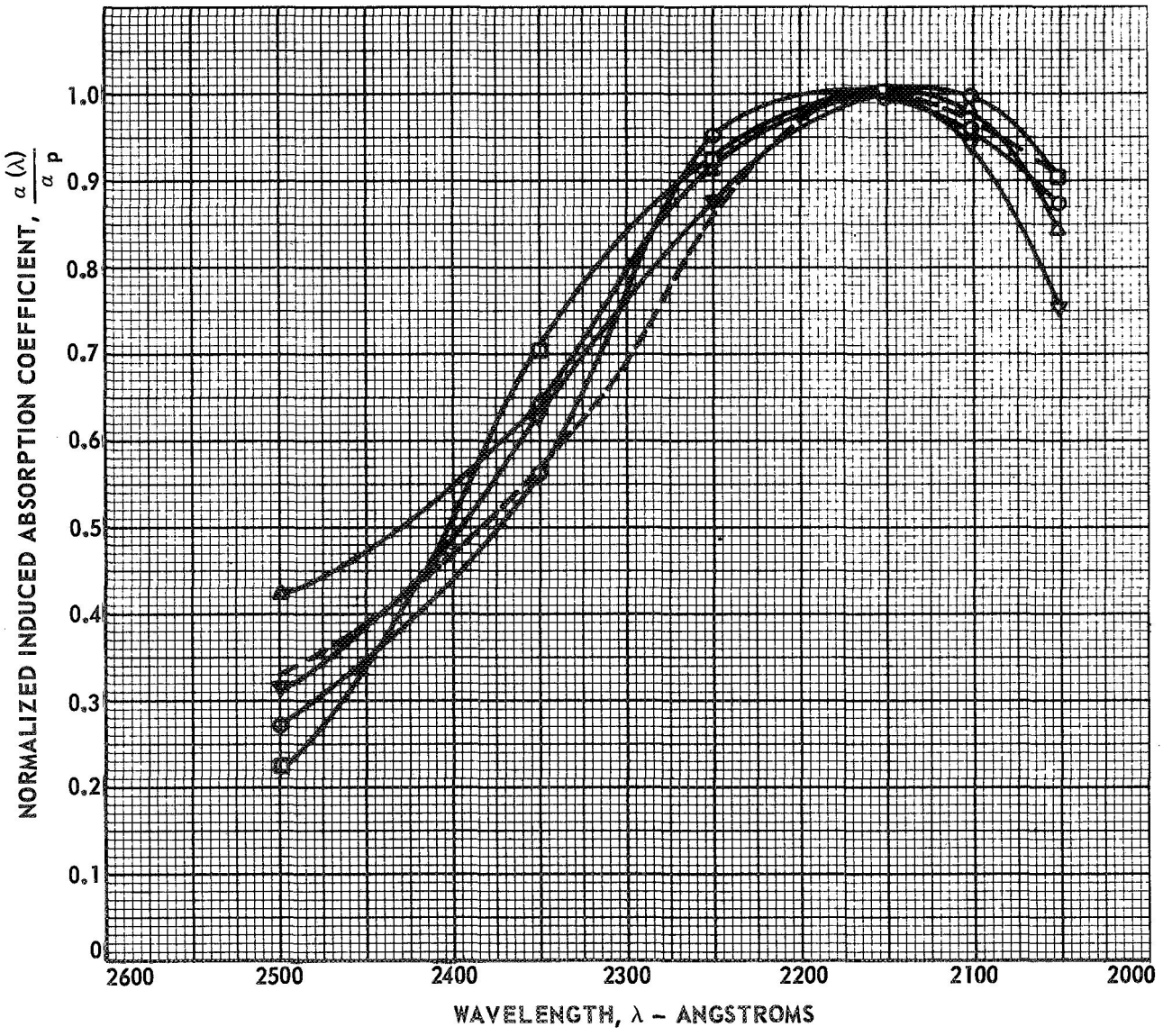

ABSORPTION SPECTRA OF ALUMINUM OXIDE AFTER REACTOR IRRADIATION TO 10^{17} n/CM^2 FAST NEUTRONS

SYMBOL	SPECIMEN
○	AL-N-1
△	AL-N-2

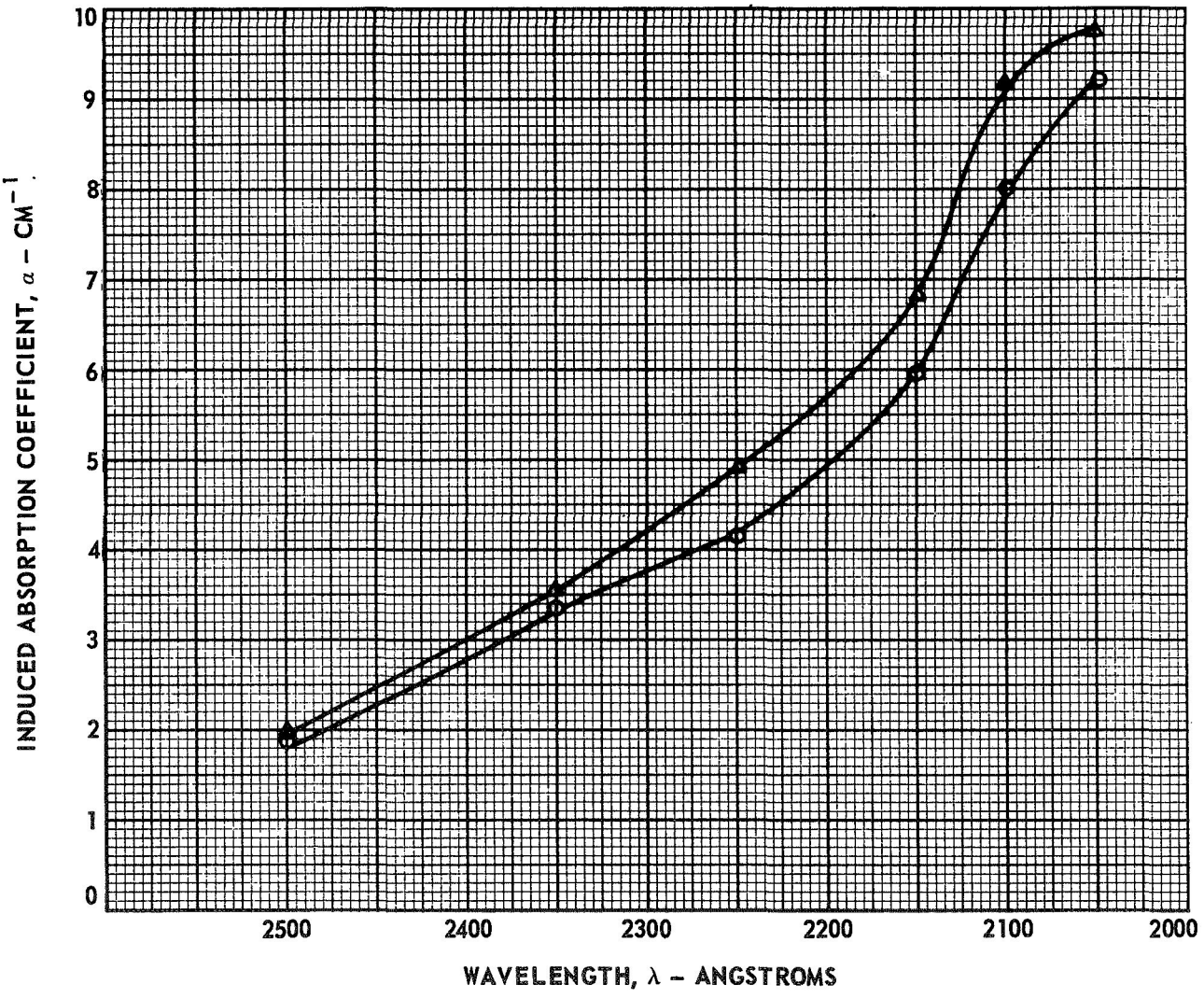

FIG. 37

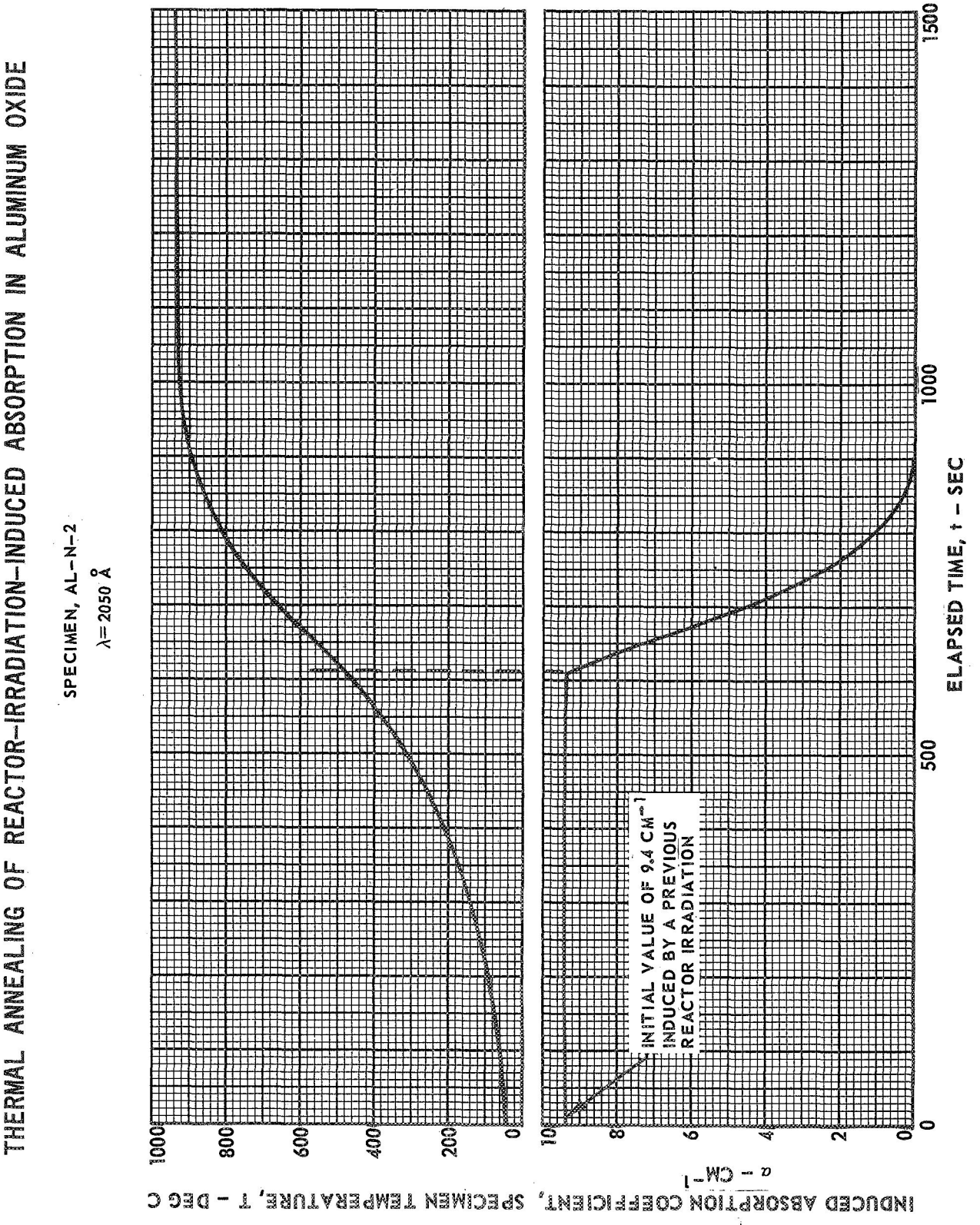
THERMAL ANNEALING OF REACTOR-IRRADIATION-INDUCED ABSORPTION IN ALUMINUM OXIDE
SPECIMEN, AL-N-2
λ= 2050 Å
INITIAL VALUE OF 9.4 CM⁻¹ INDUCED BY A PREVIOUS REACTOR IRRADIATION
INDUCED ABSORPTION COEFFICIENT, α - CM⁻¹
SPECIMEN TEMPERATURE, T - DEG C
ELAPSED TIME, t - SEC
0
200
400
600
800
1000
2
4
6
8
10
500
1000
1500

RADIATION ANNEALING OF REACTOR-IRRADIATION-INDUCED ABSORPTION IN ALUMINUM OXIDE

SPECIMEN AL-N-1
RUN NO 52
λ=2050 Å

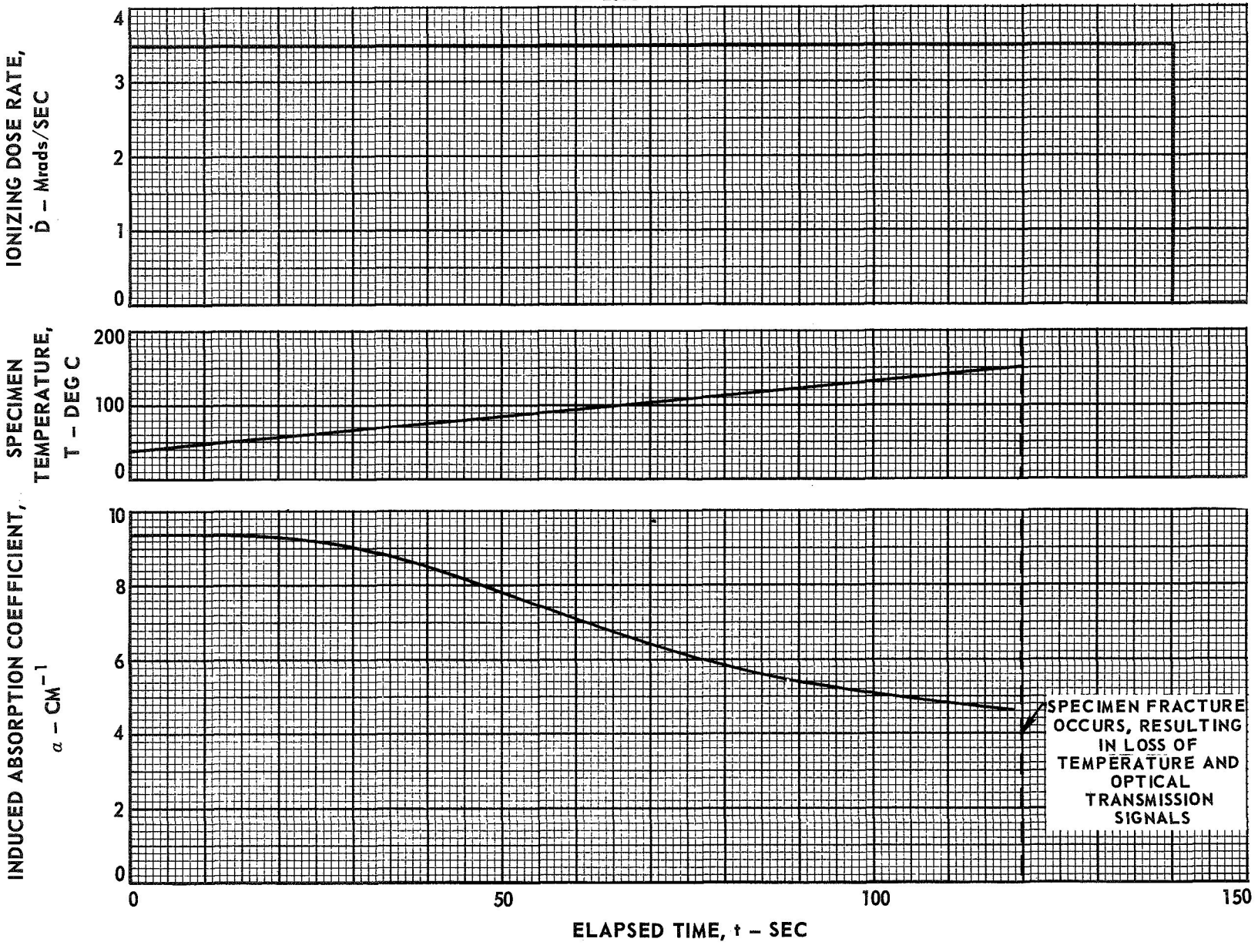

J-990929-1

FIG. 38


UNITED AIRCRAFT CORPORATION